

1990

## Inner continental shelf benthic boundary layer dynamics and suspended sediment transport

Sung Chan Kim

*College of William and Mary - Virginia Institute of Marine Science*

Follow this and additional works at: <https://scholarworks.wm.edu/etd>



Part of the [Oceanography Commons](#)

---

### Recommended Citation

Kim, Sung Chan, "Inner continental shelf benthic boundary layer dynamics and suspended sediment transport" (1990). *Dissertations, Theses, and Masters Projects*. Paper 1539616717.

<https://dx.doi.org/doi:10.25773/v5-2457-x464>

This Dissertation is brought to you for free and open access by the Theses, Dissertations, & Master Projects at W&M ScholarWorks. It has been accepted for inclusion in Dissertations, Theses, and Masters Projects by an authorized administrator of W&M ScholarWorks. For more information, please contact [scholarworks@wm.edu](mailto:scholarworks@wm.edu).

## **INFORMATION TO USERS**

**The most advanced technology has been used to photograph and reproduce this manuscript from the microfilm master. UMI films the text directly from the original or copy submitted. Thus, some thesis and dissertation copies are in typewriter face, while others may be from any type of computer printer.**

**The quality of this reproduction is dependent upon the quality of the copy submitted. Broken or indistinct print, colored or poor quality illustrations and photographs, print bleedthrough, substandard margins, and improper alignment can adversely affect reproduction.**

**In the unlikely event that the author did not send UMI a complete manuscript and there are missing pages, these will be noted. Also, if unauthorized copyright material had to be removed, a note will indicate the deletion.**

**Oversize materials (e.g., maps, drawings, charts) are reproduced by sectioning the original, beginning at the upper left-hand corner and continuing from left to right in equal sections with small overlaps. Each original is also photographed in one exposure and is included in reduced form at the back of the book.**

**Photographs included in the original manuscript have been reproduced xerographically in this copy. Higher quality 6" x 9" black and white photographic prints are available for any photographs or illustrations appearing in this copy for an additional charge. Contact UMI directly to order.**

# **U·M·I**

University Microfilms International  
A Bell & Howell Information Company  
300 North Zeeb Road, Ann Arbor, MI 48106-1346 USA  
313/761-4700 800/521-0600



**Order Number 9025869**

**Inner continental shelf benthic boundary layer dynamics and  
suspended sediment transport**

**Kim, Sung Chan, Ph.D.**

**The College of William and Mary, 1990**

**U·M·I**  
300 N. Zeeb Rd.  
Ann Arbor, MI 48106



INNER CONTINENTAL SHELF BENTHIC BOUNDARY LAYER  
DYNAMICS AND SUSPENDED SEDIMENT TRANSPORT

---

A Dissertation

Presented to

The Faculty of the School of Marine Science  
The College of William and Mary in Virginia

In Partial Fulfillment

Of the Requirements for the Degree of  
Doctor of Philosophy

---

by

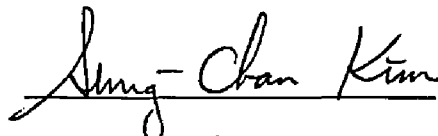
Sung Chan Kim

1990

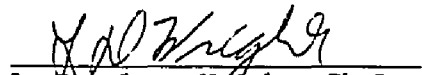
APPROVAL SHEET


This dissertation is submitted in partial fulfillment of  
the requirements for the degree of


Doctor of Philosophy


  
Sung Chan Kim


Approved, May 1990

  
L. Donelson Wright, Ph.D.  
Committee Chairman/Advisor

  
John D. Boon, III, Ph.D.

  
Robert J. Diaz, Ph.D.

  
Albert Y. Kuo, Ph.D.

  
Ole S. Madsen, Sc.D.  
Massachusetts Institute of Technology  
Cambridge, Massachusetts

## TABLE OF CONTENTS

ACKNOWLEDGEMENTS .....	v
LIST OF TABLES .....	vi
LIST OF FIGURES .....	vii
LIST OF PRINCIPAL SYMBOLS .....	x
ABSTRACT .....	xvii
1. INTRODUCTION .....	2
2. DATA ACQUISITION AND ANALYSIS .....	9
2.1 Introduction .....	9
2.2 Hydrodynamic variables .....	11
2.3 Aligning data with new coordinate system .....	19
2.4 Calibration of optical back-scattering (OBS) sensors .....	24
2.5 Suspended sediment concentrations .....	28
3. BOUNDARY LAYER MODEL .....	33
3.1 Introduction .....	33
3.2 Wave boundary layer model .....	36
3.2.1 Governing equations .....	36
3.2.2 Modeling of eddy viscosity .....	38
3.2.3 Solution and test .....	41
3.3 Wave current boundary layer model .....	48
3.3.1 Governing equations .....	48
3.3.2 Solution for current .....	53
3.3.3 Solution for wave .....	54
3.3.4 Maximum bottom shear stress .....	57
3.3.5 Bottom roughness .....	59
3.3.6 Solution and test .....	61
3.3.7 Results and discussion .....	62



4.	SUSPENDED SEDIMENT CONCENTRATION MODEL .....	70
4.1	Introduction .....	70
4.2	Governing equations .....	72
4.3	Diffusivity of suspended sediment concentration ..	74
4.4	Solution for mean concentration .....	80
4.5	Determination of model parameters from field data	81
4.6	Reference concentration .....	91
4.7	Results and discussion .....	106
5.	CROSS-SHORE SEDIMENT TRANSPORT .....	112
5.1	Introduction .....	112
5.2	An energetics model .....	115
5.3	Velocity moments .....	119
5.4	Application of the energetics model to field data	122
5.5	Discussion .....	127
6.	SUMMARY AND CONCLUSION .....	142
	LITERATURE CITED .....	146
	VITA .....	159

## ACKNOWLEDGEMENTS

This work was supported by Virginia Institute of Marine Science (VIMS). I am grateful to each of my committee members for wise counsel and encouragement. The special acknowledgement is to my supervisor Dr. Don Wright for the inspiration and support throughout my study period. I appreciate the opportunity of having discussions with Dr. Ole Madsen and his time and effort for the review of this work. I wish to thank Dr. John Boon for the advice on the instrumentation and the data acquisition and process. I also wish to thank my other committee members, Dr. Albert Kuo and Dr. Bob Diaz, for constructive reviews of this manuscript. Thanks are extended to Dr. Jerome Maa for the comments and suggestions on the dissertation. Dr. Nungjane Shi is acknowledged for introducing me numerical approaches and encouraging me throughout the first phase of this study.

I am thankful to all the staffs and students in the Division of Geological and Benthic Oceanography. I also acknowledge many friends, who have been in VIMS during the past seven years, especially Cheol Mo and Jeff List for helpful discussions and pleasant talkings.

I wish to specially thank my parents and Myung-Hee for their general encouragement.

LIST OF TABLES

1	Input data for fair weather portion .....	22
2	Input data for storm weather portion .....	23
3	Modification factors and the maximum friction velocity	46
4	Calculated values for fair weather portion .....	67
5	Calculated values for storm weather portion .....	68
6	Formulation for reference concentration and the resuspension coefficient, $\gamma$ .....	101
7	Model input parameters .....	107
8	Calculated moments for fair weather portion .....	123
9	Calculated moments for storm weather portion .....	125

## LIST OF FIGURES

1	Location map .....	10
2	Power spectra of pressure and wave height .....	13
3	Hydrodynamic variables, fair weather portion .....	15
4	A comparison of power spectra between fair weather and storm .....	16
5	Hydrodynamic variables, storm portion .....	17
6	Transformation of coordinates .....	20
7	Set-up of the calibration of an OBS sensor .....	25
8	A sample calibration of OBS sensor .....	27
9	Suspended sediment concentration profiles, fair weather portion .....	29
10	Power spectra of pressure, fair weather portion .....	30
11	Suspended sediment concentration profiles, storm portion	31
12	Power spectra of pressure, storm portion .....	32
13	Wave boundary layer model run for $\hat{f} = 1$ .....	47
14	Definition sketch for combined boundary layer .....	49
15	Effect of change in angle between current and wave propagation .....	63
16	Combined boundary layer model run for fair weather .....	64
17	Combined boundary layer model run for storm .....	66
18	Concentration profile .....	79
19	Cross-correlations between squared velocity and suspended sediment concentration, storm condition .....	82
20	Cross-correlations between squared velocity and suspended sediment concentration, fair weather condition .....	83

21	Cross-correlations between the suspended sediment concentrations at different levels, fair weather condition	84
22	Cross-correlations between the suspended sediment concentrations at different levels, storm condition	85
23	Variation of time averaged squared speed and suspended sediment concentrations, fair weather portion	86
24	Variation of time averaged squared speed and suspended sediment concentrations, storm portion	87
25	Modifying velocity scale, $V$ , versus maximum bottom friction velocity, $u_{*1}$	89
26	Reference concentration versus excess Shields parameter	95
27	The resuspension coefficient, $\gamma$ , for $C_r \propto \theta$	96
28	The resuspension coefficient, $\gamma$ , for $C_r \propto S$	97
29	The resuspension coefficient, $\gamma$ , for $C_r \propto \theta^{1/2}$	99
30	The resuspension coefficient, $\gamma$ , for $C_r \propto S^{1/2}$	100
31	Variation of the resuspension coefficient, $\gamma$ , with OBS sensor heights, fair weather portion	102
32	Variation of the resuspension coefficient, $\gamma$ , with OBS sensor heights, storm portion	103
33	The resuspension coefficient, $\gamma$ , versus the maximum bottom friction velocity, $u_{*1}$	104
34	Test run of mean concentration model for different wave conditions	108
35	Predicted suspended sediment concentrations, fair weather portion	109

36	Predicted suspended sediment concentrations, storm portion .....	111
37	Immersed weight transport rate for suspended load, fair weather portion .....	124
38	Immersed weight transport rate for suspended load, storm portion .....	126
39	Suspended sediment flux, fair weather portion .....	129
40	Suspended sediment flux, storm portion .....	130
41	Comparison of transport rates calculated by the integration of flux and the energetics approach, fair weather portion .....	134
42	Comparison of transport rates calculated by the integration of flux and the energetics approach, storm portion .....	135
43	The ratio between $\langle Q_x \rangle_{+\delta}$ and $\langle Q_x \rangle_{-\delta}$ , fair weather portion .....	137
44	The ratio between $\langle Q_x \rangle_{+\delta}$ and $\langle Q_x \rangle_{-\delta}$ , storm portion ....	138
45	Cross-correlations between cross-shore velocity and suspended sediment concentration, storm condition .....	139
46	Cross-correlations between cross-shore velocity and suspended sediment concentration, fair weather condition	140

## LIST OF PRINCIPAL SYMBOLS

$(u_i, v_i)$	Velocity vector in (E-W, N-S) coordinate system
$(u'_i, v'_i)$	Velocity vector in transformed coordinate system
$A_b$	Bottom excursion amplitude
$b$	Vertical wave displacement
$C$	Concentration of sediment
$C_m$	Mean concentration
$C_p$	Periodic concentration
$C'$	Turbulent fluctuation of concentration
$C^*$	Average volume concentration
$C_b$	Bed concentration
$C_r$	Reference concentration
$C_D$	Drag coefficient
$D_s$	Grain diameter
$f$	Frequency ( $= 1/T$ )
$\hat{f}$	Modification factor for velocity scale of wave boundary layer
$g$	Gravitational acceleration
$H$	Wave height
$H_{m0}$	Significant wave height
$h$	Water depth
$\hat{h}$	A parameter ( $= \frac{u_{*w, m}}{\omega u_{co}}$ )

$I$	Immersed weight sediment transport rate
$I_b$	Immersed weight bedload transport rate
$I_s$	Immersed weight suspended load transport rate
$\vec{I}_t$	Instantaneous transport rate vector
$\langle I_x \rangle$	Net immersed weight cross-shore transport rate
$K$	Coefficient relating transport rate to fluid power
$K'$	A variation of coefficient $K$
$K_b$	Coefficient $K$ for bedload
$K_s$	Coefficient $K$ for suspended load
$\vec{K}_t$	Vector form of $K$ for instantaneous transport
$\vec{K}_{tb}$	$\vec{K}_t$ for bedload
$\vec{K}_{ts}$	$\vec{K}_t$ for suspended load
$k_b$	Roughness height
$l$	Characteristic length scale
$N$	Available bed material
$N_s$	Number of grains in motion on the bed
$P(m)$	Pressure converted into meters
$\bar{P}$	Mean pressure
$P_{atm}$	Atmospheric pressure
$P_{read}$	Pressure recorded in mbar
$p$	Pressure
$P_c$	Mean $p$



$p_w$	Periodic fluctuation of $p$
$p'$	Turbulent fluctuation of $p$
$\langle Q_x \rangle$	Net cross-shore suspended sediment transport rate
$\langle Q_x \rangle_{-\delta}$	Net cross-shore suspended sediment transport rate inside wave boundary layer
$\langle Q_x \rangle_{+\delta}$	Net cross-shore suspended sediment transport rate above wave boundary layer
$\langle Q_x \rangle_{\text{energetics}}$	Net cross-shore suspended sediment transport rate calculated from energetics model
$q_b$	Immersed bedload rate
$\langle q_x \rangle$	Net cross-shore suspended sediment flux
$r$	Correlation coefficient
$S$	Excess shear stress
$S_p$	Power spectrum of pressure
$s_p$	Standard deviation of pressure
$s_u$	Standard deviation of $u_i$
$s_v$	Standard deviation of $v_i$
$s_{uv}$	Covariance of $u_i$ and $v_i$
$s_u$	Standard deviation of $u_i'$
$T$	Wave period
$T_{zp}$	zero-upcrossing period calculated from pressure spectrum
$U_\infty$	Amplitude of bottom excursion velocity
$U_0$	Wave orbital velocity

$U_\delta$	Amplitude of defect velocity
$U^*$	Dimensionless variable for velocity
$\bar{U}_s$	Mean flow velocity
$u$	Current in x-direction
$\bar{u}$	Average $u_i$
$\bar{u}'$	Average of $u_i'$
$u_c$	Mean current velocity in x-direction
$u_w$	Wave velocity in x-direction
$u'$	Turbulent fluctuation of $u$
$u_b$	Average bedload transport velocity
$\vec{u}_s$	Velocity vector for particle
$\vec{u}_t$	Instantaneous velocity
$\bar{u}_t$	Mean current $(= (u_c^2 + v_c^2)^{1/2})$
$u_\theta$	Velocity in direction $\theta$
$u_\infty$	Free stream velocity
$u_\delta$	Defect velocity
$u_{*c}$	Critical friction velocity
$u_{*w,m}$	Maximum bottom friction velocity due to wave
$u_{*1}$	Velocity scale of wave boundary layer
$u_{*2}$	Velocity scale for current boundary layer
$V$	Velocity scale for the modification of turbulent diffusion

$ v_i $	Speed of velocity vector ( $u_i, v_i$ )
$v$	Current in y-direction
$\bar{v}$	Average $v_i$
$\bar{v}'$	Average of $v_i'$
$v_c$	Mean current velocity in y-direction
$v_w$	Wave velocity in y-direction
$v'$	Turbulent fluctuation of $v$
$w$	Current in z-direction
$w_w$	Periodic fluctuation of $w$
$w'$	Turbulent fluctuation of $w$
$w_{fs}$	Settling velocity
$X(z)$	Real amplitude of $u_w$
$Y(z)$	Real amplitude of $v_w$
$z_0$	Roughness length scale
$z_1$	Apparent roughness for current boundary layer
$z_r$	Reference height
$z^*$	Dimensionless variable for space
$\alpha_1$	A constant related to the distance from the bed
$\alpha_i$	Angle between $u_i$ and $v_i$
$\beta$	Bed slope
$\gamma$	Resuspension coefficient
$\delta$	Parameter normalizing current velocity with wave velocity
$\delta_u$	Parameter normalizing u-velocity with wave velocity

$\delta_v$	Parameter normalizing v-velocity with wave velocity
$\delta_c$	Thickness of current boundary layer
$\delta_w$	Thickness of wave boundary layer
$\delta_t$	Delay time
$\epsilon$	Viscous dissipation
$\epsilon_b$	Efficiency for bedload transport
$\epsilon_s$	Efficiency for suspended load transport
$\epsilon_p$	Irregularity calculated from pressure spectrum
$\eta$	Surface elevation
$\eta_b$	Height of roughness element
$\theta'$	Shields parameter for skin friction
$\theta$	Angle of the wave propagation counter-clockwise from East
$\kappa$	Von Karman constant
$\lambda$	Width of roughness element
$\nu_t$	Eddy viscosity
$\nu_{ts}$	Eddy diffusivity
$\nu_w$	Diffusivity due to the factors other than turbulent diffusion
$\rho$	Density of water
$\rho_s$	Density of sediment
$\tau$	Shear stress
$\tau'_{b,m}$	Maximum bottom shear stress due to skin friction
$\tau_{bw,m}$	Maximum bottom shear stress exerted by wave

$\vec{\tau}_c$	Current shear stress
$\vec{\tau}_t$	Instantaneous shear stress
$\vec{\tau}_{cw}$	Combined shear stress
$\vec{\tau}_{w,m}$	Maximum shear stress induced by wave
$\phi$	Angle of repose for sand
$\Psi$	Mobility number
$\Psi_0$	First moment, representing bed agitation
$\Psi_1^*$	Second moment, related with wave asymmetry
$\Psi_1'$	Third moment, related with dissipation of energy
$\Psi_2^*$	Fourth moment, related with wave asymmetry
$\Psi_3$	Fifth moment, related with dissipation of energy
$\Omega$	Fluid power available
$\omega$	Radian frequency ( $= 2\pi/T$ )
A,B,C,D	Parameter for calculation of wave boundary layer
$A^*, B^*, C^*, D^*$	Parameters for calculation of transport rate
$X^*, Y^*, Z^*$	Dimensionless variables
X1,X2,X3,X4	Dimensionless variables

INNER CONTINENTAL SHELF BENTHIC BOUNDARY LAYER  
DYNAMICS AND SUSPENDED SEDIMENT TRANSPORT

ABSTRACT

An experiment conducted over the shoreface at Duck, North Carolina in 1985 embraced both fair-weather low energy and storm-related high energy conditions. To differentiate the diffusion and advection processes of suspended sediments under the high energy conditions from those under the low energy conditions, numerical modeling and the analysis of field data are exercised. A simple two-layer eddy viscosity wave-current combined boundary layer model is developed. The modeled characteristics of the boundary layer are incorporated with a diffusion equation to give suspended sediment concentration profiles. A velocity scale related to factors other than turbulent diffusion is formulated, representing the diffusion under varying energy conditions. With increasing bed friction, the vertical diffusion of sediment is reduced due to stratification, thus reducing velocity. From the measured suspended sediment concentration profiles, the resuspension coefficient,  $\gamma$ , shows a tendency to decrease with increased flow intensity, suggesting the role of the armoring effect. The coefficient,  $\gamma$ , varies between 0.0003 for high-energy conditions and 0.002 for low-energy conditions. The energetics approach to predicted sediment transport overestimates the role of wave transport for the low energy conditions. Cross-correlations between cross-shore velocity and sediment concentration show that the role of wave for the transport under low energy conditions is not substantial. The direction of transport under low energy conditions is governed by the mean current. Under high energy conditions, transport by waves is onshore but superseded by offshore transport by the mean current, resulting in net offshore transport. The energetics model based on the surfzone dynamics underestimates the transport rate by an order of magnitude compared to the depth integration of the average product of mean cross-shore velocity and mean concentration. This indicates that the calibration of the efficiency factors  $\epsilon_s$  and  $\epsilon_b$  in an energetics model is essential.

Sung Chan Kim  
SCHOOL OF MARINE SCIENCE  
THE COLLEGE OF WILLIAM AND MARY IN VIRGINIA

Dissertation Supervisor: L. Donelson Wright, Ph.D.  
Title : Professor of Marine Science  
Virginia Institute of Marine Science

INNER CONTINENTAL SHELF BENTHIC BOUNDARY LAYER  
DYNAMICS AND SUSPENDED SEDIMENT TRANSPORT

## 1. INTRODUCTION

An inner continental shelf occupies the shoreward edge of a continental shelf and serves as the active zone of on-offshore sediment transport. Exchange of sediments between inshore and offshore regions determines the geomorphologies and sediment budgets of both regions. In order to understand the consequent sedimentary characteristics, we need to define both the direction and the magnitude of the exchange processes.

In terms of the direction, across-shore exchange affects the inshore sediment storage more effectively than an alongshore exchange (Wright, 1987). Whereas the directions of transport are estimated by the directions of low frequency flow and the odd moments of high frequency flows, the magnitudes are determined by the magnitudes of low frequency flows and the even moments of high frequency flows (e.g. Green, 1987). In addition to the hydrodynamical factors, further complications come for the determination of the magnitudes from sediment characteristics and bedforms. The quantification of the process thus requires the comprehension of both sediment dynamics and hydrodynamics.

Cross-shore exchange processes over an inner continental shelf are slow and often episodic (Niedora et al., 1984). The on-offshore cycling of sediments have periods in the order of a year and are not perfectly closed (Wright et al., 1985). The incompleteness of the



cycle results in the long-term change in geometry. The storm-related high energy is believed to be responsible for this long-term change. Thus, the processes should be understood by the comparison of high energy conditions with low energy conditions.

The two different transport systems, that is, surf zone and continental shelf systems encounter transitions over an inner shelf. Inside a surf zone, a wide spectrum of gravity waves exist. In this region, the principal source of momentum flux is the radiation stresses exerted by the waves (Longuet-Higgins and Stewart, 1964, Chappell and Eliot, 1979). In addition, tidal currents, wave groupiness, longshore currents, and rip currents induce lower frequency motions. Seaward of the surf zone, mesoscale motions dominate the hydrodynamics over a continental shelf. An inner shelf provides an effective coastal boundary layer to the mesoscale flows (e.g. Csanady, 1982).

Over an inner continental shelf, wave energies are dissipated by bottom friction and waves interact with quasi-steady currents of variable sources such as tidal currents, wind-driven downwelling and upwelling (Niedora et al., 1984, Wright et al., 1986), lower frequency flows of amplitude modulated waves (Shi and Larsen, 1984), and gravity-driven motion (Seymour, 1986). I pose an a priori assumption that waves accompany currents over an inner continental shelf regardless of the sources of the forcings. The sediment size distribution over the inner shelf of the Middle Atlantic Bight is somewhat simple with well-sorted fine sand ( $D_s \approx 0.1$  mm) to coarse silt sized sediments.

The study of on-offshore sediment transport over inner continental shelves has been limited because of the amount and the quality of the data available. There have been a few attempts to solve this problem (e.g. Niedora et al., 1984; Swift et al., 1985). During September and October, 1989, a multi-institutional nearshore processes experiment (Duck'85) was conducted at the U.S. Army Engineer Waterways Experiment Station Coastal Engineering Research Center's Field Research Facility in Duck, North Carolina (Figure 1). Mason et al. (1987) described the overview of the Duck'85 experiment. Virginia Institute of Marine Science participated by deploying a tripod equipped with a Marsh-McBirney electro-magnetic current meter, a pressure sensor, and a vertical array of optical back-scattering sensor's (OBS's) on the bottom in a water depth of about 8 m (Wright et al., 1986). The data set represents both fair weather and storm conditions. It is believed that the data set not only provides information on sediment transport processes but also enables us to deduce the basic physics involved.

The suspended sediment concentration at a distance from the bed is the consequence of the agitation of bed materials by flow stresses over the bed and the subsequent diffusion of the sediments by turbulence. The magnitude of agitation is best described by the shear stresses exerted on the bed by flows. Thus, the bed shear stress must be the first variable to be determined. The shear stress is used to estimate flow structure. The next important variable is the concentration of suspended sediments. With known velocity and concentration profiles, the third important quantity, the direction and the magnitude of transport, is determined.

A benthic boundary layer comprises the first place where transfers of mass, momentum, and energy between fluid parcels and sediment particles are active. Thus the understanding of the dynamics of a benthic boundary layer is prerequisite to any model of sediment transport. Recent advancement in the study of marine benthic boundary layers, however, still does not give optimistic prognosis in the sediment transport (e.g. Glenn, 1983). This is mainly due to the relatively poor ability to define important parameters in the sediment diffusion process such as reference concentration, diffusion coefficient, and grading effects (e.g. Nielsen, 1979; Shi, 1983). There is no best way to reveal all the above-mentioned parameters. We need to start with an understanding of the physics involved and then estimate the parameters responsible for the agitation of bed materials and the diffusion and advection of suspended sediments.

For the estimation of suspended sediment concentration profiles, diffusivity and reference concentration should be known. The diffusion of sediment particles does not conform with the diffusion of flow momentum (e.g. Dobbins, 1943). Even with the neglected inertia of sediment particle motion, the complications come from the wave advection and the burst of vortex developed during oscillation of flow. Away from the bottom, the role of wave advection increases. Wang and Liang (1975) elaborate on this problem and imposed a constant length scale. Kennedy and Locher (1972) solve for the extreme cases of near bottom and far away from bottom and give qualitative description of the diffusion. When bedforms exist, the developed vortex contains sediments and bursts into the flow

with the flow reversals (Nielsen, 1979). Correlations between bottom shear stresses and concentrations are investigated to relate the sediment diffusion by turbulence to flow momentum diffusion. As the bottom shear stress increases, the near-bottom suspended sediment concentration increases, resulting in the dampening of turbulence (e.g. Yalin, 1977). To embrace this effect, the velocity scale is modified. Simple linear coupling of a velocity scale onto the turbulence velocity scale is assumed. The modifying velocity scale is set to be calculated from the suspended sediment concentration measurements for varying energy conditions.

The calculation of reference concentration starts with the definition of the reference height and the concentration. Because the mechanisms involved in the bedload and suspended load transport are totally different, the reference height should be scaled with the bedload layer thickness. After defining the reference height, we need to determine the reference concentration. One approach is to relate the concentration to the excess shear stress (e.g. Smith and McLean, 1977). The proportionality varies with the physical properties of bottom sediments (e.g. Drake and Cacchione, 1985). The variation of the proportionality between high and low energy conditions is investigated by using different formulations on the reference concentration.

The model gives the transport rate as the vertical integration of the product of the mean cross-shore current and the mean concentration. To investigate the role of waves for the net transport of sediments, an energetics approach is applied to

calculate the immersed weight transport rates by the currents, waves, and gravity-induced transport. Energetics approaches consider the available fluid power to entrain and advect sediments via empirical efficiency factors (Bagnold, 1963). Because energetics models cannot resolve the acceleration of flows, the correlations between cross-shore velocities and concentrations are investigated.

The objective of this study is to provide an on-offshore suspended sediment transport model for a wave-current combined boundary layer and to distinguish storm-related high energy process from fair-weather low energy process. In Chapter 2, hydrodynamic variables are calculated from the analysis of data. The variables are to be the input variables for the boundary layer model developed in Chapter 3. The time variations of suspended sediment concentration profiles are also presented. In Chapter 3, an oscillatory boundary layer model is developed to test model sensitivity to assumed eddy viscosity distributions. The results are extended to building a simple wave-current boundary layer model in case of substantial mean flow with a monochromatic wave. In Chapter 4, a model for mean suspended sediment concentration is built upon the result from the wave-current combined boundary layer model. Focus is on the diffusion and the reference concentration, by utilizing suspended sediment concentration data. In Chapter 5, the contributions of currents and waves to the net transports are studied, based on an energetics model. The applicability and the limit of the energetics approach is tested by comparing with the mean transport rate calculated as the depth integration of the

product of the mean concentration and the mean cross-shore velocity.

Chapter 6 summarizes the study and draws conclusions.

## 2. DATA ACQUISITION AND ANALYSIS

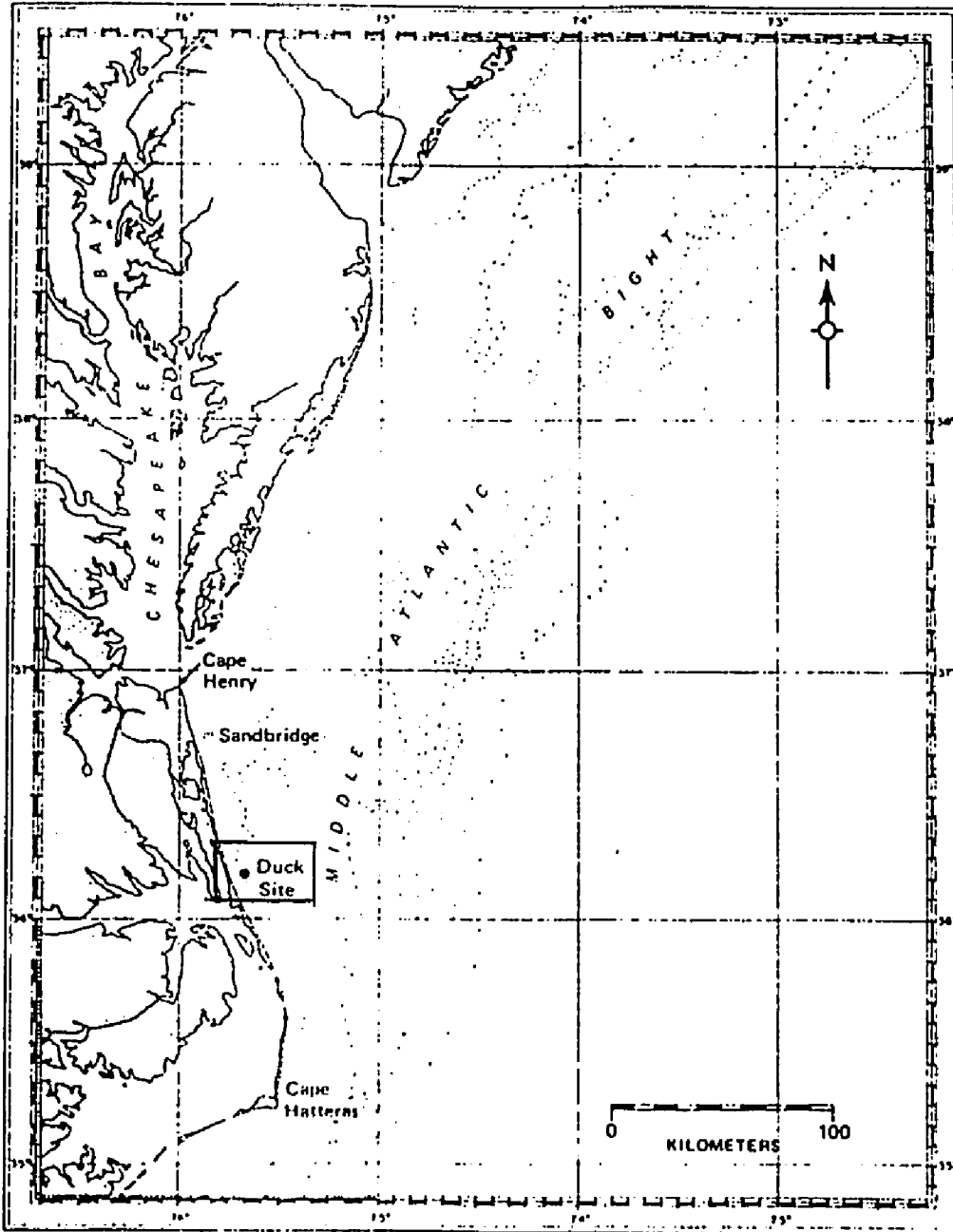
### 2.1 Introduction

During the period between 1 and 19 September, 1985, VIMS collected data for both hydrodynamic and sedimentary variables, participating Duck'85 experiment (Figure 1). A tripod, equipped with a Marsh-McBirney electro-magnetic current meter (EMCM), a pressure gauge, and a vertical array of OBS sensors, was deployed on the shoreward edge of inner shelf (depth  $\approx$  8 m). The first week of the deployment was subject to low energy condition. The remaining period was exposed to high energy conditions, induced by strong northeasterly wind.

Two separate portions of data from the Duck'85 experiment, representing both fair weather and onset of storm, are processed. High frequency sampling of hydrodynamic variables and suspended sediment concentrations enables us to observe the suspended sediment transport activity and the interactions among the hydrodynamic forcings in terms of frequency. The data representing fair weather has been processed and reported by Green et al. (1989). In this chapter, more emphasis is given to the comparison of high energy processes to the low energy processes.

Figure 1 Location map. The study area is the shoreface fronting the Field Research Facility (FRF) of U.S. Army Corps of Engineering at Duck on the Outer Banks of North Carolina in the southern Mid-Atlantic Bight.





## 2.2 Hydrodynamic variables

In order to compare the storm event and the fair weather condition, 11 consecutive bursts were selected for each cases to sample pressure, velocities, and suspended sediment concentrations. Each burst is comprised of 2048 samples with the sampling rate of 1 Hz. The burst interval is 4 hours, so that each portion of selected data set covers approximately a 2-day period.

The pressure sensor was set at the height of 119.5 cm above the bottom. The reading of pressure sensor is in the unit of millibar. The reading is converted into meters by the following formulation:

$$P \text{ (m)} = \frac{P_{\text{read}}(\text{mb}) - P_{\text{atm}}}{\rho g} \quad (2.1)$$

Here, the  $P$  is the converted pressure in m,  $P_{\text{read}}$  is the pressure record in mbar.  $P_{\text{atm}}$  is the atmospheric pressure and set to 1013 mbar.  $\rho$  is the density ( $1026.97 \text{ Kg/m}^3$ ) and  $g$  is the gravitational acceleration ( $9.81 \text{ m/sec}^2$ ). The water depth,  $h$ , is approximated by the use of mean pressure,  $\bar{P}$ .

$$h \approx \bar{P} + 1.195 \quad (2.2)$$

To work with elevation instead of pressure, we use the spectral relationships between pressure and elevation from linear wave theory.

$$S_{\eta}(f) = \left( \frac{\cosh kh}{\cosh kd} \right)^2 S_p(f) \quad (2.3)$$

Here,  $f = 1/T$  is frequency in hertz where  $T$  is period in second.  $S_{\eta}(f)$  is spectral values of elevation,  $k$  is wave number, and  $d$  is the height of the pressure gauge from the bottom (119.5 cm this case). Figure 2 shows the depth attenuation effect gives the bias in the estimation of power spectrum for high frequency. We chose the frequency 0.33 Hz for the upper limit of height spectrum. The spectral relationship enables us to calculate the significant wave height.

$$H_{m0} = 4 \left( \int_0^{0.33} S_{\eta}(f) df \right)^{1/2} \quad (2.4)$$

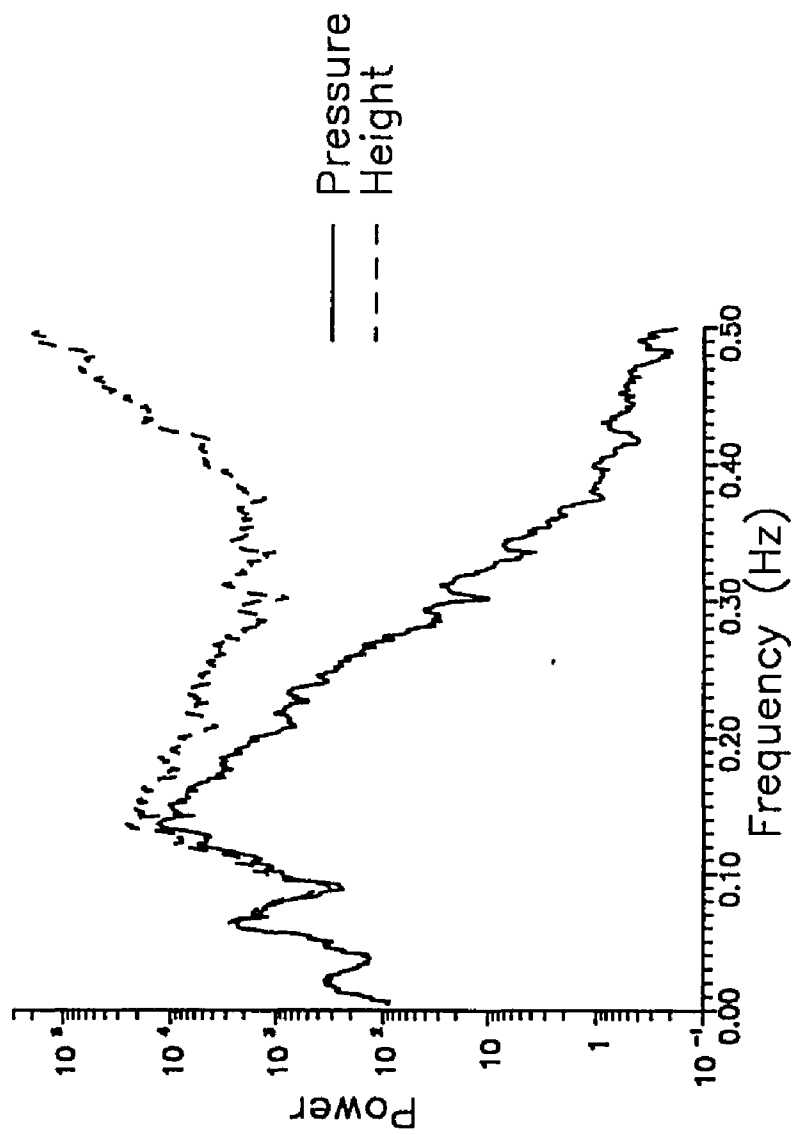
The significant wave height becomes the estimate of the wave height,  $H$ , in this study. The zero-upcrossing period,  $T_{zp}$ , and the irregularity,  $\epsilon_p$ , are calculated from the power spectra of pressure,  $S_p(f)$  (WMO, 1976).

$$T_{zp} = \frac{\left( \int_0^{0.5} S_p(f) df \right)^{1/2}}{\left( \int_0^{0.5} f^2 S_p(f) df \right)^{1/2}} \quad (2.5)$$

$$\epsilon_p^2 = 1 - \frac{\left( \int_0^{0.5} f^2 S_p(f) df \right)^2}{\int_0^{0.5} S_p(f) df \int_0^{0.5} f^4 S_p(f) df} \quad (2.6)$$

An EMCM sensor was calibrated before and after the deployment. For the calibration, steady currents generated in the flume with

Figure 2 Power spectra of pressure and wave height. The solid line represents the power spectrum of pressure signal. The dashed line is the spectrum of transformed wave height.



approximately 2 m wide and 10 m long. The water depth was about 1 m. To make homogeneous flow, honeycomb-shaped filters with thickness of about 10 cm were located at the head of the flow. To suppress the unsteady current, a heavy canvas with 1 m width was located after the filters. A rod with vertical vane was floated with the flow and the traveling distance and time was measured. The sensor was fixed at the same level as the vane. Dividing the distance by time, velocity was calculated. The traveling distance was about 2 m in the mid of the stream. The currents measured were found to behave reasonably with an rms error of about 2 cm/sec.

The EMCM sensor was set at 20 cm above the bottom. The velocities are obtained to align with right-hand coordinate, so that positive  $u$  is offshore (East) and positive  $v$  is North bound. Measured velocities are processed in the unit of cm/sec.

Figure 3 shows the hydrodynamics for the fair weather portion: Surface elevations fluctuate with tidal frequency. Wave height is as low as 40 cm. The mean flow is very low ( $\approx 2$  cm/sec). Referring the rms error of 2 cm/sec, this suggests almost negligible current during fair weather.

Toward the onset of storm, the wave energy is increased by an order of magnitude (Figure 4). The peak frequency is shifted toward high frequency (from 0.1 Hz to 0.13 Hz). Figure 5 shows the hydrodynamics for the storm portion: The surface elevation still shows the tidal fluctuation. Wave height is increased to 150 cm almost by a factor of four. Substantial southeasterly mean

Figure 3 Hydrodynamic variables, fair weather portion.  $\eta$  is the water surface elevation in cm.  $H$  is the wave height in cm calculated by equation (2.4).  $u$  is the cross-shore velocity in cm/sec in which positive is offshore and negative is onshore.  $v$  is the along-shore velocity in cm/sec in which positive is north-bound and negative is south-bound.

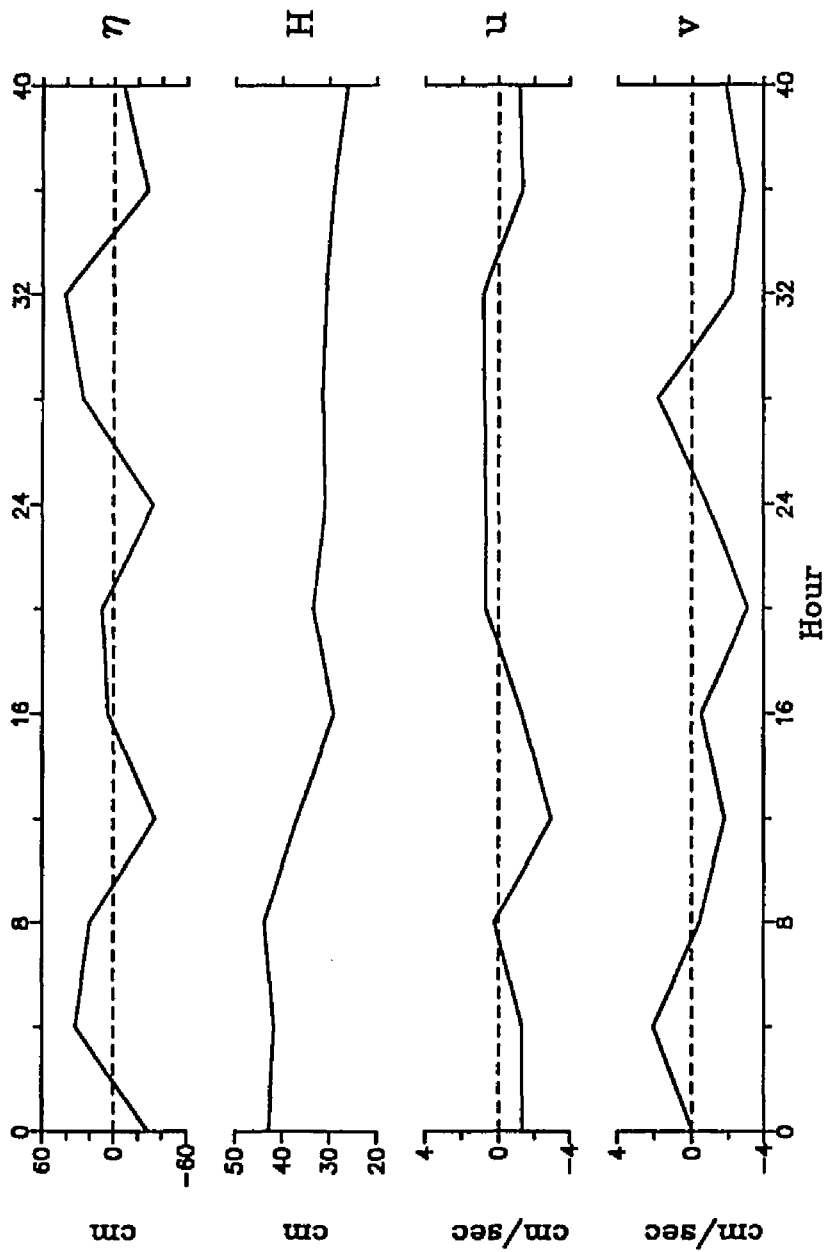




Figure 4 A comparison of power spectra between fair weather and storm. The solid line is the power spectrum of pressure signal of a fair weather sample. The dashed line is the power spectrum of pressure signal of a storm sample.

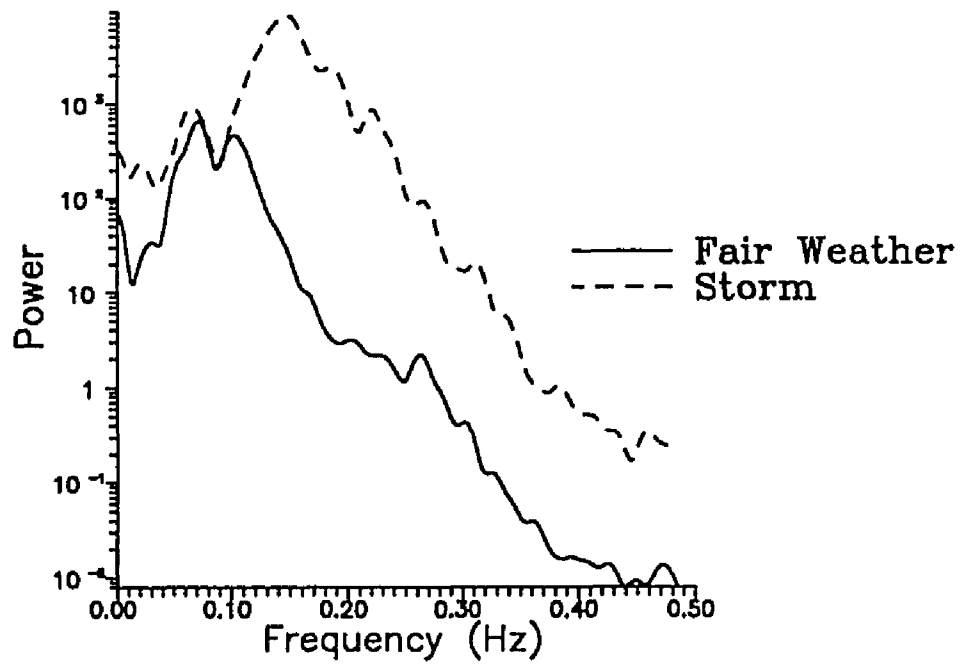
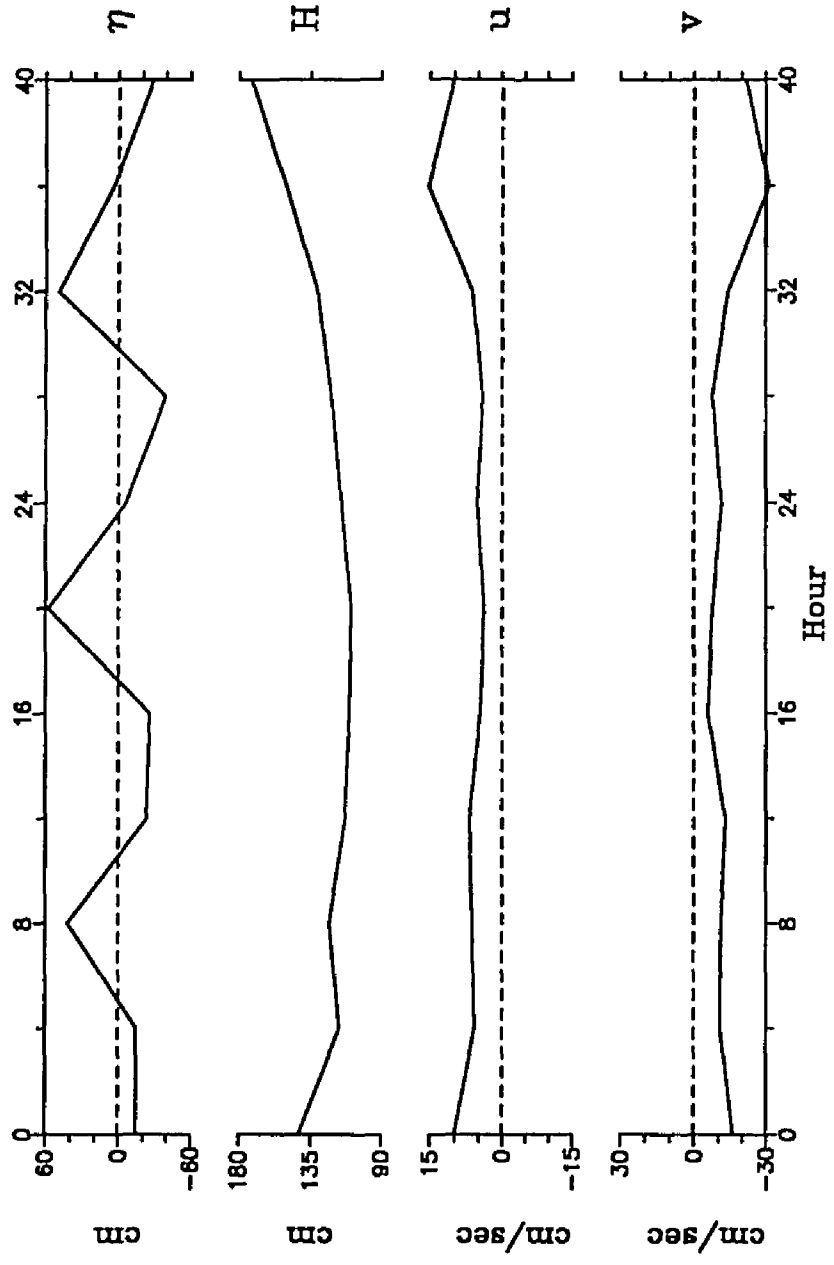


Figure 5 Hydrodynamic variables, storm portion.  $\eta$  is the water surface elevation in cm.  $H$  is the wave height in cm calculated by equation (2.4).  $u$  is the cross-shore velocity in cm/sec in which positive is offshore and negative is onshore.  $v$  is the along-shore velocity in cm/sec in which positive is north-bound and negative is south-bound.



currents, seemingly related to the prevailing northeasterly wind, were observed (for example,  $u = 10$  cm/sec and  $v = -20$  cm/sec).

### 2.3 Aligning data with new coordinate system

In order to utilize the model developed, we have to rotate the axes to conform with the x-axis being in the direction of wave propagation. The direction of wave propagation is set as the direction of maximum variance in velocity.

Suppose we have a velocity vector  $(u_i, v_i)$  in an x-y coordinate. After rotating the axes by  $\theta$  in the counterclockwise direction, the vector becomes  $(u'_i, v'_i)$  in the new x'-y' coordinate system (Figure 6). Define the internal angle and the magnitude of the velocity vector in the old coordinate system.

$$\alpha_i = \tan^{-1}(v_i / u_i) \quad (2.7)$$

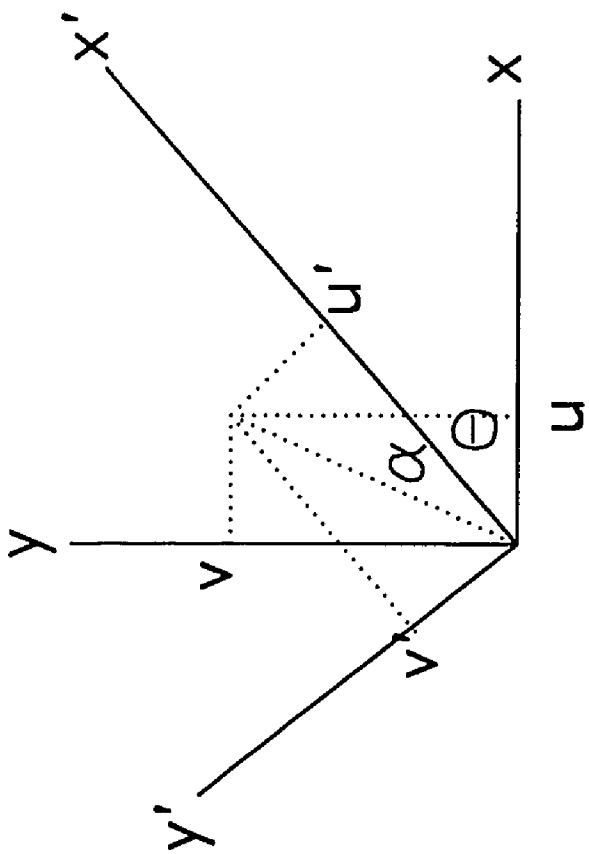
$$|V_i| = (u_i^2 + v_i^2)^{1/2} \quad (2.8)$$

Define the averages  $\bar{u}$  and  $\bar{v}$ , the variances  $s_u^2$  and  $s_v^2$ , and covariance  $s_{uv}$ . In the new coordinate system, the magnitude of a velocity vector  $|V_i|$  remains same but the internal angle becomes  $\alpha_i - \theta$ .

Suppose we have N - velocity vectors  $(i=1,2,\dots,N)$ . Then, we have new statistical parameters in the new coordinate system: New averages are

$$\bar{u}' = \cos \theta \cdot \bar{u} + \sin \theta \cdot \bar{v} \quad (2.9)$$

Figure 6 Transformation of coordinates.  $(x', y')$  is the transformed coordinate from  $(x, y)$ . Corresponding vector expression for the velocity is  $(u, v)$  and  $(u', v')$ , respectively. The transformation is by the angle of  $\theta$  in counter-clockwise direction. The angle  $\alpha$  is the internal angle of vector  $(u, v)$ . Thus, the new internal angle of vector  $(u', v')$  is  $\alpha - \theta$ .





$$\bar{v}' = \cos \theta \cdot \bar{v} - \sin \theta \cdot \bar{u} \quad (2.10)$$

New variance of  $u_i'$  becomes

$$s_u^2 = \cos^2 \theta \cdot s_u^2 + \sin^2 \theta \cdot s_v^2 + \sin 2\theta \cdot s_{uv} \quad (2.11)$$

In order for this new variance to be the maximum, the angle of rotation should be

$$\theta = n\pi + \pi/4 - \theta'/2 \quad (2.12)$$

where

$$\theta' = \tan^{-1} \left( \frac{1}{2} (s_u^2 + s_v^2) / s_{uv} \right) \quad (2.13)$$

Now, we have transformed the velocity vector which is aligned with the direction of wave propagation. The angle is again given in degree. All the hydrodynamic variables estimated are tabulated in Table 1 for the fair weather portion and in Table 2 for the storm portion; water depth (h), wave height (H), cross-shore velocity ( $u_c$ ), along-shore velocity ( $v_c$ ), peak period (T), and the angle of wave propagation counter-clockwise from east ( $\theta$ ).

Table 1. Input data for fair weather portion

Hour	h (cm)	$u_c$ (cm/sec)	$v_c$ (cm/sec)	H (cm)	$\theta$ (degree)	T (sec)
0	872.65	-1.28	-0.04	41.94	196	10.08
4	933.82	-1.29	2.04	40.30	196	10.21
8	921.64	0.23	-0.44	42.94	198	10.75
12	867.17	-3.00	-1.76	36.69	195	10.54
16	905.74	-1.30	-0.52	28.30	198	9.91
20	910.69	0.71	-3.10	30.36	192	10.63
24	868.32	0.68	-0.83	29.72	194	10.67
28	926.55	0.76	1.78	31.51	194	10.91
32	943.02	0.82	-2.20	28.16	194	10.72
36	873.52	-1.32	-2.83	26.50	191	10.81
40	893.78	-1.16	-1.86	23.99	190	11.09

\*  $D_s = 0.1$  mm

\* Current velocity,  $(u_c, v_c)$ , is given at the height,  $z = 20$  cm, away from the bottom.

Table 2. Input data for storm weather portion

Hour	h (cm)	$u_c$ (cm/sec)	$v_c$ (cm/sec)	H (cm)	$\theta$ (degree)	T (sec)
0	925.99	9.93	-16.23	102.28	225	6.59
4	926.20	5.85	-10.99	80.28	219	6.94
8	982.86	6.38	-11.15	77.13	219	6.50
12	917.44	6.90	-13.00	76.07	210	7.09
16	914.90	4.61	-5.80	73.63	210	6.97
20	998.81	3.73	-7.82	85.98	201	8.28
24	935.06	5.27	-11.44	87.70	203	8.06
28	901.25	4.02	-7.55	86.24	205	7.00
32	989.83	6.39	-14.01	84.26	209	6.81
36	945.12	15.44	-31.38	99.41	223	6.59
40	912.45	10.19	-21.69	125.11	217	6.69

\*  $D_s = 0.01$  mm

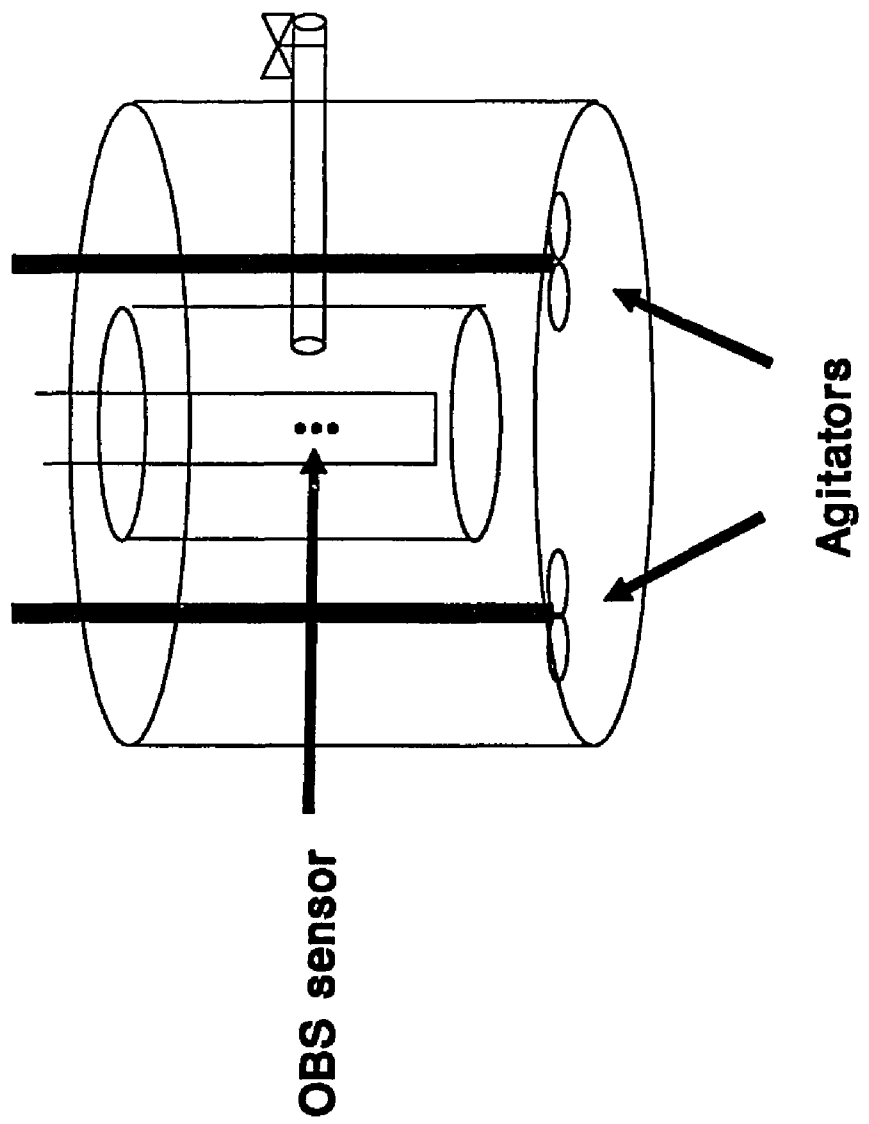
\* Current velocity,  $(u_c, v_c)$ , is given at the height,  $z = 20$  cm, away from the bottom.

#### 2.4 Calibration of optical back-scattering (OBS) sensors

Bottom sediments from the field site (Duck, North Carolina) were used to calibrate the OBS sensors. Figure 7 is the sketch of the set-up: The sediments were put into a cylinder of about 50 cm diameter and 30 cm deep. In the center of the cylinder, another small cylinder of about 10 cm diameter was set about 3 cm from the bottom of the big cylinder. To make the distribution of suspended sediments homogeneous, many small holes (diameter = 1 cm) were made in the small cylinder. Each sensor was put into the small cylinder about 8 cm from the bottom. At the same height as the sensor, a pipe with 1 cm diameter was inserted to collect suspended sediments. Two electric drills with propellers were used to agitate bottom sediments. The output voltages from a sensor were measured. When the output voltage is stabilized, the water samples through the pipe were collected into a bottle.

After the measurement of the output voltages and the sampling of suspended sediments, the amount of bottom sediments was reduced by almost a half. The calibration for each sensor was done over seven different suspended sediment concentrations. The water samples with suspended sediments were filtered on pre-weighed glassfiber filters with 1  $\mu\text{m}$  of pore sizes. The sediments collected on the filters were dried in the oven with 350 °F of temperature and weighed. The difference of the sample weight from the filter weight was divided by the volume of the water sample to give the suspended sediment concentration. The concentrations vary between 500 and 10,000 mg/l. The corresponding output voltages vary between 0.2 and 2.1 Volts.

Figure 7 Set-up of the calibration of an OBS sensor. Many small holes of 1 cm diameter are made on the small cylinder inside the tank to make the distribution of suspended sediments homogeneous in the tank.



Before and after the calibration, all the sensors were put into water without sediments and the output voltages were measured to assure that no drift had taken place.

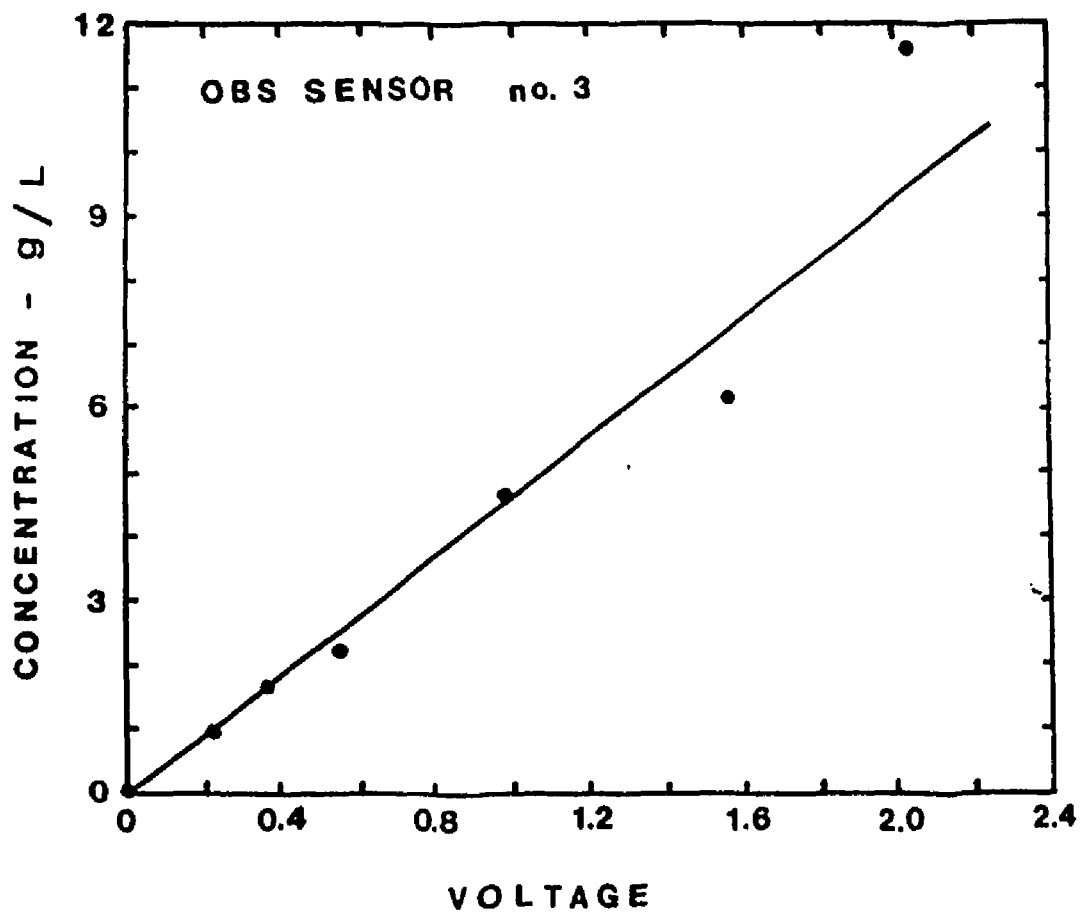
Regression analysis was applied: The line fitting through the origin was adopted because the zero Volt with zero concentration was applied. For the  $V_e$  Volts of output signal, the corresponding concentration  $C_{cal}$  is

$$C_{cal} = \hat{\beta} V_e + \text{Err} \quad (2.14)$$

Here,  $\hat{\beta}$  is the slope of the regression line and Err is the random error. For the estimation of  $\hat{\beta}$ , there are three unbiased estimates, that is,  $\Sigma V_e C_{cal} / \Sigma V_e^2$ ,  $\Sigma C_{cal} / \Sigma V_e$ , and  $\Sigma(C_{cal} / V_e) / n$  where  $n$  is the number of points used for the line fitting. The precision of the estimation depends on the variance of the random error, Err. The most precise estimate is the first, second, or third above depending on the variance of Err is constant, proportional to  $V_e$ , or proportional to  $V_e^2$  (Snedecor and Cochran, 1967). Figure 8 is a sample from the calibration and shows that the third estimation is suitable. The estimate gives an error of  $\pm 10 \%$ .

Figure 8 A sample calibration of an OBS sensor. The points represent measurements. The solid line is the regression line.





## 2.5 Suspended sediment concentrations

We use the readings of the optical back-scattering sensors set at 15, 35, 65, and 105 cm above bottom, respectively. The suspended sediment concentrations are processed in the unit of  $\text{Kg/m}^3$ . Figure 9 shows the burst averaged concentration profile for fair weather portion. Figure 10 shows the power spectra variations for the same portion. Comparing Figure 9 (suspended sediment concentration profiles) with Figure 10 (power spectra), we can see that the concentration distribution is closely related with the wave energy change. For lowered energy, the reversals in the concentration profile were observed. This may be related with the increased role of advection from other sources instead of the diffusion of bottom sediments under fair weather condition. This would decrease the importance of the fair weather data set. The storm data set, however, always shows the conventional log-log linear relationships between the concentration and the height from the bottom (Figure 11). This well-behavior of the storm data, obtained after the fair weather data set, excludes the possibility of the malfunction of the particular sensor at the height 65 cm from the bottom. Figure 11 (suspended sediment concentration profile) and Figure 12 (power spectra) also show the close relations for the storm portion. The concentration at the bottom sensor for storm portion ( $\approx 2 \text{ Kg/m}^3$ ) are an order higher than the concentration for fair weather portion ( $\approx 0.4 \text{ Kg/m}^3$ ).

Figure 9 Suspended sediment concentration profiles, fair weather portion.

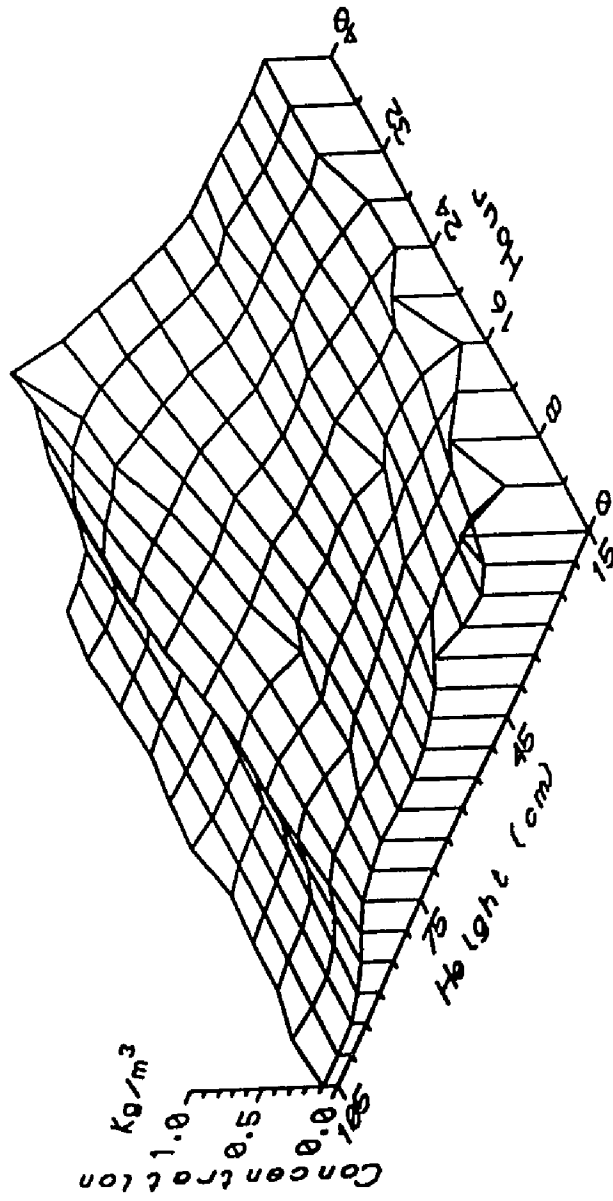


Figure 10 Power spectra of pressure, fair weather portion.

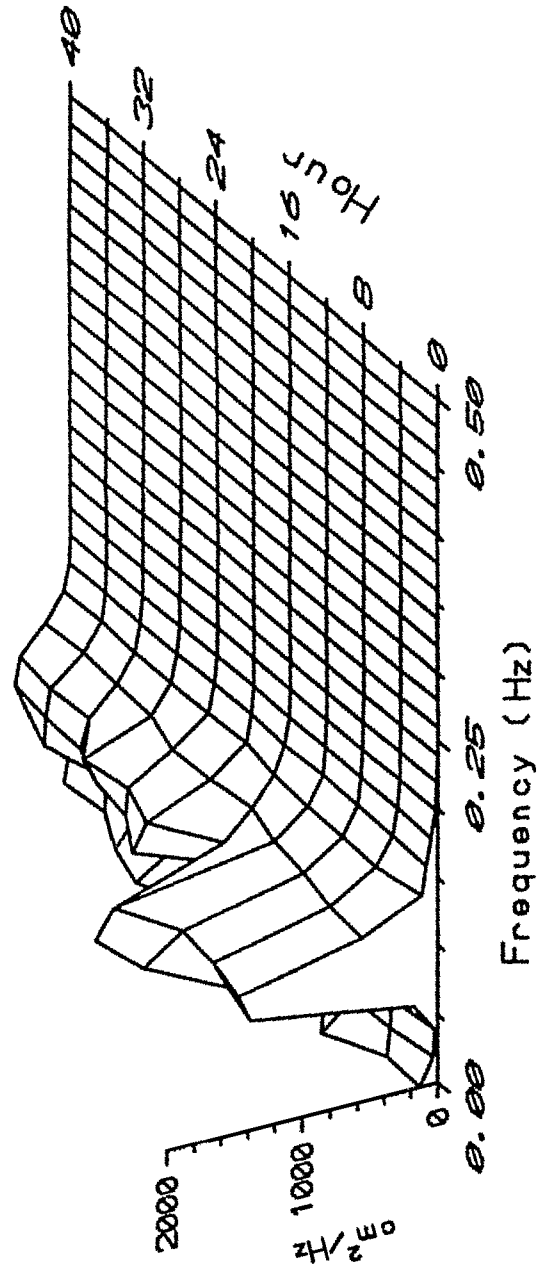


Figure 11 Suspended sediment concentration profiles, storm portion.

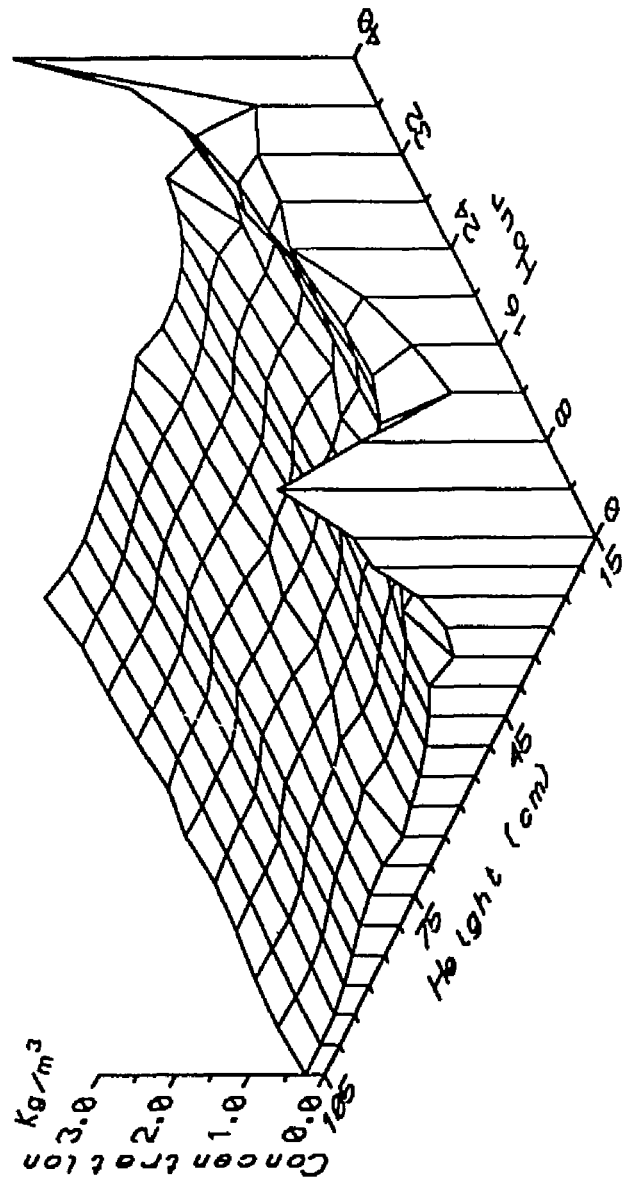
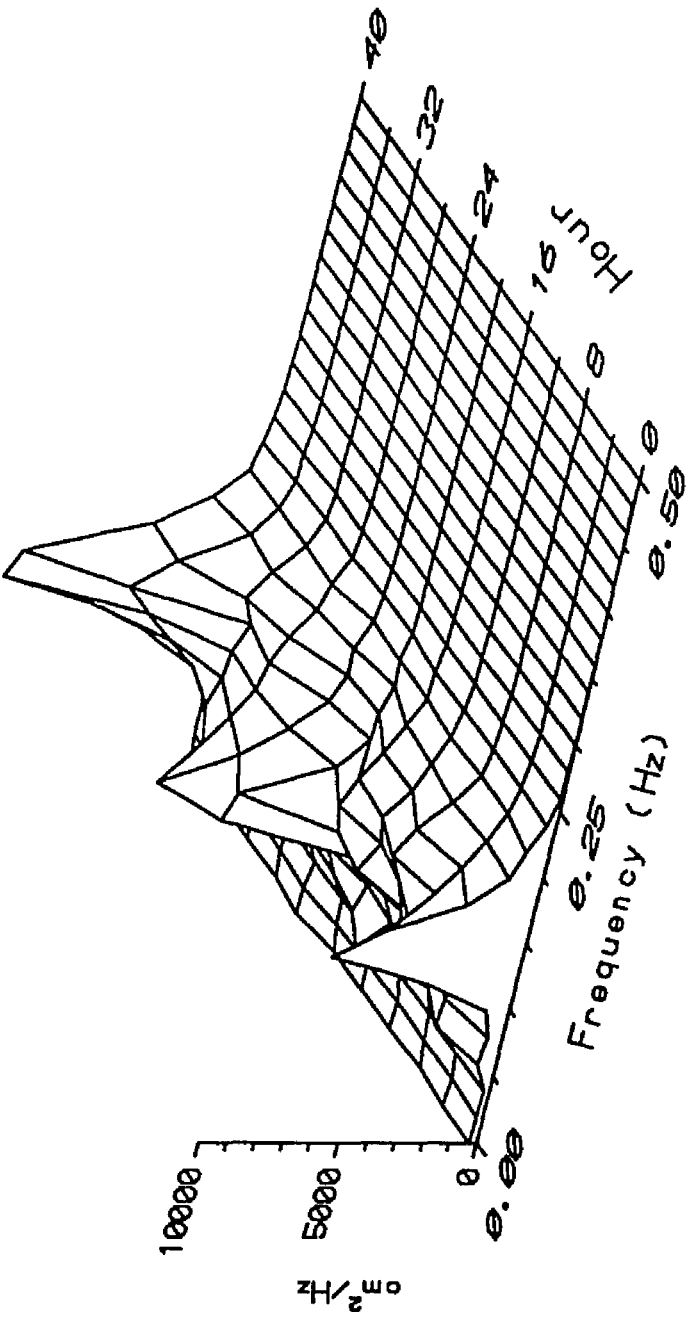




Figure 12 Power spectra of pressure, storm portion.



### 3. BOUNDARY LAYER MODEL

#### 3.1 Introduction

The existence of a solid bed, commonly comprised of sediment particles, imposes constraints on the flow behavior through the no-slip boundary conditions at the sediment water interface. Turbulent flows are associated with multiple length scales such as a viscosity-dominated characteristic length, a characteristic length of the roughness element, and the thickness of boundary layer (e.g. Tennekes and Lumley, 1972): Near the boundary, viscosity dissipates momentum, so that the viscosity length scale governs the flow near the solid boundary. Far away from the bottom, velocity of the flow approaches the free stream velocity, so that the boundary layer thickness itself becomes the most significant length scale. Between these two distinctive regions, there exists a transitional layer in which a logarithmic velocity profile is observed. In this inertial sublayer, the dominant length scale is the distance from the bed. The structure and the behavior of a steady turbulent boundary layer is depicted by Clauser (1956) and this becomes the basis for the further investigation of unsteady boundary layer flows.

An analogy to the steady boundary layer can be drawn for a wave boundary layer. The efforts to recognize the velocity distribution and to estimate the bottom stresses are related to variable modeling schemes on eddy viscosity. Jonsson (1963) assumed a constant stress logarithmic flow in analogy to a steady flow. He proposed a semi-empirical model in which maximum bed shear stress is related to

the square of the maximum velocity outside the boundary layer through a wave friction factor. The friction factor is set to be the function of relative roughness length only. Kajiura (1968) appears to be the first who adopted the steady boundary layer structure of Clauser (1956) to develop a theory for turbulent oscillatory boundary layer flows. Other laboratory investigations have also confirmed the wave boundary layer structure at least qualitatively (e.g. Jonsson, 1966 and 1980, Kalkanis, 1964, Horikawa and Watanabe, 1968, Sleath, 1970, Kamphuis, 1975, Jonsson and Carlsen, 1976, Bakker and van Doorn, 1978). Collins (1963) provided an insight of wave boundary layer structure in field. Here, we have to note that all the studies mentioned above are for the case of large excursion amplitude compared to the bed roughness scale. The reproduction of a near-logarithmic velocity profile in the lower portion of the wave boundary layer has been successful utilizing a time-invariant eddy viscosity model (e.g. Kajiura, 1968, Grant, 1977, Smith, 1977, Jonsson, 1980, Brevik, 1981, Long, 1981, and Myrhaug, 1982).

For the case of a combined wave-current boundary layer, the modeling effort becomes complicated by the complexity of the structure and the lack of the availability of quality data for calibration. In this context, it may be safe to adopt a linear coupling of boundary layers induced by variable flows in terms of time scale (e.g. Grant and Madsen, 1979). For the first-order approximation, we assume two different time-scaled flows, that is, a steady current and an unsteady oscillatory flow cause two different boundary layers. To provide insight into the coupling, we must

first try to model the thinner wave boundary layer. For this, four different sets of eddy viscosity formulations are tested. We are mainly concerned with the boundary layer thickness and the magnitude of bottom shear stress. The result of the numerical experiment provides a basis for the further application of the time-invariant eddy viscosity model for the combined wave-current boundary layer flow. Whereas the obtained bottom shear stress determines the sediment entrainment, the eddy viscosity controls the diffusion of both momentum and suspended sediments.

## 3.2 Wave boundary layer model

### 3.2.1 Governing equations

Assume that horizontal pressure gradient and bed friction are the only relevant driving forces for a wave boundary layer. Assume homogeneity in the y-direction. Then, the momentum equation becomes

$$\frac{\partial u_w}{\partial t} = -\frac{1}{\rho} \frac{\partial p_w}{\partial x} + \frac{\partial}{\partial z} \left( \frac{\tau}{\rho} \right) \quad (3.1)$$

Here  $u_w$  is periodic velocity in the x-direction,  $p_w$  is periodic pressure, and  $\tau$  is shear stress.  $\rho$  is the density of water. We set  $z = z_0$  at bottom boundary. Consider that the shear becomes negligible far away from the bottom. Then, the free stream condition is

$$\frac{\partial u_\infty}{\partial t} = -\frac{1}{\rho} \frac{\partial p_w}{\partial x} \quad (3.2)$$

where  $u_\infty$  is the free stream velocity. Substituting equation (3.2) in equation (3.1), we get

$$\frac{\partial}{\partial t} (u_w - u_\infty) = \frac{\partial}{\partial z} \left( \frac{\tau}{\rho} \right) \quad (3.3)$$

The solution depends on the shear  $\tau/\rho$ . Decompose the velocity such that the amplitude is a function of  $z$  only:

$$u_w(z, t) = \{X(z) + i \cdot Y(z)\} e^{i\omega t} \quad (3.4)$$

Here,  $\omega = \frac{2 \cdot \pi}{T}$  is radian frequency where T is a wave period and  $i = \sqrt{-1}$ . Only real part is considered as the solution here.

We impose two boundary conditions: At the bottom, we impose the no-slip boundary condition.

$$\text{Re}\{u_w(z_0, t)\} = X(z_0) \cdot \cos \omega t - Y(z_0) \cdot \sin \omega t = 0 \quad (3.5)$$

Thus, we have

$$X(z_0) = Y(z_0) = 0 \quad (3.6)$$

Far away from the bottom, the velocity is given by linear wave theory which incorporate the negligible shear.

$$u_w(\infty, t) = \{X(\infty) + i \cdot Y(\infty)\} e^{i\omega t} = u_\infty \cdot e^{i\omega t} \quad (3.7)$$

Thus, we have

$$X(\infty) = u_\infty \quad (3.8)$$

$$Y(\infty) = 0 \quad (3.9)$$

### 3.2.2 Modeling of eddy viscosity

Now, the nature of shear stress is investigated. Adopting an eddy viscosity model (e.g. Rodi, 1980), we assume the shear stress is proportional to the velocity gradient:

$$\frac{\tau}{\rho} = \nu_t \frac{\partial u_w}{\partial z} \quad (3.10)$$

The eddy viscosity  $\nu_t$  should be modeled in order to have the solution for the governing equation. Conventionally,  $\nu_t$  is regarded to consist of the combination of a velocity scale and a length scale. The velocity scale is a function of the bottom friction as well as the location and the wave frequency. The size of eddy is comparable to the distance from the bottom and chosen to be a length scale. In order to approximate the eddy viscosity, it is usually assumed that

$$\nu_t = \kappa u_{*w,m} z \hat{f}(z, u_{*w,m}, \omega) \quad (3.11)$$

where maximum wave friction velocity  $u_{*w,m} = (\tau_{bw,m})^{1/2}$  and  $\tau_{bw,m}$  is the maximum bottom shear stress exerted by a wave. The von Karman constant  $\kappa$  is approximated by 0.4. The length scale is  $\kappa z$  and the velocity scale is  $u_{*w,m} \hat{f}$ . The modification factor  $\hat{f}$  is a function of  $z$ ,  $u_{*w,m}$ , and  $\omega$ . We picked four different  $\hat{f}$  values to apply for the time-invariant eddy viscosity model.



Assume the velocity scale is independent of the distance from the bottom. Then, we can set

$$\hat{f} = 1 \quad (3.12)$$

For this case, Smith (1977) gives the exact solution in terms of Kelvin functions. From the solution, he depicted that the shear is appreciable only within a certain limit from the bottom. This limit is given as the top of boundary layer.

$$\delta_w = \frac{u_{*w,m}}{\omega} \quad (3.13)$$

The disappearance of shear above  $\delta_w$  leads to the inconsistency of the assumption of a constant velocity scale. The disappearance of mean shear indicates that the turbulent kinetic energy is balanced by turbulent diffusion. Because the diffusion is confined only to a region near the bottom boundary, the turbulent kinetic energy should be small away from the bottom. The constant velocity scale conflicts with this physical argument.

In order to incorporate the physics of turbulence, we can assume the velocity scale is modified by an exponentially decaying function. Assume that velocity scale becomes very small at large distance compared to  $\delta_w$  and approaches unity at small distance compared to  $\delta_w$  ( $\approx \kappa \delta_w$ ).

$$\hat{f} = \exp\left(-\frac{z}{\kappa \delta_w}\right) \quad (3.14)$$

Following Businger and Arya (1974), Long (1981) showed that for small  $z$  the shear stress is given by

$$\frac{\tau_{w,m}}{\rho} = u_{*w,m}^2 (1 - z/\hat{h}) \quad (3.15)$$

$$\text{where } \hat{h} = u_{*w,m}^2 / (\omega \cdot u_{\infty}) \quad (3.16)$$

Assuming a logarithmic velocity profile, they found

$$\nu_t = \kappa z u_{*w,m} (1 - z/\hat{h}) \quad (3.17)$$

To apply this result to the whole boundary layer, we have

$$\hat{f} = \exp(-z/\hat{h}) \quad (3.18)$$

For small  $z$ , turbulent kinetic energy production balances the viscous dissipation.

$$\tau \frac{\partial u}{\partial z} = \rho \cdot \epsilon \quad (3.19)$$

where  $\epsilon$  is viscous dissipation. From dimensional analysis, one can find

$$\epsilon = (\tau/\rho)^{3/2} / (\kappa z) \quad (3.20)$$

Combining equations (3.19) and (3.20), we have

$$\frac{\partial u}{\partial z} = \frac{(\tau/\rho)^{1/2}}{\kappa z} \quad (3.21)$$

Since  $\frac{\tau}{\rho} = \nu_t \frac{\partial u}{\partial z}$ , we have

$$\frac{\tau/\rho}{\nu_t} = \frac{(\tau/\rho)^{1/2}}{\kappa z} \quad (3.22)$$

Rearrange, then

$$\nu_t = \kappa z u_{*w,m} (1 - z/h)^{1/2} \quad (3.23)$$

To apply this to the whole boundary layer, we have

$$\hat{f} = \exp(-z/2h) \quad (3.24)$$

### 3.2.3. Solution and test

Returning to the governing equation, the simple eddy viscosity model gives

$$\frac{\partial}{\partial t} (u_w - u_\infty) = \frac{\partial}{\partial z} (\kappa u_{*w,m} z \hat{f} \frac{\partial u}{\partial z}) \quad (3.25)$$

using equation (3.5), we have

$$-Y + i \cdot (X - u_\infty) = \frac{\kappa u_{*w,m}}{\omega} \frac{d}{dz} \left\{ z \hat{f} \left( \frac{dX}{dz} + i \cdot \frac{dY}{dz} \right) \right\} \quad (3.26)$$

Introduce dimensionless variables.

$$X^* = \frac{X - u_\infty}{u_\infty} \quad (3.27)$$

$$Y^* = \frac{Y}{u_\infty} \quad (3.28)$$

$$Z^* = \frac{z}{\kappa u_{*w, m} / \omega} \quad (3.29)$$

The equation (3.26) becomes

$$-Y^* + i \cdot X^* = \frac{d}{dZ^*} (Z^{*\hat{f}} \left( \frac{dX^*}{dZ^*} + i \cdot \frac{dY^*}{dZ^*} \right)) \quad (3.30)$$

Comparing the arguments for complex variables, we have

$$-Y^* = \frac{d}{dZ^*} (Z^{*\hat{f}} \cdot \frac{dX^*}{dZ^*}) \quad (3.31)$$

$$X^* = \frac{d}{dZ^*} (Z^{*\hat{f}} \cdot \frac{dY^*}{dZ^*}) \quad (3.32)$$

The boundary conditions become

$$X^*(Z_0^*) = -1 \quad (3.33)$$

$$Y^*(Z_0^*) = 0 \quad (3.34)$$

$$X^*(\infty) = 0 \quad (3.35)$$

$$Y^*(\infty) = 0 \quad (3.36)$$

Let

$$X1 = X^* \quad (3.37)$$

$$X2 = Y^* \quad (3.38)$$

$$X3 = \frac{dX^*}{dZ^*} \quad (3.39)$$

$$X4 = \frac{dY^*}{dZ^*} \quad (3.40)$$

Then the equations (3.31) and (3.32) become a set of four simultaneous first order ordinary differential equations.

$$X1' = X3 \quad (3.41)$$

$$X2' = X4 \quad (3.42)$$

$$X3' = -\frac{1}{Z^* f} \cdot X2 - \left( \frac{1}{Z^*} + \frac{\hat{f}'}{f} \right) \cdot X3 \quad (3.43)$$

$$X4' = \frac{1}{Z^* f} \cdot X1 - \left( \frac{1}{Z^*} + \frac{\hat{f}'}{f} \right) \cdot X4 \quad (3.44)$$

The boundary conditions become

$$X1(Z_0^*) = -1 \quad (3.45)$$

$$X2(Z_0^*) = 0 \quad (3.46)$$

$$X1(\infty) = 0 \quad (3.47)$$

$$X2(\infty) = 0 \quad (3.48)$$

Now, we have a two point boundary value problem. In this problem, the boundary conditions at the starting point do not determine a unique solution to start with, while in initial value problem we are able to start an acceptable solution at its initial values and just march it along by numerical integration to final values. There are two distinct classes of numerical methods for solving two point boundary value problems; shooting method and relaxation method (Press et al., 1986). We adopt a variation of the shooting methods, multiple shooting, because finite difference methods for relaxation seem to be more complicated and expensive. The maximum friction velocity can be calculated by iteration procedures.

$$u_{*w,m} = \kappa u_{\infty} Z_0^* \hat{f} \cdot \{X3(Z_0^*)^2 + X4(Z_0^*)^2\}^{1/2} \quad (3.49)$$

The velocity distribution is given by

$$\frac{u(Z^*)}{u_\infty} = (X1(Z^*) + 1) \cos \omega t - X2(Z^*) \sin \omega t \quad (3.50)$$

The shear stress is calculated by

$$\frac{\tau(Z^*)/\rho}{\kappa u_\infty u_{*w,m}} = Z^* \hat{f}(Z^*) (X3(Z^*) \cos \omega t - X4(Z^*) \sin \omega t) \quad (3.51)$$

For the test, we use the same data set used by Smith (1977): Free stream velocity,  $u_\infty = 1$  m/sec and period of  $T = 10$  sec. The bottom roughness  $z_0 = 10^{-5}$  m. Table 3 summarizes the calculated maximum friction velocities  $u_{*w,m}$  for the different eddy viscosity formulations. We see that the variations in eddy viscosity outside the wave boundary layer does not affect much the bottom shear stress which is directly responsible to the calculation of sediment concentrations. Thus, we may use the simplest assumption of  $\hat{f} = 1$ , that is time and space invariant velocity scale in the application to sediment transport under the influence of waves.

Figure 13 shows that the velocity shear for  $\hat{f} = 1$  is appreciable only within a short distance from bottom. This height is defined as the top of the wave boundary layer and approximated by  $\delta_w$ . From this result, we are confident that the oscillating flow does not affect much the distribution of turbulent kinetic energy above the wave boundary layer. Thus, we can impose a simple model that the thin wave boundary layer ( $\delta_w \approx 0(\text{cm})$ ) is nested inside the current boundary layer ( $\delta_c \approx 0(\text{m})$ ).

Table 3. Modification factors and the maximum friction velocity

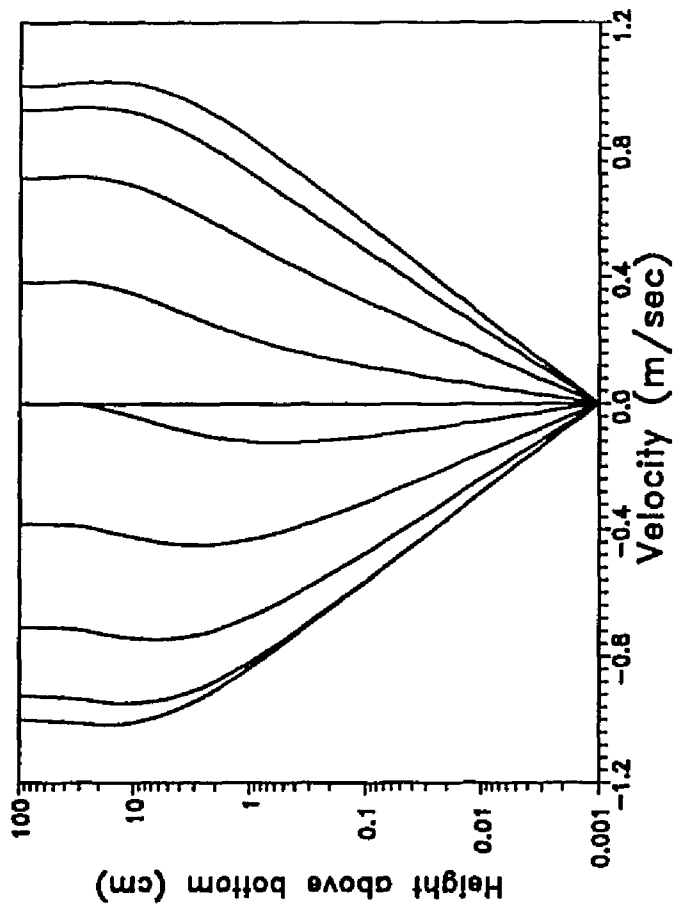
$\hat{f}$	$u_{*w,m}$ (cm/sec)
1	5.01
$\exp(-\frac{z}{\kappa \delta_w})$	4.96
$\exp(-\frac{z}{\kappa h})$	4.41
$\exp(-\frac{z}{2h})$	4.74

$$* \quad \hat{h} = \frac{u_{*w,m}^2}{\omega u_\infty}$$

$$* \quad \delta_w = \frac{u_{*w,m}}{\omega}$$



Figure 13 Wave boundary layer model run for  $\hat{f} = 1$ . Input variables are  $u_{\infty} = 1$  m/sec,  $T = 10$  sec, and  $z_0 = 10^{-5}$  m (Smith, 1977).



### 3.3. Wave current boundary layer model

#### 3.3.1 Governing equations

Models of the combined boundary layer have been built upon our knowledge of the two different individual flow components, that is, currents and waves. By analogy to the steady boundary layer, we relate the velocity scale to the total shear stress which results from the coupling of shear stresses exerted by mean flow and wave orbital motion.

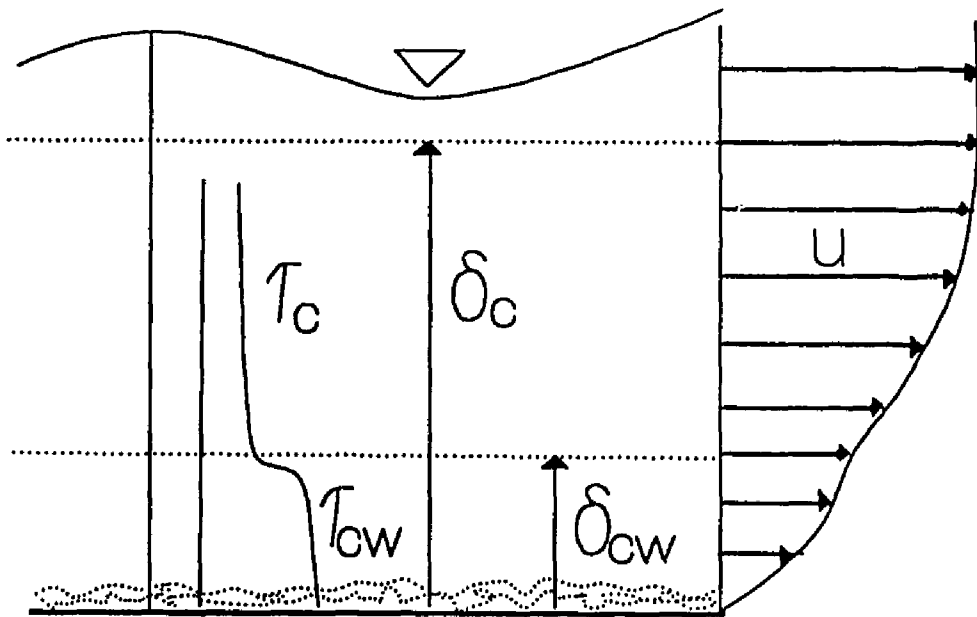
$$\vec{\tau}_{cw} = \vec{\tau}_c + \vec{\tau}_{w,m} \quad (3.52)$$

Here,  $\vec{\tau}_c$  is the shear stress of the current and  $\vec{\tau}_{w,m}$  is the maximum shear stress exerted by the wave.

The numerical experiments of the previous section also depict that the shear related to oscillatory motion is relevant only within a wave boundary layer thickness. Because the thickness is very small compared to the current boundary layer thickness ( $\delta_w \ll \delta_c$ ), we can say the total shear stress has the contribution only from the current away from the bottom ( $\vec{\tau}_{cw} \approx \vec{\tau}_c$  as  $z > \delta_w$ ). This enables us to build a two-layer time-invariant eddy viscosity model of boundary layer (Grant and Madsen, 1979) (Figure 14). We adopt the model utilizing two different velocity scales.

$$\nu_t = \kappa \cdot u_* \cdot z \quad (3.53)$$

Figure 14 Definition sketch for combined boundary layer (Grant and Madsen, 1979). Here,  $\tau_{cw}$  is the shear stress induced by the combined effect of wave and current,  $\tau_c$  is the shear stress induced solely by current.  $\delta_c$  and  $\delta_{cw}$  represent the thickness of current boundary layer and the combined boundary layer, respectively.



where

$$u_* = \begin{cases} u_{*1} & \text{for } z \leq \delta_w \\ u_{*2} & \text{for } \delta_w \leq z \leq \delta_c \end{cases} \quad (3.54)$$

Here, the thickness of the wave boundary layer is given by equation (3.13). Both  $u_{*1}$  and  $u_{*2}$  are related to the bottom stress exerted by the flow field. The velocity scale  $u_{*1}$  is directly related to the maximum bottom shear stress - thus is under the influence of the combined flow. The velocity scale  $u_{*2}$  represents the diffusion of turbulence produced at the bottom by the mean current shear. When we apply the law of the wall to the data obtained outside the wave boundary layer, which is one of the most common practices, we have to keep in mind that the friction velocity calculated by the least square is not the real bottom friction velocity but the velocity scale  $u_{*2}$ . By the same reason, we also obtain from the outer flow a determination of apparent roughness  $z_1$  which differs from the actual bottom roughness length scale  $z_0$ .

The advantage of this model is that analytical expression for both the mean and the oscillating velocity profiles and thus the shear profile can be obtained. There exist weak assumptions such as the discontinuous and time-invariant eddy viscosity distribution, the definition of the wave boundary layer thickness, and the existence of constant shear stress layer. There have been several modified versions of the two-layer models (e.g. Lavelle and Mofjeld, 1983). However, as Wiberg and Smith (1983) pointed out, the ambiguity in the preference of a model, this simple two-layer model

is quite attractive especially when the main purpose is to study sediment transport.

We align the x-axis with the direction of wave propagation and decompose variables by different time scales:

$$u = u_c + u_w + u' \quad (3.55)$$

$$v = v_c + v' \quad (3.56)$$

$$w = w_w + w' \quad (3.57)$$

$$p = p_c + p_w + p' \quad (3.58)$$

Here, the subscripts c and w denote current and wave, respectively. The prime represents turbulent fluctuations.

Adopt Boussinesq approximation, neglect second-order terms, and average over turbulent time scales. Neglecting Coriolis force and horizontal advection, the momentum equation becomes

$$\frac{\partial u_w}{\partial t} = - \frac{1}{\rho} \frac{\partial}{\partial x} (p_c + p_w) + \frac{\partial}{\partial z} (- \overline{u' w'}) \quad (3.59)$$

$$0 = - \frac{1}{\rho} \frac{\partial}{\partial y} (p_c + p_w) + \frac{\partial}{\partial z} (- \overline{v' w'}) \quad (3.60)$$

$$\frac{\partial w_w}{\partial t} = - \frac{1}{\rho} \frac{\partial}{\partial z} (p_c + p_w) - g \quad (3.61)$$

Adopt simple eddy viscosity model.

$$-\overline{u'w'} = \nu_t \frac{\partial}{\partial z} (u_c + u_w) \quad (3.62)$$

$$-\overline{v'w'} = \nu_t \frac{\partial v_c}{\partial z} \quad (3.63)$$

Average over several wave periods.

$$0 = -\frac{1}{\rho} \frac{\partial p_c}{\partial x} + \frac{\partial}{\partial z} \left( \nu_t \frac{\partial u_c}{\partial z} \right) \quad (3.64)$$

$$0 = -\frac{1}{\rho} \frac{\partial p_c}{\partial y} + \frac{\partial}{\partial z} \left( \nu_t \frac{\partial v_c}{\partial z} \right) \quad (3.65)$$

$$0 = -\frac{1}{\rho} \frac{\partial p_c}{\partial z} - g \quad (3.66)$$

Subtract equations (3.64) through (3.66) from equations (3.59) through (3.61). Then, we have

$$\frac{\partial u_w}{\partial t} = -\frac{1}{\rho} \frac{\partial p_w}{\partial x} + \frac{\partial}{\partial z} \left( \nu_t \frac{\partial u_w}{\partial z} \right) \quad (3.67)$$

$$0 = -\frac{1}{\rho} \frac{\partial p_w}{\partial y} \quad (3.68)$$

Equations (3.64) through (3.66) are solved for currents whereas equations (3.67) and (3.68) are solved for waves.



### 3.3.3. Solution for current

Assume a constant shear stress for current boundary layer.

Outside wave boundary layer,  $z \geq \delta_w$ , we have

$$u_{*2} \cdot u_{*2,x} = \kappa u_{*2} z \frac{\partial u_c}{\partial z} \quad (3.69)$$

$$u_{*2} \cdot u_{*2,y} = \kappa u_{*2} z \frac{\partial v_c}{\partial z} \quad (3.70)$$

Here, subscripts x and y denote the horizontal components in x- and y-directions, respectively. From the above equations, we get

$$u_c = \frac{u_{*2,x}}{\kappa} \ln(z/z_1) \quad (3.71)$$

$$v_c = \frac{u_{*2,y}}{\kappa} \ln(z/z_1) \quad (3.72)$$

Here, we set zero velocity at  $z = z_1$  because the velocity scale is valid only above the wave boundary layer. This height  $z_1$  is defined as apparent roughness.

Inside wave boundary layer  $z \leq \delta_w$ , we have

$$u_{*2} \cdot u_{*2,x} = \kappa u_{*1} z \frac{\partial u_c}{\partial z} \quad (3.73)$$

$$u_{*2} \cdot u_{*2,y} = \kappa u_{*1} z \frac{\partial v_c}{\partial z} \quad (3.74)$$

Thus, we get

$$u_c = \frac{u_{*2}}{u_{*1}} \cdot \frac{u_{*2,x}}{\kappa} \ln(z/z_0) \quad (3.75)$$

$$v_c = \frac{u_{*2}}{u_{*1}} \cdot \frac{u_{*2,x}}{\kappa} \ln(z/z_0) \quad (3.76)$$

Matching velocities at top of wave boundary layer  $z = \delta_w$ , we have

$$\ln(\delta_w/z_1) = \frac{u_{*2}}{u_{*1}} \ln(\delta_w/z_0) \quad (3.77)$$

Here,  $\delta_w$  is given again by equation (3.13). Provided we know  $u_{*1}$  and  $u_{*2}$  in addition to  $z_0$ , we can calculate apparent roughness  $z_1$  by iteration using the equation (3.77).

### 3.3.3 Solution for wave

Separate the oscillatory component so that the velocity amplitude  $U$  is the function of  $z$  only.

$$u_w = U(z) e^{i\omega t} \quad (3.78)$$

Substitute equation (3.78) into equation (3.64).

$$i\omega U = -\frac{1}{\rho} \frac{\partial p_w}{\partial x} + \frac{\partial}{\partial z} (\kappa u_{*1} z \frac{\partial U}{\partial z}) \quad (3.79)$$

Boundary conditions are

$$\operatorname{Re}(U|_{z=z_0}) = 0 \quad (3.80)$$

$$\operatorname{Re}(U|_{z=\delta_w}) = U_\infty \quad (3.81)$$

where  $U_\infty$  is the amplitude of bottom excursion velocity. The boundary condition given by equation (3.81) is different from the boundary condition for the pure wave model. But, the difference does not have any significance on the predictions. Because shear is negligible above the wave boundary layer, we set

$$i\omega U_\infty = - \frac{1}{\rho} \frac{\partial p_w}{\partial x} \quad \text{for } z \geq \delta_w \quad (3.82)$$

Substitute equation (3.81) into equation (3.78). Then, we have an ordinary differential equation.

$$i\omega(U - U_\infty) = \frac{d}{dz} (\kappa u_*^2 z \frac{dU}{dz}) \quad (3.83)$$

Define defect velocity amplitude  $U_\delta$ .

$$U_\delta = U - U_\infty \quad (3.84)$$

Then, equation (3.83) becomes

$$i\omega U_\delta = \frac{d}{dz} (\kappa u_*^2 z \frac{dU_\delta}{dz}) \quad (3.85)$$

The boundary conditions become

$$\operatorname{Re}(U_\delta |_{z=z_0}) = -U_\infty \quad (3.86)$$

$$\operatorname{Re}(U_\delta |_{z=\delta_w}) = 0 \quad (3.87)$$

Define a dimensionless variable for velocity.

$$U^* = \frac{U_\delta}{U_\infty} \quad (3.88)$$

Define another dimensionless variable for space.

$$z^* = 2 (z/l)^{1/2} \quad (3.89)$$

Here,  $l$  is a characteristic length scale.

$$l = \frac{\kappa u_* l}{\omega} \quad (3.90)$$

Combining equation (3.13) and equation (3.89), we have

$$\delta_w^* = 2 \kappa^{-1/2} \quad (3.91)$$

Then, equation (3.85) is non-dimensioned. After manipulation, we have

$$(z^*)^2 \cdot (U^*)'' + z^* \cdot (U^*)' - i (z^*)^2 \cdot U^* = 0 \quad (3.92)$$

with the boundary conditions

$$\operatorname{Re}(U^* \Big|_{z^* = z_0^*}) = -1 \quad (3.93)$$

$$\operatorname{Re}(U^* \Big|_{z^* = \delta_w^*}) = 0 \quad (3.94)$$

Following Abramowitz and Stegun (1964), we have the solution

$$U^* = A (\operatorname{ber} z^* + i \cdot \operatorname{bei} z^*) + B (\operatorname{ker} z^* + i \cdot \operatorname{kei} z^*) \quad (3.95)$$

where A and B are constants. The constants are obtained from boundary conditions.

$$A = \frac{-\operatorname{kei} \delta_w^*}{\operatorname{ber} z_0^* \cdot \operatorname{kei} \delta_w^* - \operatorname{ker} z_0^* \cdot \operatorname{bei} \delta_w^*} \quad (3.96)$$

$$B = \frac{\operatorname{bei} \delta_w^*}{\operatorname{ber} z_0^* \cdot \operatorname{kei} \delta_w^* - \operatorname{ker} z_0^* \cdot \operatorname{bei} \delta_w^*} \quad (3.97)$$

### 3.3.4 Maximum bottom shear stress

Using simple eddy viscosity model, the maximum bottom shear stress is given by

$$\left( \frac{\tau_{b, \max}}{\rho} \right)_x = \kappa u_*^2 z_0 \left. \frac{\partial u_c}{\partial z} \right|_{z=z_0} + \kappa u_*^2 z_0 \left( \left. \frac{\partial u_w}{\partial z} \right|_{z=z_0} \right)_{\max} \quad (3.98)$$

$$\text{Since } \frac{\vec{r}_{b, \max}}{\rho} = \hat{i} \cdot u_{*1} \cdot u_{*1, x} + \hat{j} \cdot u_{*1} \cdot u_{*1, y} \quad (3.99)$$

we have

$$u_{*1, x} = \kappa z_0 \left( \frac{\partial u_c}{\partial z} \Big|_{z=z_0} + \text{Max} \left( \frac{\partial u_w}{\partial z} \Big|_{z=z_0} \right) \right) \quad (3.100)$$

$$u_{*1, y} = \kappa z_0 \frac{\partial v_c}{\partial z} \Big|_{z=z_0} \quad (3.101)$$

From equation (3.95), we get

$$\begin{aligned} \frac{dU^*}{dz^*} &= (A \text{ber}' z^* + B \text{ker}' z^*) + i (A \text{bei}' z^* + B \text{kei}' z^*) \\ &= C(z^*) + i \cdot D(z^*) \end{aligned} \quad (3.102)$$

We know

$$\frac{\partial u_w}{\partial z} = \frac{U_\infty}{(z \cdot 1)^{1/2}} \cdot (C + i \cdot D) \cdot e^{i\omega t} \quad (3.103)$$

Thus,

$$\text{Max} \left( \frac{\partial u_w}{\partial z} \right) = U_\infty \left( \frac{C^2 + D^2}{z \cdot 1} \right)^{1/2} \quad (3.104)$$

Combining this with equations (3.75) and (3.76) and substitute into equations (3.100) and (3.101), we get

$$u_{*1,x} = \frac{u_{*2}}{u_{*1}} \cdot u_{*2,x} + 0.5 \cdot \kappa U_{\infty} z_0^* (C(z_0^*)^2 + D(z_0^*)^2)^{1/2} \quad (3.105)$$

$$u_{*1,y} = \frac{u_{*2}}{u_{*1}} \cdot u_{*2,y} \quad (3.106)$$

### 3.3.5. Bottom roughness

In addition to the maximum bottom friction velocity  $u_{*1}$ , the height of zero velocity  $z_0$  should be defined to solve the governing equations for both currents and waves. Nikuradse (1933) relates  $z_0$  to the roughness height  $k_b$  (Yalin, 1977).

$$z_0 = k_b / 30 \quad (3.107)$$

He expressed  $k_b$  in terms of grain diameter  $D_s$ , in case of no sediment movement. The skin friction is the boundary shear stress acting on the sediment grains in the bed thus calculated by using the Nikuradse roughness.

Bedforms increase the roughness height and thereby the bottom boundary shear stress by form drag (Smith and McLean, 1977; Grant and Madsen, 1982). Moveable bed extracts momentum from the flow thus increasing bottom shear stress and the effective roughness length (Grant and Madsen, 1983). Suspended sediments affect the boundary layer structure by density stratification which reduces downward diffusion of momentum from the currents. The result of stratification effect is the reduced bottom shear stress with the

increased bottom roughness (Adams and Weatherly, 1981; Cacchione and Drake, 1982; Glenn and Grant, 1987). Wave-current interaction increases both  $z_0$  and  $u_{*1}$  (Grant and Madsen, 1979; Glenn, 1983; Nielsen et al., 1982).

We adopt Nielsen et al.'s (1982) method to calculate bottom roughness height  $k_b$ .

$$k_b = 2.5 \cdot D_s \quad \text{for } \theta' \leq 0.05 \quad (3.108)$$

$$k_b = 190 (\theta' - 0.05)^{1/2} \cdot D_s + 8 \eta_b^2 / \lambda \quad \text{for } 0.05 \leq \theta' \leq 1 \quad (3.109)$$

$$k_b = 190 (\theta' - 0.05)^{1/2} \cdot D_s \quad \text{for } \theta' \geq 1 \quad (3.110)$$

Here,  $\theta'$  is skin friction Shields parameter.

$$\theta' = \frac{\tau'_{b,max} / \rho}{(\rho_s / \rho - 1) \cdot g \cdot D_s} \quad (3.111)$$

Here,  $\tau'_{b,max}$  is the maximum bottom shear stress for skin friction, calculated using the roughness height given by equation (3.108).  $\eta_b$  is the height of roughness element and  $\lambda$  is the width of roughness element. Form drag effect is resolved in equation (3.109) through  $\eta_b$  and  $\lambda$ . Because the information of bedforms is not available, we need to estimate  $\eta_b$  and  $\lambda$  from the flow and sedimentary characteristics. Nielsen (1981) give this formulation through experimental data from surf zones. Mobility number  $\Psi$  is defined as



$$\Psi = \frac{(A_b \omega)^2}{(\rho_s/\rho - 1) g D_s} \quad (3.112)$$

Here,  $A_b$  is the bottom excursion amplitude. The ripple steepness is given as a function of Shields parameter.

$$\eta_b/\lambda = 0.342 - 0.34 (\theta')^{1/4} \quad (3.113)$$

The ripple height  $\eta_b$  is related to the excursion amplitude  $A_b$  by

$$\eta_b/A_b = 21 \Psi^{-1.85} \quad (3.114)$$

### 3.3.6 Solution and test

The solution requires iterative procedures. At the starting point, we assume  $u_{*1} = 0.1 \cdot U_b$  where  $U_b$  is the amplitude of bottom excursion velocity. Then, we calculate a length scale  $l = \frac{\kappa u_{*1}}{\omega}$  and the thickness of the wave boundary layer  $\delta_w = 1/\kappa$ . Equation (3.108) gives the roughness height from the grain diameter. Assigning an initial values as  $0.1 u_{*1}$ , we find  $u_{*2}$  by iteration using equations (3.71) and (3.72). Now, equations (3.105) and (3.106) give  $u'_{*1}$  which is the friction velocity for the skin friction. Going back to the calculation of  $l$  and  $\delta_w$ , new  $u_{*2}$  is obtained and then the new  $u'_{*1}$  is calculated. The skin friction Shields parameter  $\theta'$  is also obtained by equation (3.111). After the iteration procedure gives a converged value of  $u'_{*1}$ , another iteration is required to obtain  $u_{*1}$  and  $u_{*2}$ : Assume  $u_{*1} = u'_{*1}$ . Calculate  $l$  and  $\delta_w$ . With the equations

(3.108) through (3.114),  $z_0$  is calculated via equation (3.107). We find  $u_{*2}$  by iteration using equations (3.71) and (3.72). At this point, we also have a calculated apparent roughness  $z_1$  via equation (3.77). The iteration goes back to the calculation of  $z_0$ . After obtaining  $z_0$ , we can use equations (3.105) and (3.106) to calculate new  $u_{*1}$ . We return to the calculation of  $l$  and  $\delta_w$  and repeat the procedure until the calculated  $u_{*1}$  value converges.

To see the effect of the change in angle between current and wave propagation, we use  $U_\infty = 1$  m/sec,  $T = 10$  sec. Diameter of bottom sediments is assumed to be 0.1 mm. Steady current of 1 m/sec at the height 100 cm from the bottom is assumed. We can see that the shear is maximum when the wave propagation and the steady current are in the same direction (Figure 15). This has been shown by many researchers (e.g. Glenn, 1983). We also tested the effect of varying wave velocity. We use four different  $U_\infty$  values, 1, 0.75, 0.5, and 0.25 m/sec. We can see the increased effect of wave on the bottom friction. The effect of oscillating component on the mean flow is to increase  $z_1$ ,  $u_{*2}$ , and velocity gradient (Larsen et al., 1981).

### 3.3.7 Results and discussion

The input data is tabulated in Table 1 for low energy condition and in Table 2 for high energy condition. Under low energy condition, the maximum bottom friction represented by  $u_{*1}$  is around 2 cm/sec. By comparing Figure 16 with Figure 3, the increase in  $z_0$  with decreasing wave height  $H$  can be seen. This implies an

Figure 15 Effect of change in angle between current and wave propagation.

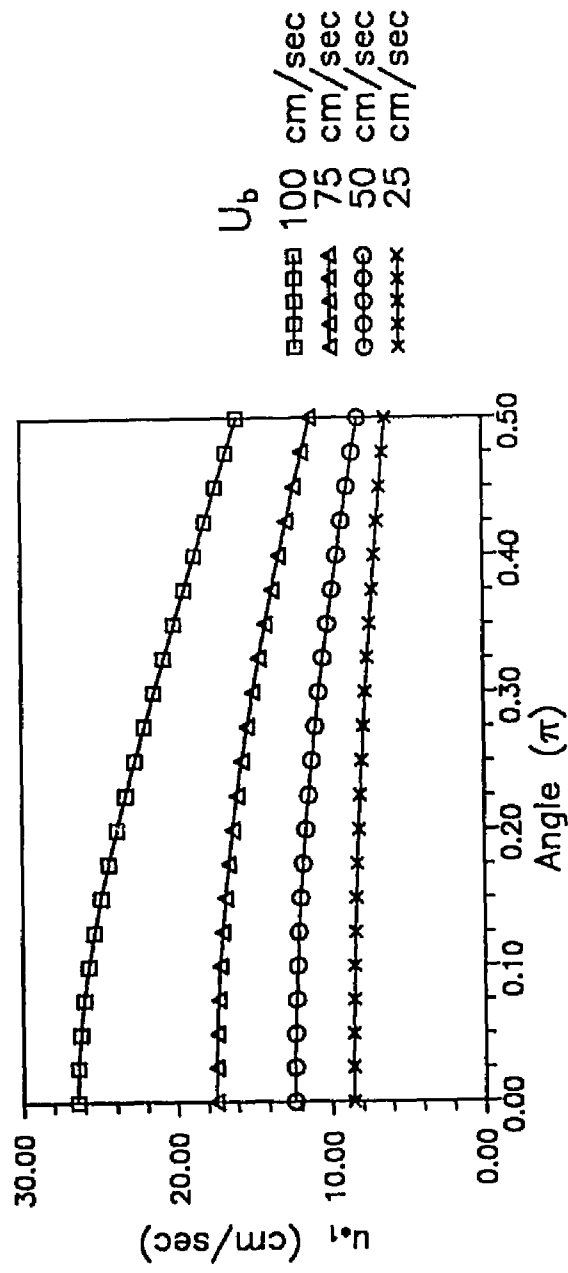
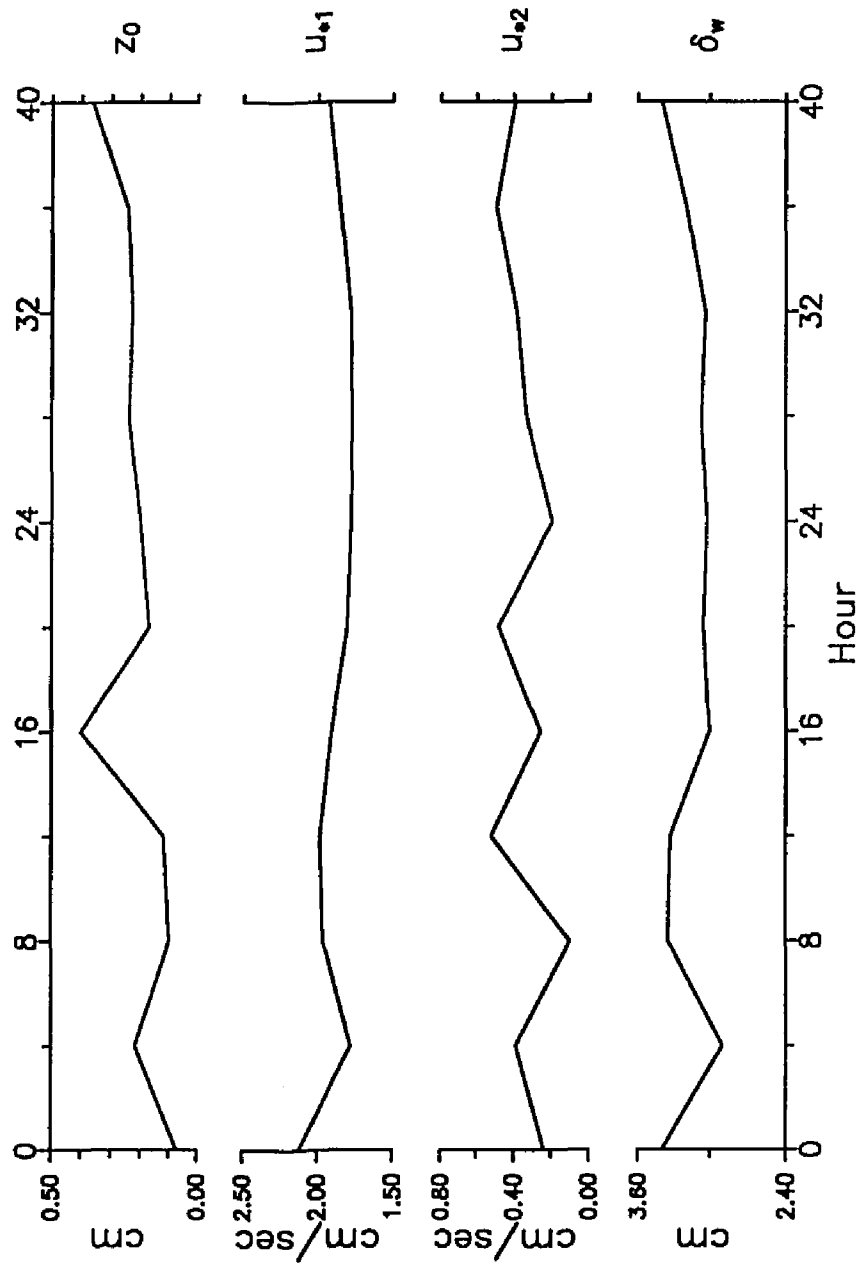


Figure 16 Combined boundary layer model run for fair weather.  $z_0$  is the roughness length scale in cm.  $u_{*1}$  is the maximum bottom friction velocity in cm/sec.  $u_{*2}$  is the velocity scale related with the shear induced by current in cm/sec.  $\delta_w$  is the thickness of wave boundary layer in cm.



increased bedform size with decreasing wave energy. The velocity scale for current boundary layer  $u_{*2}$  varies with varying mean current from 0.2 to 0.4 cm/sec. The wave boundary layer thickness varies between 3 to 3.5 cm.

Under high energy condition,  $z_0$  is reduced, as a result of decreased size of the wave generated ripples. Maximum bottom friction velocity  $u_{*1}$  is increased upto 10 cm/sec. The velocity scale  $u_{*2}$  also increases by an order of magnitude. Comparing with hydrodynamic conditions (Figure 5), we notice  $u_{*1}$ ,  $z_0$ , and  $\delta_w$  are sensitive to the variation in the wave height (Figure 17). The current boundary layer velocity scale  $u_{*2}$  varies with mean current. The calculated model values are tabulated in Table 4 for low energy condition and in Table 5 for high energy condition. These values become input parameters for the concentration model developed in Chapter 4.

The two-layer time-invariant eddy viscosity model is based on the linearized equation of motion. The non-linear interaction is modelled through  $u_{*1}$ . Still there exist weak assumptions such as the discontinuous and time-invariant eddy viscosity distribution, the ambiguity in the definition of the wave boundary layer thickness  $\delta_w$ , and the existence of constant shear stress layer. Wiberg and Smith (1983) uses a continuous eddy viscosity model and the results of two models are almost identical. Thus, there is no serious basis upon which to single out any of the assumption underlying the simple discontinuous eddy viscosity distribution.

Figure 17 Combined boundary layer model run for storm.  $z_0$  is the roughness length scale in cm.  $u_{*1}$  is the maximum bottom friction velocity in cm/sec.  $u_{*2}$  is the velocity scale related with the shear induced by current in cm/sec.  $\delta_w$  is the thickness of wave boundary layer in cm.



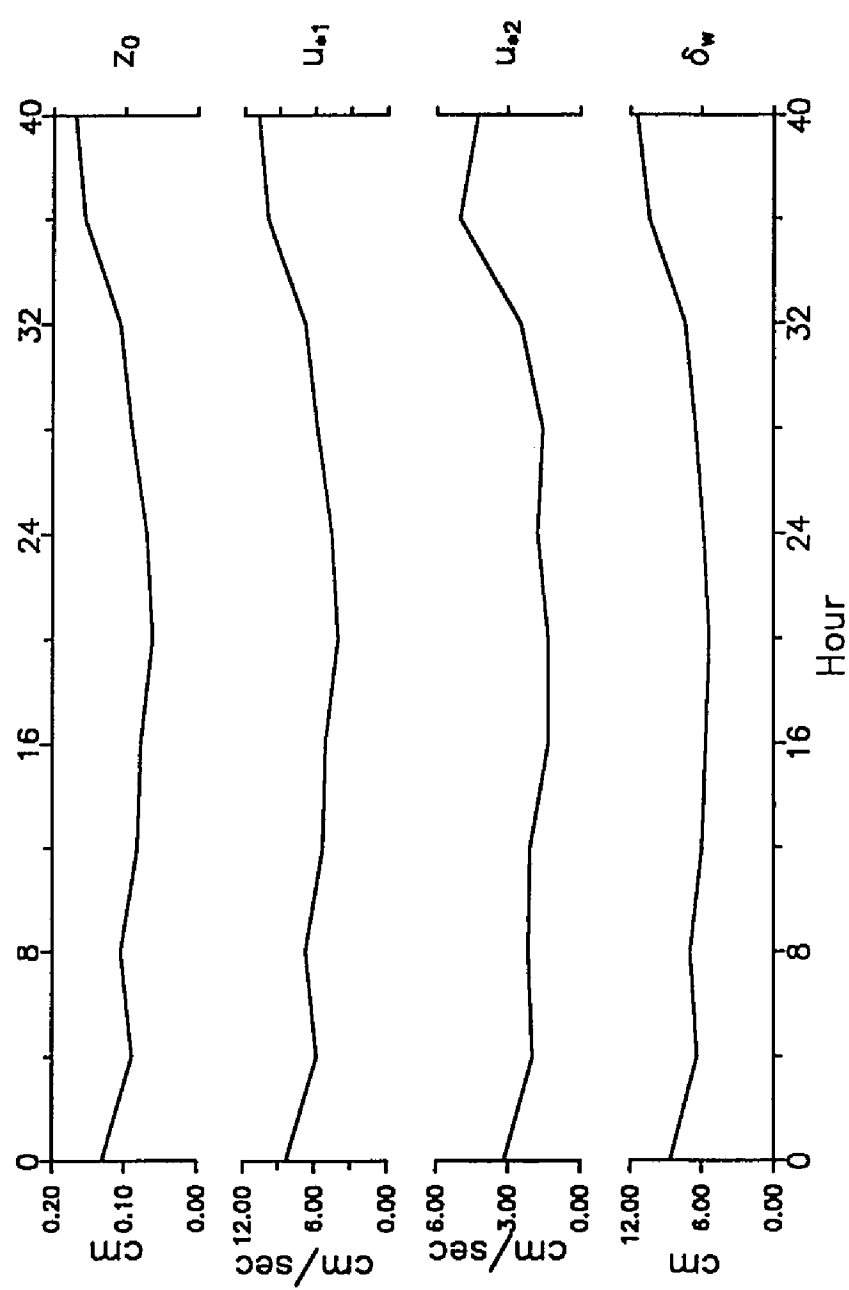


Table 4. Calculated values for fair weather portion

Hour	$z_0$ (cm)	$z_1$ (cm)	$u_{*1}$ (cm/sec)	$u_{*2}$ (cm/sec)	$\delta_w$ (cm)
0	0.0707	2.2171	2.12	0.23	3.40
4	0.2184	1.6511	1.78	0.39	2.90
8	0.0971	2.7974	1.96	0.10	3.35
12	0.1177	1.3847	1.98	0.52	3.33
16	0.4026	2.2882	1.90	0.26	3.00
20	0.1695	1.4158	1.81	0.48	3.06
24	0.1989	2.2459	1.78	0.20	3.03
28	0.2384	1.9085	1.77	0.33	3.07
32	0.2277	1.7381	1.78	0.38	3.04
36	0.2430	1.6057	1.85	0.50	3.19
40	0.3640	2.1578	1.93	0.39	3.40

Table 5. Calculated values for storm weather portion

Hour	$z_0$ (cm)	$z_1$ (cm)	$u_{*1}$ (cm/sec)	$u_{*2}$ (cm/sec)	$\delta_w$ (cm)
0	0.1301	1.7757	8.31	3.14	8.71
4	0.0898	1.5271	5.77	1.94	6.37
8	0.1048	1.8212	6.72	2.14	6.95
12	0.0822	1.1351	5.30	2.05	5.97
16	0.0785	1.9308	5.07	1.27	5.62
20	0.0618	1.2994	4.01	1.27	5.29
24	0.0699	1.0778	4.53	1.72	5.81
28	0.0904	2.1126	5.81	1.52	6.47
32	0.1063	1.6093	6.81	2.44	7.38
36	0.1559	1.2406	9.94	5.03	10.41
40	0.1689	2.1374	10.76	4.29	11.45...

We still have many unsolved questions such as the validity of logarithmic velocity profile. Field evidence shows mixed interpretations. For example, Soulsby and Dyer (1981) and Lavelle and Mofjeld (1983) dispute the ambiguity of the logarithmic velocity profile whereas Gross and Nowell (1983) show the evidences for it. For the further application to the sediment transport model, we also need to understand the coupling of form drag and moveable bed effects on the bottom shear stress and bottom roughness height. The model developed here is believed to be sufficiently accurate to reproduce the bottom shear stress, at least to the first degree which is essential for the further application. The magnitude of the maximum bottom shear stress becomes the most important input variable for the sediment concentration model.

## 4. SUSPENDED SEDIMENT CONCENTRATION MODEL

### 4.1 Introduction

The most common approach to the prediction of suspended sediment distribution is based on the assumption that the sediment phase as well as the fluid phase is a continuum. That is, the largest size of the sediment particles is small compared with the smallest length scale of the flow parameter (Monin and Yaglom, 1971). In this continuum theory, the continuity is applied to both phases (e.g. Graf, 1971). This becomes the basis for the estimation of concentration profile.

To improve the suspended sediment concentration model, the diffusion term which appears in the governing equation should be defined with a certain level of accuracy. The diffusion of sediment mass within a flow is related to the multi-phase flow dynamics and thus complicated by the unknown correlations in terms of time scales (e.g. Hunt, 1969). Because both the turbulence and the wave movements contribute to the diffusion processes, this should be determined in such a way that resolves at least turbulent and periodic time scales. Moreover, the analogy of sediment mass diffusion to the fluid momentum diffusion can be questioned (e.g. Dobbins, 1943).

The determination of diffusion coefficient is complicated by the bedforms developed. Especially when the magnitude of the quasi-steady current is much smaller than the amplitude of oscillating

flow, it is the vortex bursting that dominates the supply of suspended sediments into the water column (Bhattacharya, 1971). Nielsen (1979) pointed out that a model for the suspended sediment should be based on a periodically pulsating input of sand at the lower boundary.

The concentration model also requires the knowledge of the concentration at a reference level. Because suspended sediments are transported under different mechanisms from bedload sediments, the reference height is related to the thickness of bedload layer which in turn is related to grain diameter. The boundary conditions should be expressed in terms of both the flow and the sediment characteristics (e.g. Einstein, 1950).

In this Chapter, a sediment concentration model is developed and the estimation of diffusion and reference concentration is elaborated.

## 4.2 Governing equations

The change of mass in a closed system equals the sum of the mass changes due to convection and diffusion.

$$\frac{\partial C}{\partial t} + \nabla \cdot C \vec{u}_s = \nu \cdot \nabla^2 C \quad (4.1)$$

Here,  $C$  is the volume concentration of sediments,  $\vec{u}_s$  is the vector of sediment particle velocity, and  $\nu$  is the molecular velocity. Analogous to the flow field analysis, we decompose the particle velocity into mean, periodic, and turbulent parts.

$$\vec{u}_s = \vec{u}_{sc} + \vec{u}_{sw} + \vec{u}'_s \quad (4.2)$$

Subscripts  $c$  and  $w$  represent current and wave, respectively.

Analogous decomposition is given to the sediment concentration.

$$C = C_m + C_p + C' \quad (4.3)$$

Here, the subscripts  $m$  and  $p$  represent mean and periodic concentrations, respectively. Assume negligible horizontal convection and molecular diffusion compared with vertical turbulent diffusion. Substitute equations (4.3) and (4.2) into equation (4.1) and average over turbulent time scale.

$$\frac{\partial C_p}{\partial t} + \frac{\partial}{\partial z} (w_{sc} + w_{sw}) (C_m + C_p) = \frac{\partial}{\partial z} \overline{(-w'_s \cdot C')} \quad (4.4)$$

The particle velocity is given by the conservation of momentum for a single particle (Hinze, 1959). If the length scale and time scale of particle are smaller than turbulence length and time scales, then the particle velocity differs from the flow velocity only by the settling velocity.

$$w_s = w - w_{fs} \quad (4.5)$$

Tooby et al.(1977) argued that particle Reynolds number instead of flow Reynolds number characterizes the flow in the immediate vicinity of a suspended particle. Thus, the above equation is modified by the fluid drag and gravity-induced buoyancy. In unsteady flows, the discrepancy is interpreted using delay distance (Hattori, 1969), time lag (Bhattacharya, 1971), and the reduced settling velocity due to non-linear drag forces (Nielsen, 1983). However, Nielsen (1983) showed that the approximation of particle velocity by equation (4.5) is valid for oscillatory flow within a certain level of accuracy especially for coarse sediments. Substituting equation (4.5) into equation (4.4), we have

$$\frac{\partial C_p}{\partial t} - w_{sf} \cdot \frac{\partial}{\partial z} (C_m + C_p) + \frac{\partial}{\partial z} [w_w \cdot (C_m + C_p)] = \frac{\partial}{\partial z} (\overline{-w' C_s'}) \quad (4.6)$$



### 4.3 Diffusivity of suspended sediment concentration

It has been recognized that the turbulent diffusion of fluid momentum is responsible for the sediment mass transfer in a flow field (e.g. Rouse, 1939, Kalinske and Pien, 1943). The correlation term  $\overline{w' C'}$  in the above equation reflects the turbulent diffusion of sediment mass. Analogy to the eddy viscosity for flow, the turbulent diffusion of sediment mass is assumed to be related to the gradient of mean concentration by eddy diffusivity  $\nu_{ts}$  (O'Brien, 1933).

$$-\overline{w' C'} = \nu_{ts} \frac{\partial}{\partial z} (C_m + C_p) \quad (4.7)$$

The diffusivity is assumed to be related to eddy viscosity of fluid momentum transfer (Vanoni, 1941).

$$\nu_{ts} = \alpha_1 \cdot \nu_t \quad (4.8)$$

Rouse (1939) showed that the coefficient  $\alpha_1$  is constant for the sediments with diameter less than 1/16 mm. Vanoni (1941) suggested  $\alpha_1 = 1$  for relatively low concentration of small grains. Even though there is ambiguity (e.g. Dobbins, 1943), we assume  $\alpha_1 = 1$  for simplicity. Then, equation (4.6) becomes

$$\frac{\partial C_p}{\partial t} - w_{sf} \cdot \frac{\partial}{\partial z} (C_m + C_p) + \frac{\partial}{\partial z} w_w (C_m + C_p) = \frac{\partial}{\partial z} [\nu_t \frac{\partial}{\partial z} (C_m + C_p)] \quad (4.9)$$

Average over wave periods. Then, we have

$$-w_{sf} \cdot \frac{\partial C_m}{\partial z} + \frac{\partial \langle w_w C_p \rangle}{\partial z} = \frac{\partial (\nu_t \cdot C_m)}{\partial z} \quad (4.10)$$

In the equation, we now have a new unresolved correlation term  $\langle w_w C_p \rangle$ . Kennedy and Locher (1972) elaborated this problem, giving asymptotic solutions. They choose two extreme cases: Far above the bed, turbulent diffusion is negligible whereas wave advection is negligible close to the bed. Wang and Liang (1975) defined a diffusivity  $\nu_w$  for periodic diffusion analogous to  $\nu_t$  for turbulent diffusion.

$$\langle -w_w C_p \rangle = \nu_w \frac{\partial C_m}{\partial z} \quad (4.11)$$

Then, equation (4.10) becomes

$$\frac{\partial}{\partial z} \{ w_{sf} \cdot C_m + (\nu_t + \nu_w) \cdot \frac{\partial C_m}{\partial z} \} = 0 \quad (4.12)$$

They assumed that the velocity is scaled with vertical wave orbital velocity and the length scale is constant for the diffusivity.

$$\nu_w = L \cdot w_w \quad (4.13)$$

Here, L is a constant proportionality representing length scale. They set  $L = 5.15$  m. This model may be valid away from the wave boundary layer nested at the bottom of current boundary layer, where

the paths of a wave orbit is about constant. Very close to the bottom boundary, turbulent diffusion is dominant over the diffusion of sediments by wave orbital motion.

Nielsen (1979) argued that the analogy of periodic sediment diffusion to that of steady flow usually fails possibly due to the character of periodic convection of sediment motion. Homma and Horikawa (1963) relates the diffusivity with potential wave motion.

$$\nu_w = (3/\alpha) \cdot b^2 \omega \quad (4.14)$$

Here,  $\alpha$  is a constant related to the distance from the bed and  $b$  is the vertical wave displacement. Homma et al. (1965) later introduced mixing length approach even if it is conflict in physics because potential flow is a non-mixing flow.

$$\nu_w = \kappa^2 \left| \frac{\partial u}{\partial z} \right|^3 / \left( \frac{\partial^2 u}{\partial z^2} \right)^2 \quad (4.15)$$

Bhattacharya (1971) tried to show the existence of an upward sediment drift caused by the periodic components. He gets periodic diffusivity is proportional to the square of the distance from the bed.

$$\nu_w = \frac{1}{2} \cdot \delta_t \cdot \left( \frac{H \cdot z}{2 \cdot h} \right)^2 \quad (4.16)$$

Here,  $\delta_t$  is the delay time,  $H$  is the wave height, and  $h$  is the water depth.

Nielsen (1979) sees the diffusivity as the combination of turbulent diffusivity and periodic diffusivity. He showed that  $\nu_w$  is negligible and

$$\nu_t = \kappa \cdot u_* h \cdot (1-z/h) \quad (4.17)$$

He tested this over variable empirical diffusivities. His formulation suggests that the distance from the bottom is a good length scale both for the turbulent diffusion and for the convection by waves. However, use of friction velocity is questionable because the friction represents the dissipation of turbulent energy at the bottom boundary. The friction velocity as a velocity scale holds only for the case of turbulent diffusion.

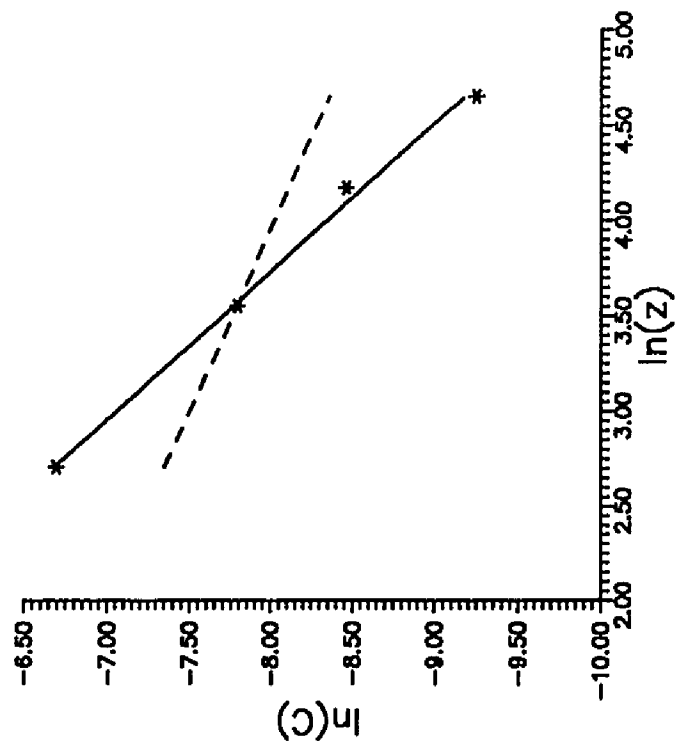
Between the bottom boundary and the free stream region, which is the active zone of suspended sediment transport, the diffusion process is complicated: At a certain height above the bottom, the role of wave orbit is not negligible any more. In addition, the role of lee vortex becomes significant when bedforms are present, which is the cases we encounter most frequently in the nature (e.g. Nielsen, 1979). The entrainment of bottom sediments are related to the skin friction. Form drag affects not only the turbulent diffusion of both momentum and sediment concentration but also the bursting of sediments trapped within the lee vortex. As bottom friction increases, form drag diminishes and the moveable bed contributes to the turbulence structure. The role of the lee vortex decreases and the turbulent diffusion is enhanced with the change of bedform into the plane bed due to increased flow intensity.

Thus, the diffusion of sediment concentration is related to the vortex size as well as the wave orbits. The size of vortex depends on the dimension of bedforms. We do not have a good apprehension of the bedforms with varying flow conditions. For the first order approximation, we assume the bed is plane and the role of steady current is significant so that we may minimize the role of periodic advective mechanism which is apparent for the case of wave boundary layer. We introduce another velocity scale,  $V$ , for the modification of turbulent diffusion. Figure 18 shows that the predicted concentration profile without the introduction of  $V$  is far from the measured profile. We set  $V$  as a function of the geometry of bedform inferring vortex bursting as well as the wave amplitude representing convective diffusion. The determination of  $V$  thus depends on the hydrodynamic conditions. Then, the diffusivity becomes

$$\nu_t + \nu_w = \kappa (u_{*1} + V) z \quad \text{for } z \leq \delta_w \quad (4.18)$$

$$\kappa (u_{*2} + V) z \quad \text{for } z \geq \delta_w$$

Figure 18 Concentration profile. The dotted line is the slope given by excluding modifying velocity scale,  $V$ . The solid line is the slope given by including  $V$ .



#### 4.4 Solution for mean concentration

Add equation (4.12) to equation (4.9). Neglect second order periodic term. Then, we have

$$\frac{\partial C_p}{\partial t} - w_{sf} \frac{\partial C_p}{\partial z} + \frac{\partial}{\partial z} w_w \cdot C_m = \frac{\partial}{\partial z} (\nu_t \cdot C_p) \quad (4.19)$$

Assume no sediment flux through upper boundary. Substituting equation (4.18), equation (4.12) becomes the governing equation for mean concentration.

$$w_{sf} \cdot C_m + \kappa(u_{*1} + V) z \cdot \frac{\partial C_m}{\partial z} = 0 \quad \text{for } z \leq \delta_w \quad (4.20)$$

and

$$w_{sf} \cdot C_m + \kappa(u_{*2} + V) z \cdot \frac{\partial C_m}{\partial z} = 0 \quad \text{for } z \geq \delta_w \quad (4.21)$$

The solution is

$$C_m(z) = C_m(z_r) \cdot (z / z_r)^{-w_{sf} / (\kappa \cdot (u_{*1} + V))} \quad \text{for } z \leq \delta_w \quad (4.22)$$

and

$$C_m(z) = C_m(\delta_w) \cdot (z / \delta_w)^{-w_{sf} / (\kappa \cdot (u_{*2} + V))} \quad \text{for } z \geq \delta_w \quad (4.23)$$

Here, we have to set reference concentration  $C_m(z_r)$ .



#### 4.5 Determination of model parameters from field data

The model starts with the assumption that the instantaneous suspended sediment concentrations respond to the instantaneous bottom shear stress exerted by the flow. To investigate the validity of this assumption, cross-correlations between the concentration and the squared velocity, which represent instantaneous shear stress, are obtained. For the high-energy environment, the correlations are high and have near-zero time lag (Figure 19). For the low-energy condition, we can hardly see the correlation and the lag between bottom shear stress and suspended sediment concentration is apparent (Figure 20). This implies that the use of the diffusivity given in the model can only be useful under high energy conditions. But, the cross-correlations between the suspended sediment concentrations at different vertical positions show, the lag between  $C_p$ 's are small under the low energy condition (Figure 21) and increases away from the bottom under high energy condition (Figure 22). This implies that we have to be careful about using the diffusivity given in this study for the model of periodic concentration. The model of  $C_p$  needs a diffusivity which resolves the time lag.

The mean concentrations, however, varies with the average shear stress in general. Figure 23 shows the variation of average squared velocities (shown without any marker) with concentrations (lines with markers) almost conform under low energy conditions. The high energy condition also shows the same tendency (Figure 24). From this, the use of a time-invariant diffusivity can be validated for

Figure 19 Cross-correlations between squared speed and suspended sediment concentration, storm condition

Cross  
Correlation  
 $U_2^2$  vs. C

Duck'85  
Storm Weather

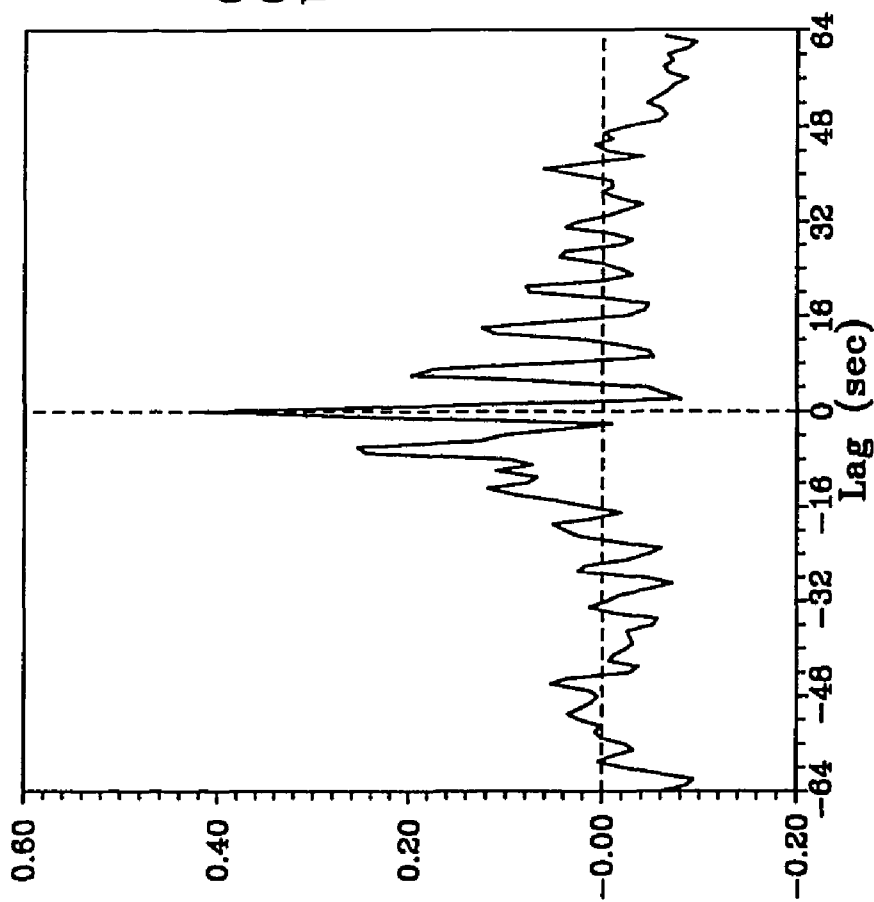


Figure 20 Cross-correlations between squared speed and suspended sediment concentration, fair weather condition

Cross  
Correlation  
 $U_2$  vs. C

Duck '85  
Fair Weather

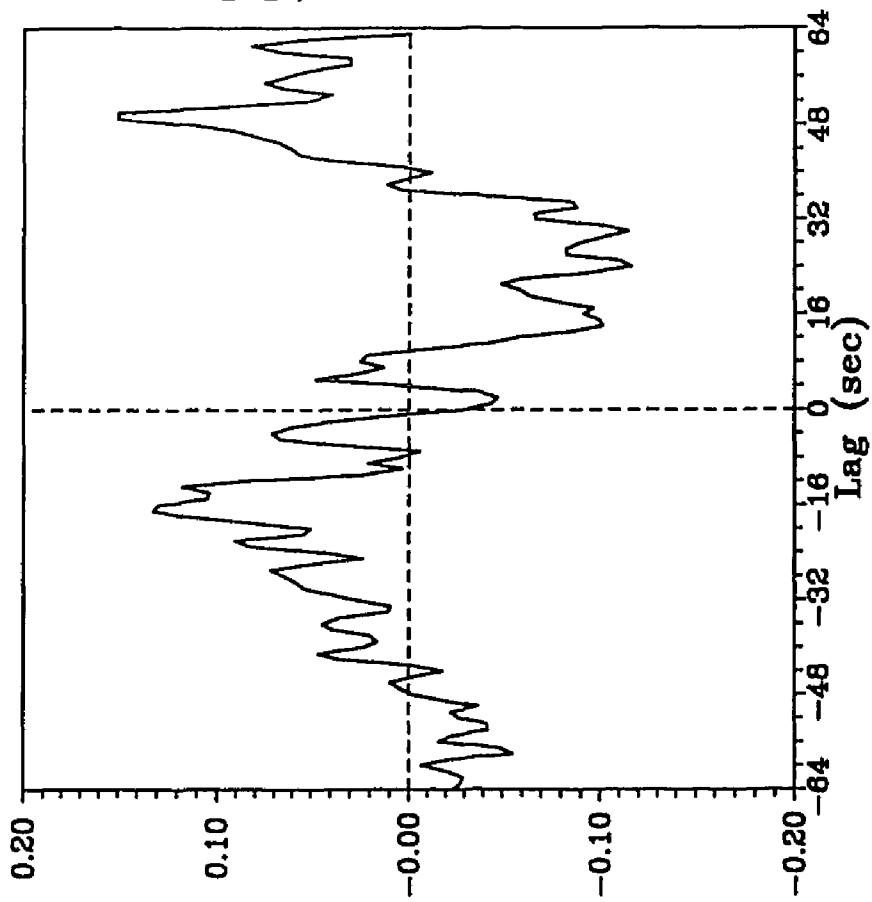


Figure 21 Cross-correlations between the suspended sediment concentrations at different levels, fair weather condition.

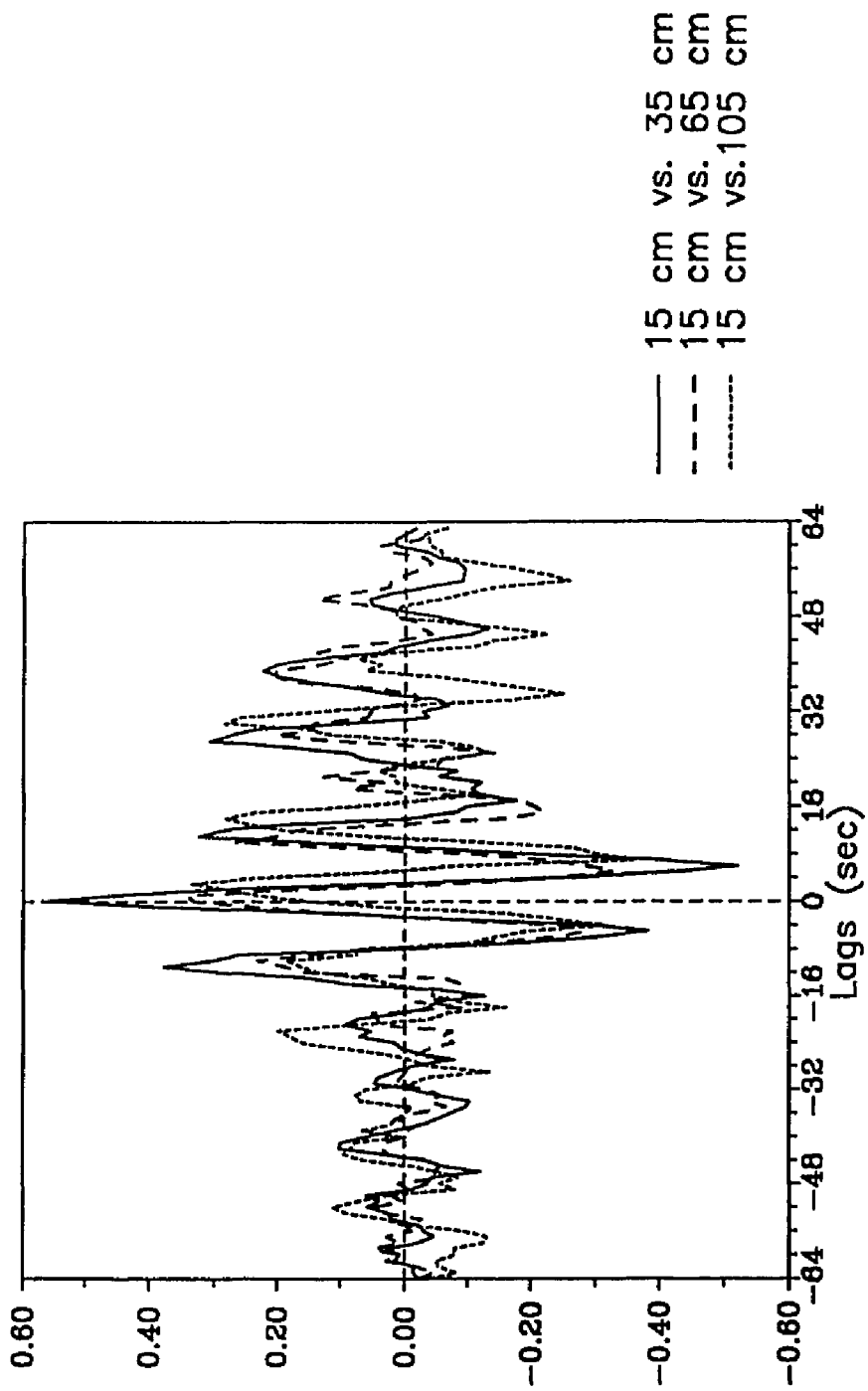


Figure 22 Cross-correlations between the suspended sediment concentrations at different levels, storm condition.



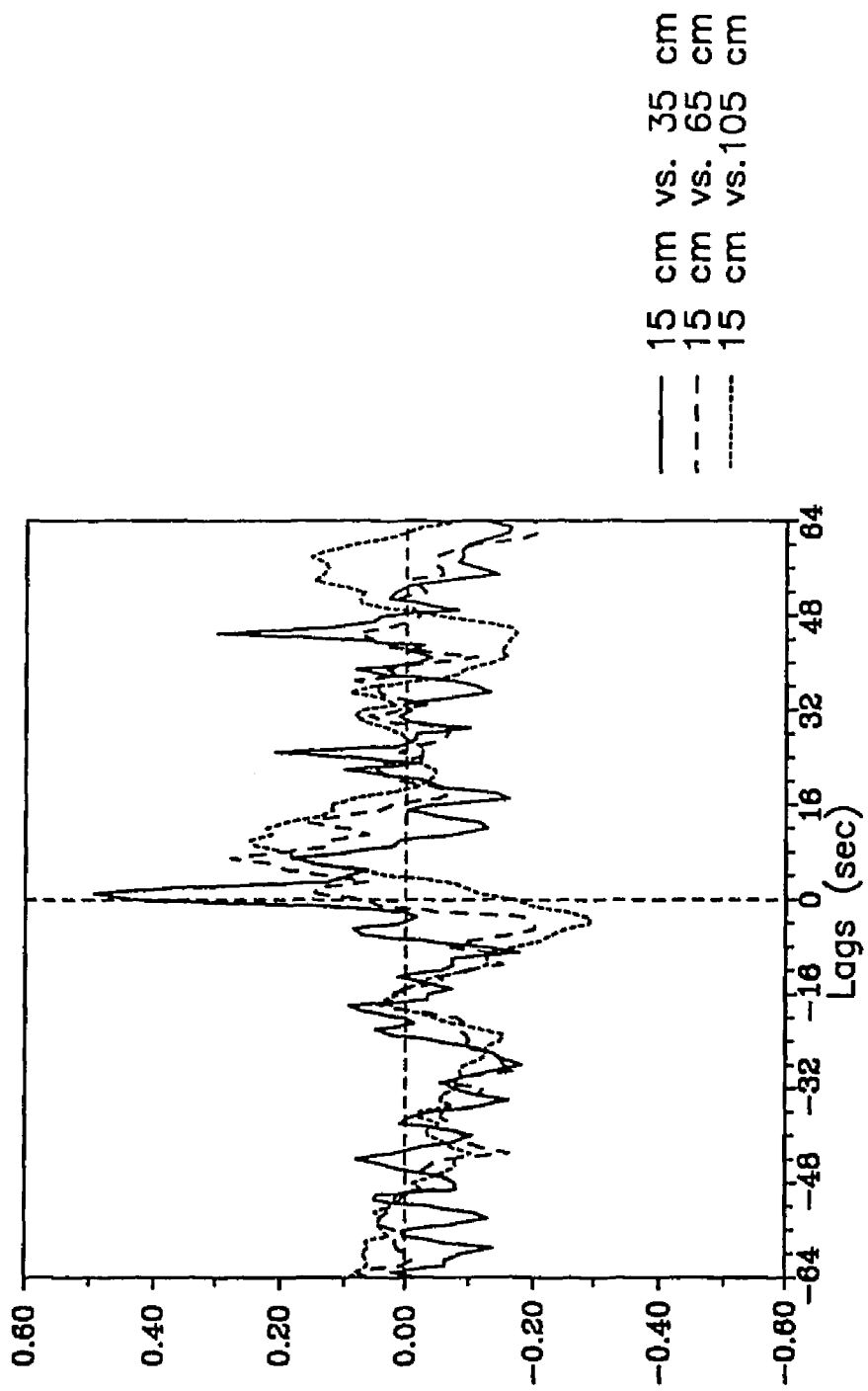
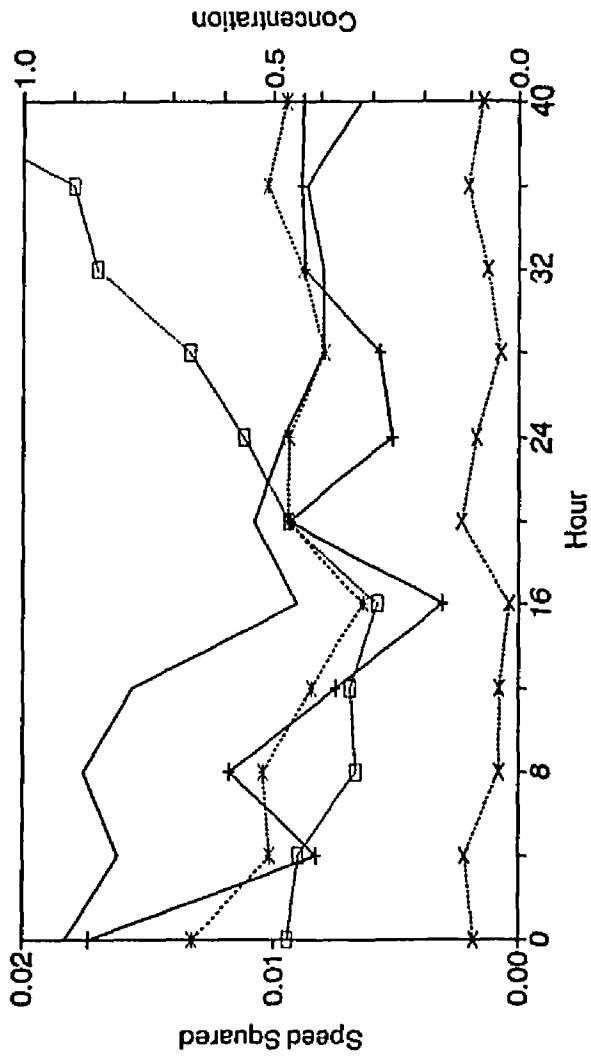
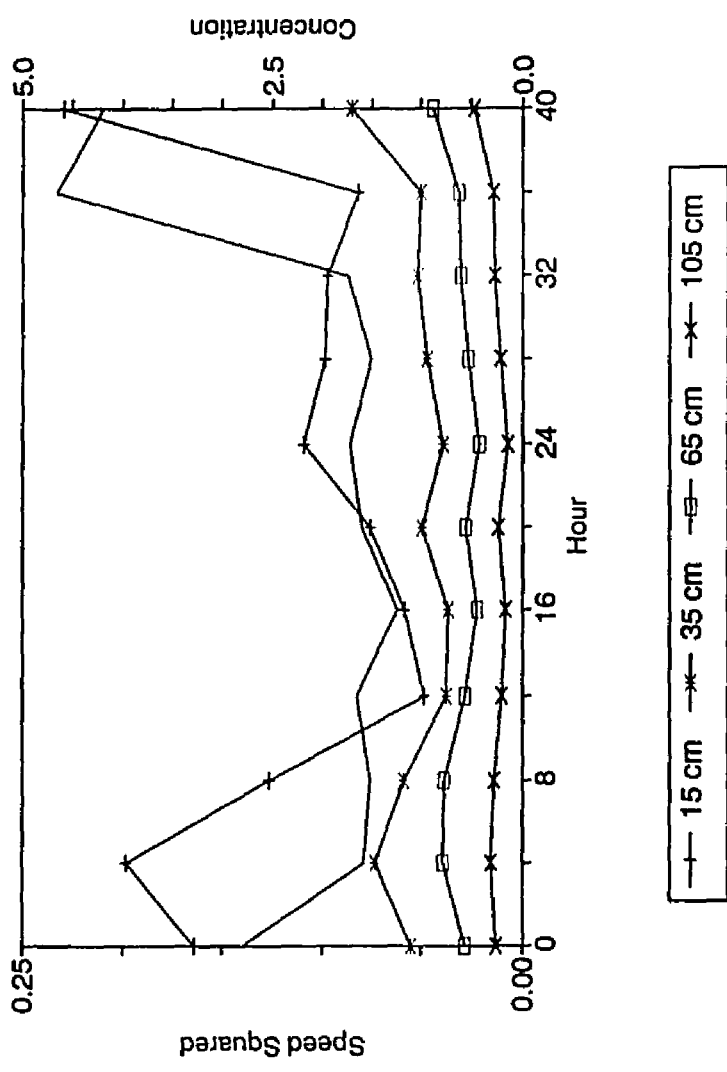


Figure 23 Variation of time averaged squared speed and suspended sediment concentrations, fair weather portion. Here, squared speed is in  $\text{cm}^2/\text{sec}^2$  and concentrations are in  $\text{Kg}/\text{m}^3$ .



—+— 15 cm    -\*- 35 cm    —□— 65 cm    -x- 105 cm

Figure 24 Variation of time averaged squared speed and suspended sediment concentrations, storm portion. Here, squared speed is in  $\text{cm}^2/\text{sec}^2$  and concentrations are in  $\text{Kg}/\text{m}^3$ .



the prediction of mean concentration  $C_m$ .

In addition to the turbulent diffusion, the contributions from other sources for the diffusion are accounted for the model developed. These effects are resolved into the velocity scale  $V$ . From the vertical profile of suspended sediment concentrations, the slope in log-log scale plot is  $-\frac{w_{sf}}{\kappa (u_{*2} + V)}$ . Corresponding  $D_s = 0.1$  mm, the settling velocity  $w_{sf}$  is set to be 0.7 cm/sec. From the linear regression,  $V$  is estimated.

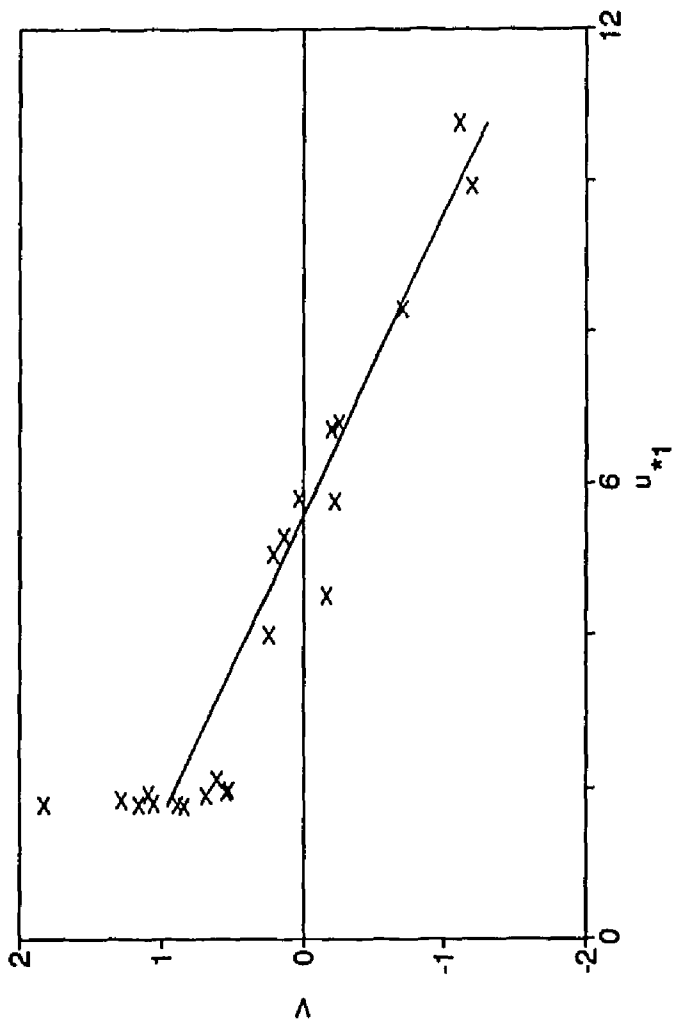
$$V = - 0.25 u_{*1} + 1.4 \quad (4.24)$$

The regression coefficient  $r^2$  is 0.86.

The energy conditions are believed to be represented by the bottom friction. Thus, the estimated  $V$  is viewed as a function of  $u_{*1}$  (Figure 25). Under the low energy condition, the total diffusion is greater than the turbulent diffusion. When the low energy conditions prevail, there always exist bedforms which cause the entrapment of suspended sediments within lee vortices. The bursting of lee vortex is a complicated procedure (e.g. Sleath, 1982). The interval of bursting is believed to be aligned with the flow reversal. However, we do not have the quantitative information on the bursting phenomenon.

Under the high energy condition, the diffusion is smaller than turbulent diffusion. Results from atmospheric studies (Mellor and

Figure 25 Modifying velocity scale,  $V$ , versus the maximum bottom friction velocity,  $u_{*1}$ . Both have the units of cm/sec.





Yamada, 1974) have been applied by many (e.g. Adams and Weatherly, 1981) to model the effect of density stratification in benthic boundary layers. Evaluating the effects of stratification due to suspended sediment concentration requires that both the velocity profile and the suspended sediment concentration profile be simultaneously modelled. The Monin-Obukov length scale and the gradient Richardson number are usually used to modify the eddy viscosity profile. The evaluation, however, is not straightforward because the process also produces moveable bed roughness. Grant et al. (1983) note that even though data from the CODE winter storm experiment showed high suspended sediment concentrations, no significant modification in the velocity profile was observed. In this context use of a modifying velocity scale,  $V$ , only for sediment concentrations is feasible. At the onset of storm, the bedforms are washed out and the turbulence becomes the relevant means for the diffusion of sediments. Because the measurements were confined to the bottom 1 meter, we expect to have negligible effect of wave diffusion proposed by Wang and Liang (1975).

#### 4.6 Reference concentration

The solution of the governing equation for the mean concentration requires the specification of a reference concentration  $C_r$  at a reference height  $z_r$ . Lane and Kalinske (1941) assumed that the composition and concentration of suspended sediments near the bed are related to the composition and concentration of bed materials and to the hydraulic conditions of the transporting system. They relate reference concentration to the bed concentration  $C_b$  and the standard deviation of vertical velocity fluctuations. From empirical data, they determined the relationships between  $w_{fs}/u_*$  and  $C_r / C_b$ .

Einstein (1950) reasoned that the relationship governing the concentration at the lower boundary of suspension could be found by setting up an expression for the exchange of sediment particles between suspended load and bedload layers: He set the top of the bedload layer as  $2 \cdot D_s$ . Then, the weight of particles per unit area is proportional to  $\frac{q_b}{u_b}$  where  $q_b$  is the immersed bedload rate in weight per unit time per unit width and  $u_b$  is the average bedload transport velocity. He again assumed  $u_b$  is proportional bottom friction velocity  $u_*$ . Thus,

$$C_r \propto \frac{q_b}{D_s \cdot u_*} \quad (4.25)$$

Yalin (1977) reasoned that bedload concentration is a function of the lift force and the weight of sediment grains. An assumption

was made that the number of grain lifted from the bed surface increases proportionally with excess shear stress S.

$$N = 0.635 \cdot S \quad (4.26)$$

Here, N is the number of grains in motion and  $S = \frac{\tau}{\tau_c} - 1$  where

$\tau_c$  is critical shear stress. In terms of concentration, this expression may be converted into

$$C_r = \gamma \cdot S \cdot C_b \quad (4.27)$$

where  $\gamma$  is an empirical coefficient. Smith (1977) modified Yalin's idea through the correction for the case of infinite S.

$$C_r = \frac{\gamma \cdot C_b \cdot S}{1 + \gamma \cdot S} \quad (4.28)$$

Smith and McLean (1977) gave  $\gamma = 0.0024$  from measurements in the Columbia river. Glenn (1983) calculated the same order value  $\gamma = 0.003$  through the investigation of the data of Kalkanis (1964) and Abou-Seida (1965). Drake and Cacchione (1985) got lower values for  $\gamma$  for cohesive sediments. The estimations of  $\gamma$  vary from the order of  $10^{-2}$  (Kachel and Smith, 1986) to the order of  $10^{-5}$  (Sternberg et al., 1985), depending on both the hydrodynamic conditions, the sediment characteristics, and the geometries of bedforms.

Shi et al. (1985) also noticed the departure of  $\gamma$  from the value of Smith and McLean. They referred the observation results of Lesht et al. (1980) and Clark et al. (1982) of a near-linear relationship between wave orbital velocity and suspended sediment concentration and reasoned that the reference concentration varies linearly with the square root of the excess shear stress.

$$C_r = \gamma \cdot C_b \cdot S^{1/2} \quad (4.29)$$

Vincent et al. (1981) viewed the data of Kalkanis (1964) and Abou-Seida (1965) of the mass of sand deposited in the trays as a measure of concentration of sand in suspension not as a measure of the transport. They defined an average volume concentration  $C^*$  which has unit of cm. They determined the empirical relationship

$$C^*(t) = (0.09 \pm 0.03) \theta_{ex}(t) \quad (4.30)$$

where  $\theta_{ex}$  is the excess Shields parameter. This result appears to be supportive of Smith's (1977) expression. However, their expression, equation (4.25), is dimensionally in conflict since  $C^*$  is the dimension of [L] whereas  $\theta_{ex}$  is dimensionless. We maintain their interpretation of the data of Kalkanis (1964) and Abou-Seida (1965), but we normalize  $C^*$  with the thickness of bedload layer which is given by  $2 \cdot D_s$ . Vincent et al. (1981) choose only rough turbulent case ( $Re > 35$ ). Here,  $Re$  is grain Reynolds number. After normalizing the concentration by the bedload layer thickness, we also can give the smooth turbulent case the same formulation. From

the relationships between the normalized concentration and the excessive Shields parameter (Figure 26), we get

$$C_r = 0.09 \cdot \theta_{ex} \quad (4.30)$$

The bed agitation is related to shear stress exerted on the bottom. Linear relationships between reference concentrations and shear stresses are formulated either using excess shear stress (equation 4.28) or Shields parameter  $\theta$ . Proportionality with the square root of shear stress has also been suggested, as in equation (4.29).

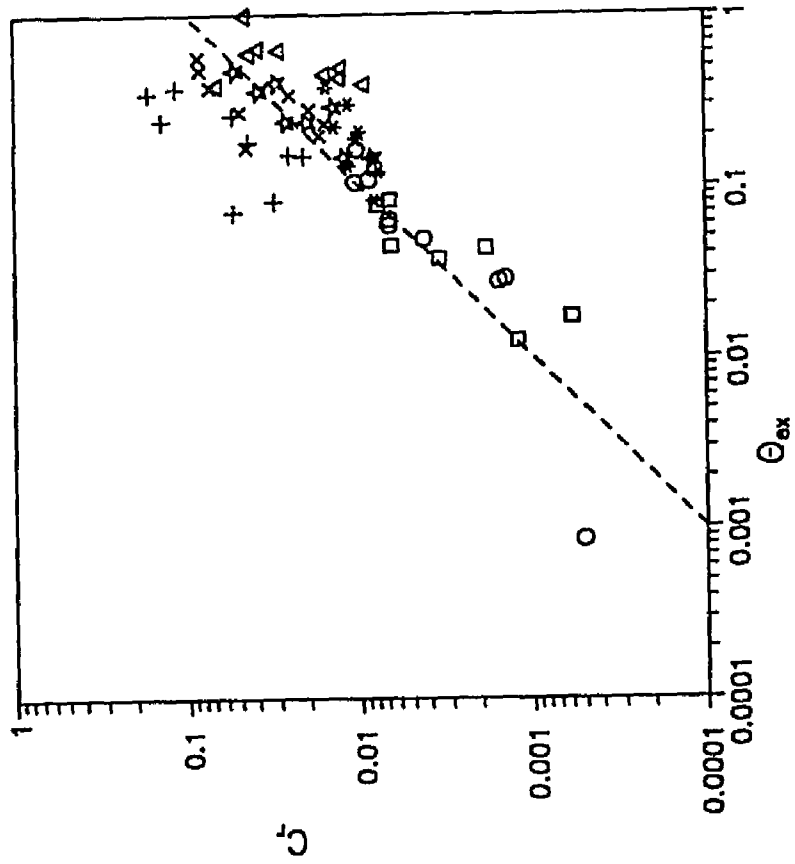
Combining equations (4.22) and (4.23), reference concentration is calculated.

$$C_m(z_r) = \frac{C_m(z)}{(\delta_w/z_r)^{-w_{sf}/\kappa(u_{*1}+V)} (z/\delta_w)^{-w_{sf}/\kappa(u_{*2}+V)}} \quad (4.27)$$

Both the excess shear stress  $S$  and Shields parameter  $\theta$  are calculated setting the critical friction velocity  $u_{*c} = 0.75$  cm/sec for  $D_s = 0.1$  mm. The bed concentration  $C_b = 0.65$ . The density of sediments  $\rho_s = 2.65$  g/cm<sup>3</sup>.

Figure 27 shows the estimated coefficient  $\gamma$  for the case of linear relationships of reference concentration with Shields parameter  $\theta$ . The coefficient  $\gamma$  under low energy condition is high by an order compared with  $\gamma$  under high energy condition. The same trend is seen for excess shear stress  $S$  (Figure 28). For the

Figure 26 Reference concentration versus excess Shields parameter.



$D_s$   
 ○○○○○ 1.68 mm  
 □□□□□ 2.18 mm  
 △△△△△ 0.14 mm  
 ☆☆☆☆☆ 0.30 mm  
 \* \* \* \* \* 2.60 mm  
 + + + + + 1.21 mm  
 x x x x x 0.70 mm

Figure 27 The resuspension coefficient,  $\gamma$ , for  $C_r \propto \theta$ .



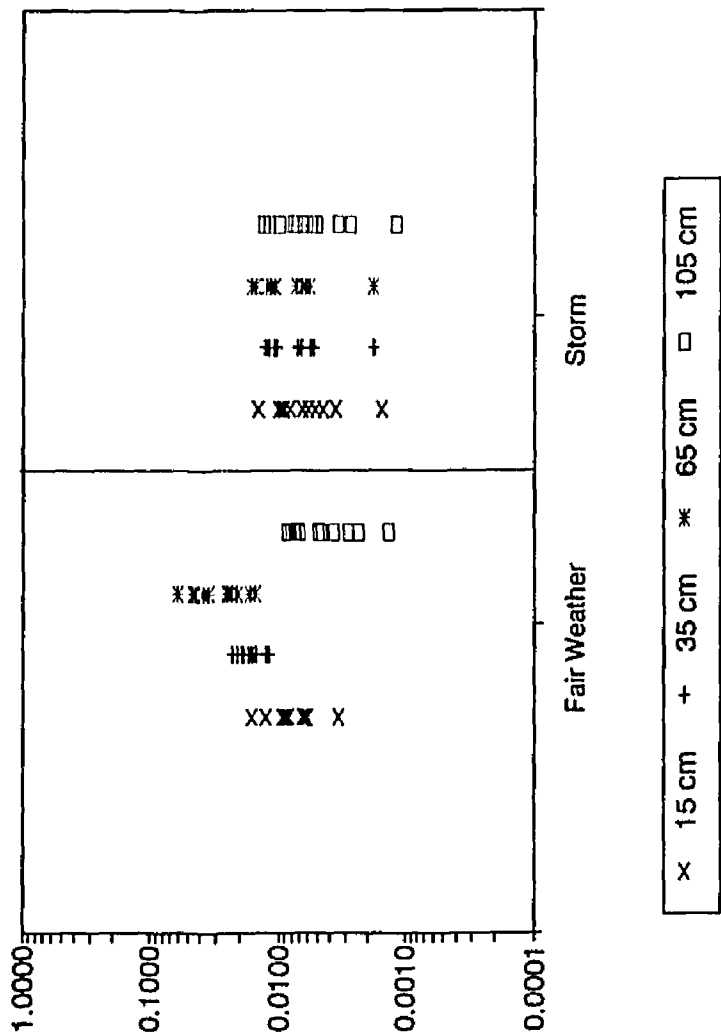
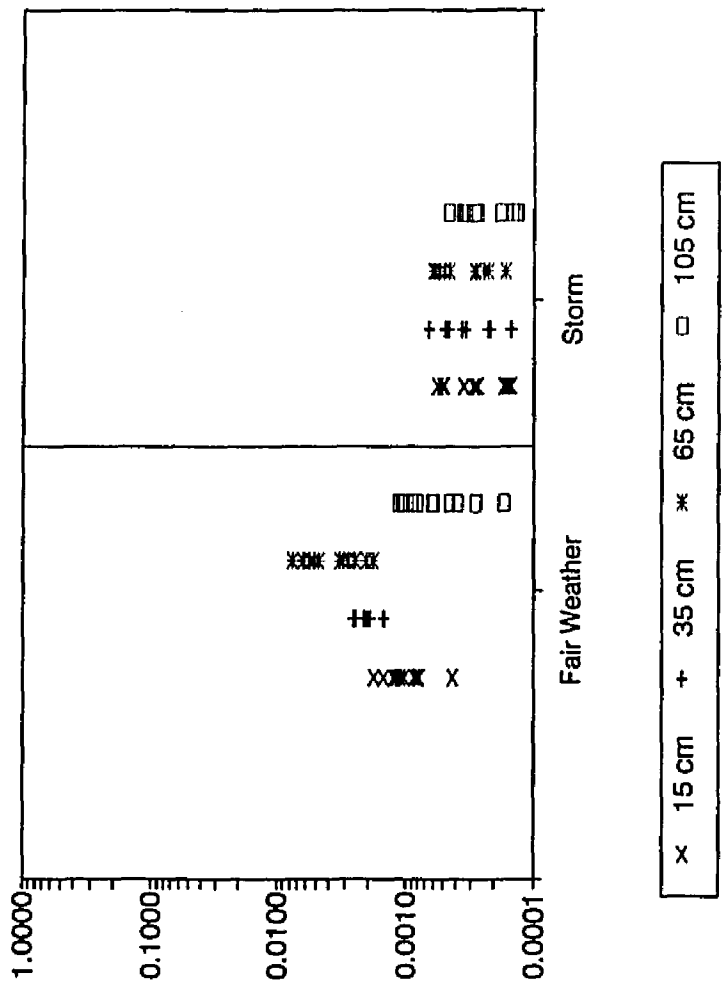


Figure 28 The resuspension coefficient,  $\gamma$ , for  $C_r \propto S$ .



proportionality to the square root of shear stress, values of  $\gamma$  from using either  $\theta^{1/2}$  (Figure 29) or  $S^{1/2}$  (Figure 30) vary by two or three factors with different energy conditions. The average values of  $\gamma$  are tabulated in Table 6. Considering the variability of the values of  $\gamma$  from the different formulae, it is hard to set the definite preference of any specific formula. In consistence with the laboratory result given by equation (4.31) as the linear relationships of the reference concentration,  $C_r$ , with shear stress in terms of Shields parameter,  $\theta$ , we chose the linear relationship of  $C_r$  with excess shear stress,  $S$ , given by equation (4.28).

For the low energy condition, the vertical variation of the coefficient  $\gamma$  shows no apparent relationships (Figure 31). The coefficient  $\gamma$  for the high energy condition, however, shows the estimates do not vary appreciably with different sensor heights (Figure 32). This near-independence of height above bottom under high energy condition suggests that any deduction about  $\gamma$  from fair weather data is questionable. Also apparent in Figure 32 is the reduced  $\gamma$  for hour 36 which corresponds to the rapid increase in flow intensity. One possibility is the armoring effect with increased bottom friction. As Drake and Cacchione (1989) noted, the coefficient  $\gamma$  decreases with increasing bottom shear stress (Figure 33). This tendency is retained only for the case when the bottom shear stress exceeds a certain value, representing high energy condition. This implies the possible change of the supply of bed materials into the water column due to the armoring effect which increases with increasing bottom friction (Drake and Cacchione, 1989). But, the correlation coefficient  $r^2$  is less than 0.6. Thus,

Figure 29 The resuspension coefficient,  $\gamma$ , for  $C_r \propto \theta^{1/2}$ .

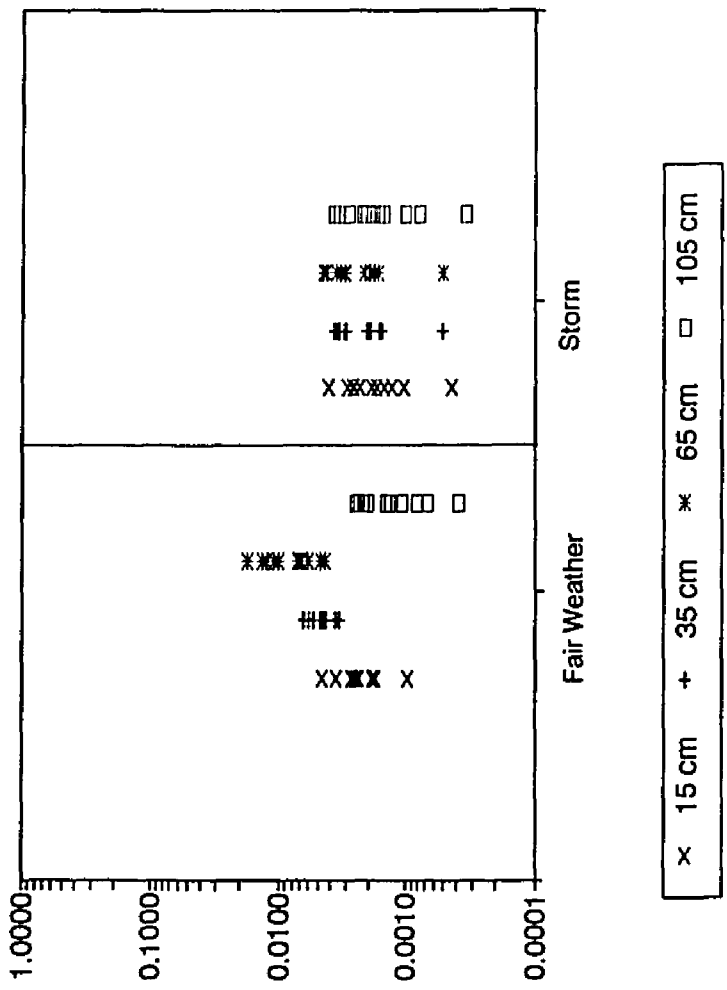


Figure 30 The resuspension coefficient,  $\gamma$ , for  $C_r \propto S^{1/2}$ .

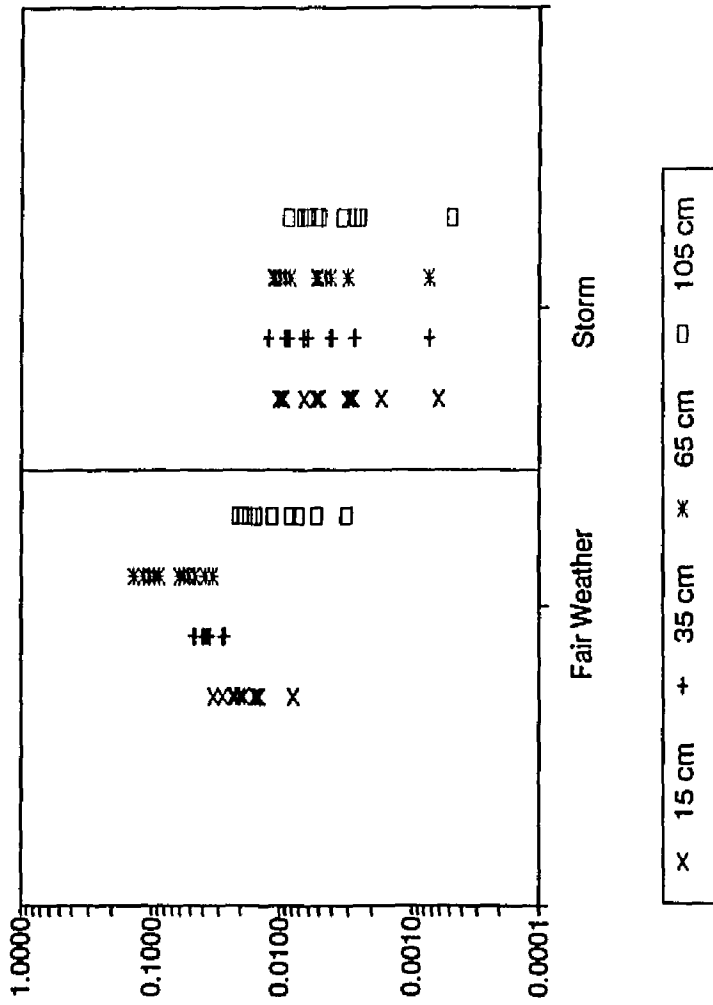




Table 6. Formulation for reference concentration and the coefficient  $\gamma$

Formulation	Fair Weather	Storm
$C_r = \gamma \theta_{ex}$	0.040	0.006
$C_r = \frac{\gamma C_b S}{1 + \gamma C_b S}$	0.002	0.0003
$C_r = \gamma \theta_{ex}^{1/2}$	0.020	0.008
$C_r = \gamma C_b S^{1/2}$	0.004	0.002

\*  $\theta_{ex} = \frac{\tau_{b,max} - \tau_{cr}}{(\rho_s - \rho) g D_s}$

\*  $S = (\tau/\tau_{cr}) - 1$

Figure 31 Variation of the resuspension coefficient,  $\gamma$ , with OBS sensor height, fair weather portion.

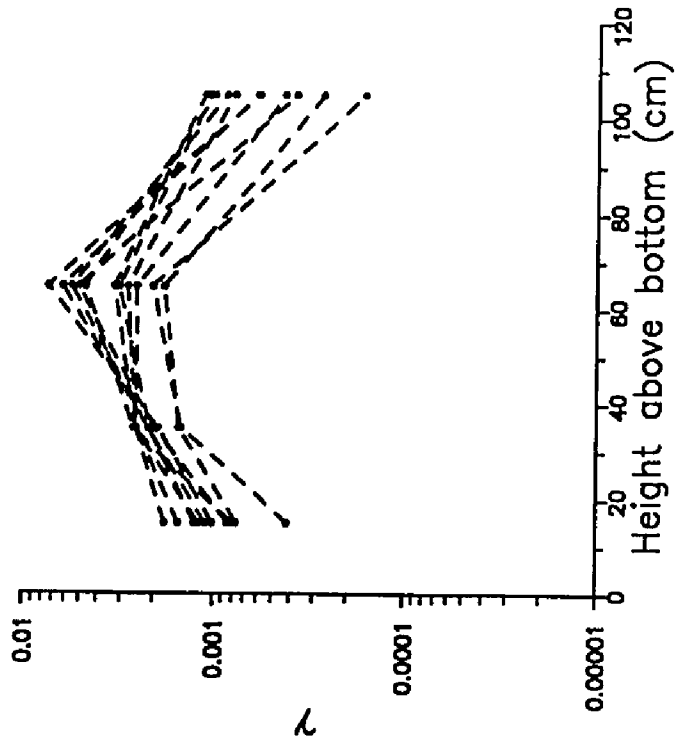


Figure 32 Variation of the resuspension coefficient,  $\gamma$ , with OBS sensor height, storm portion. The isolated line with low values in the order of  $10^{-5}$  corresponds to Hour 36.

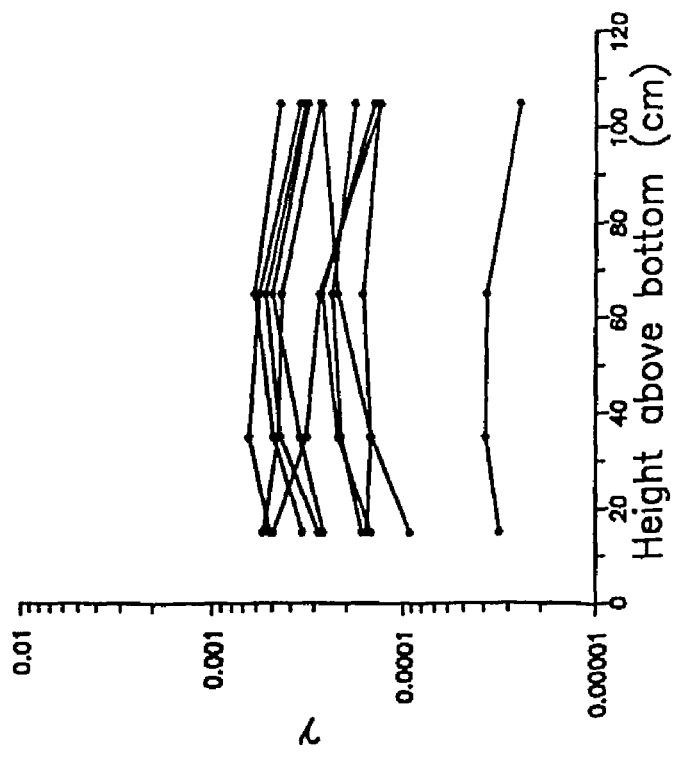
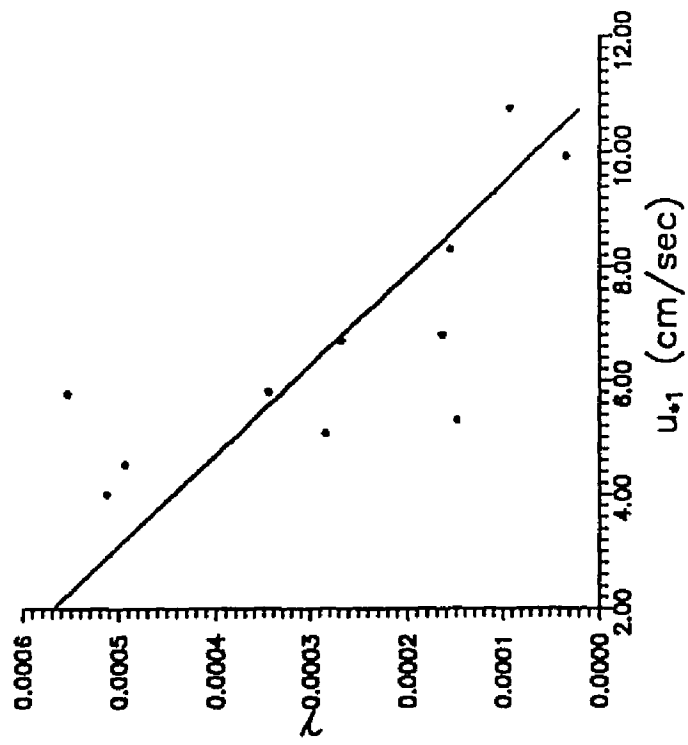


Figure 33 The resuspension coefficient,  $\gamma$ , versus the maximum bottom friction velocity  $u_{*1}$  (cm/sec).



it is unsafe to set a formulation for this relationships at this stage. We need more data to reveal this relationships. In this context, the use of the average value 0.0003 for the coefficient  $\gamma$  under high-energy condition and 0.002 for  $\gamma$  under low-energy condition seems to be appropriate.



#### 4.7 Results and discussion

The mean concentration model is tested using Glenn's (1983) data for variable wave conditions which is tabulated in Table 7. The bottom concentrations increase with increasing shear stresses (Figure 34). The concentrations far away from the bottom increase with decreasing shear stresses. This is because of the relative increase of the diffusion in current boundary layer under low wave condition.

For the fair weather portion, data in Table 4 is applied. The predicted concentrations at the height 15 cm, 35 cm, 65 cm and 105 cm are compared with the measurements (Figure 35). The prediction reproduces the profile within an acceptable range of error only for the first 8 hour samplings. From hours 12 to 40, the overestimation at the bottom and top and the underestimation at the middle are apparent. Because the model does not include any advection term and there could be possible error in some of the measurements, the model does not guarantee the prediction of suspended sediment concentration under the low energy condition. Both the suspended sediment concentration and the current velocity under fair weather condition is low by an order of magnitude compared with those under storm condition, which results two-orders of magnitude low in flux. Thus, the discrepancy between the prediction and the measurement under low-energy condition is insignificant for the study of net transport of suspended sediments.

Table 7. Model input parameters (Glenn, 1983)

$D_s = 0.01$  (cm)

	$z_0$ (cm)	$z_1$ (cm)	$u_{*1}$ (cm/sec)	$u_{*2}$ (cm/sec)	$\delta_w$ (cm)
Small wave	0.514	1.79	7.88	4.97	15.1
Medium wave	0.162	1.41	8.78	4.69	16.8
Large wave	0.170	2.27	11.30	5.28	21.8

Figure 34 Test run of mean concentration model for different wave conditions.

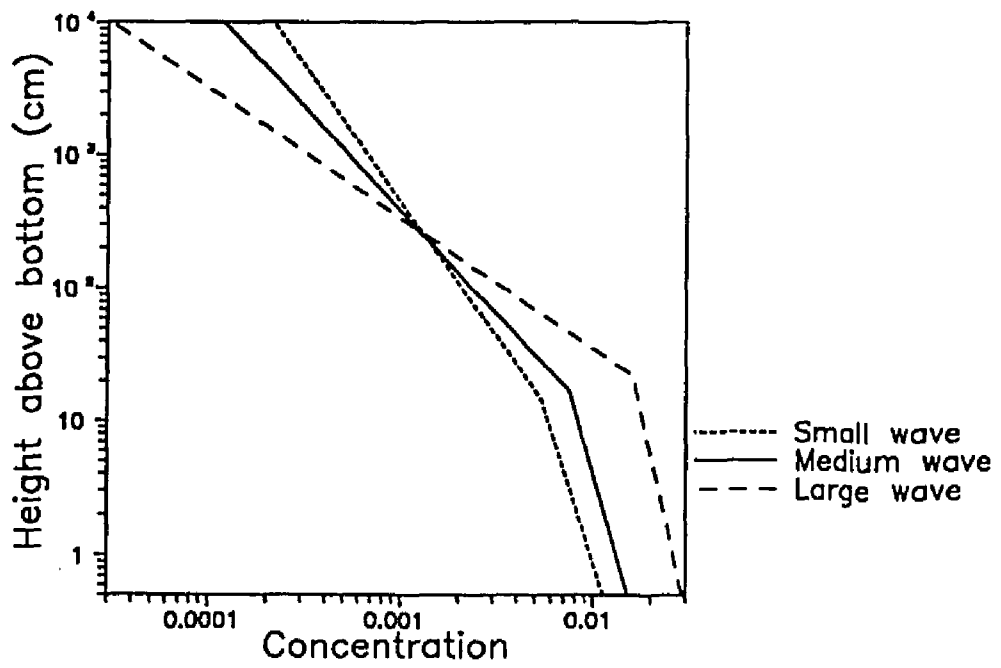
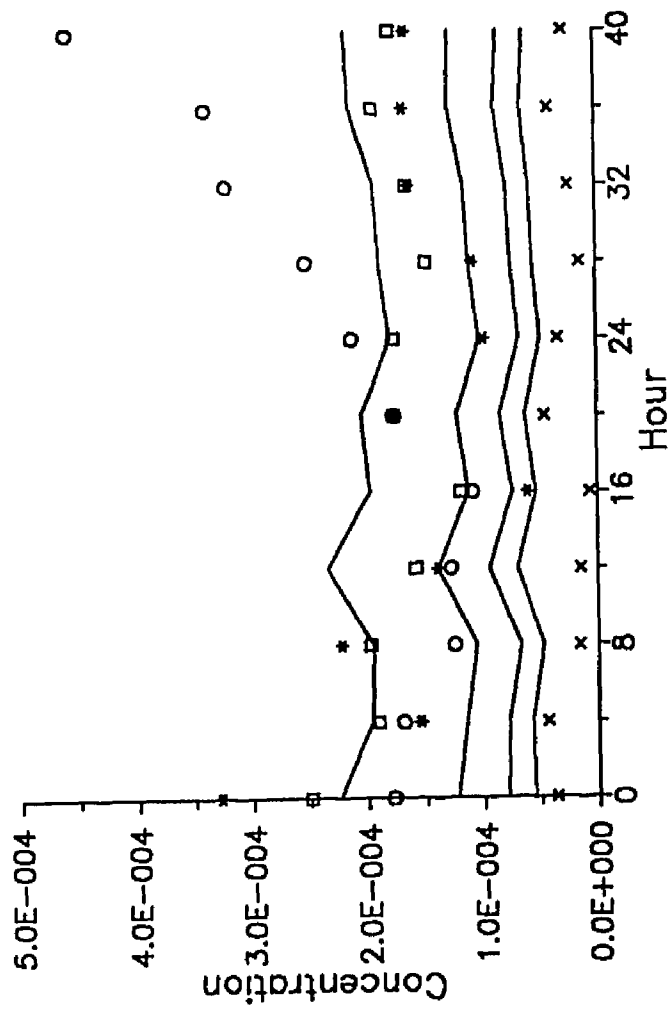


Figure 35 Predicted suspended sediment concentrations, fair weather portion.

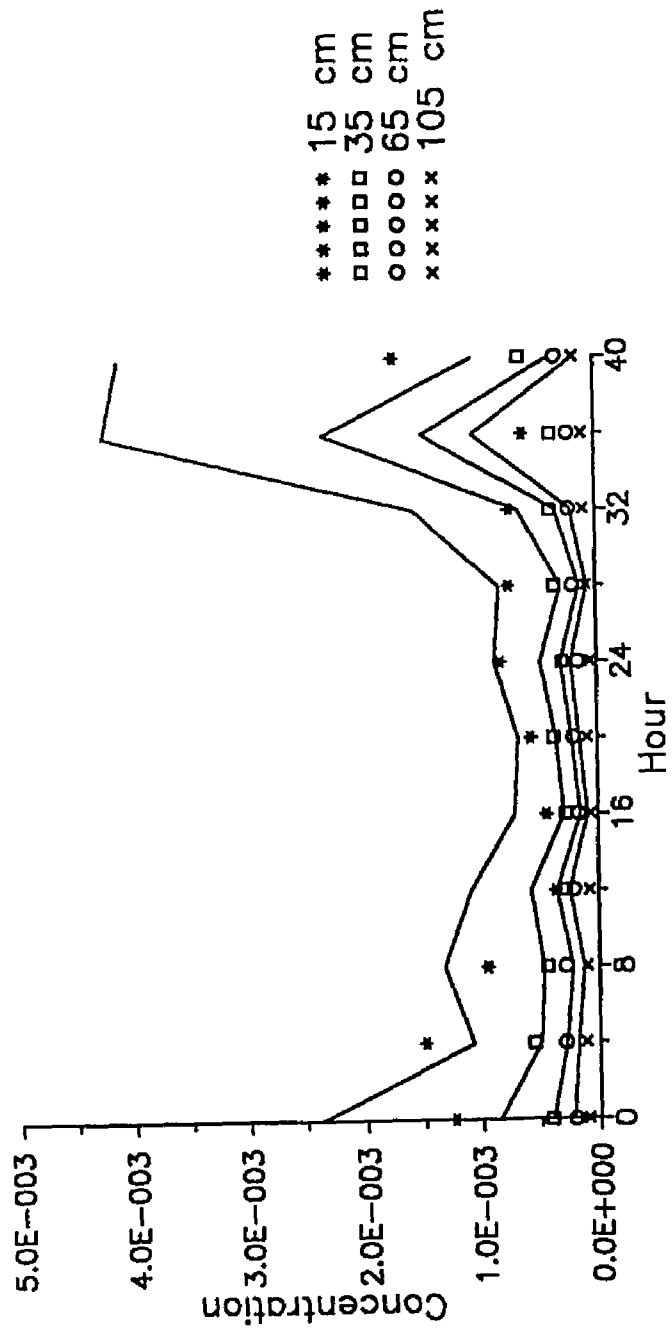


\*\*\*\* 15 cm  
 □□□□ 35 cm  
 ○○○○ 65 cm  
 xxxxx 105 cm

For the storm weather portion, the values in Table 5 become the input variables. The prediction almost matches the measurement (Figure 36). The overestimation at hour 36 is apparent. This burst coincides with very strong current ( $\approx 35$  cm/sec) with increasing wave energy, representing onset of the storm. The strong current results in high  $u_{*2}$  ( $\approx 5$  cm/sec) which is responsible for the diffusion of sediments inside current boundary layer in the model developed in this study. This could be the limitation of this model. When the current becomes strong, particle interacts to suppress the diffusion (Adams and Weatherly, 1981). Armoring effect is also increasing with rapid increase in bottom shear stress (Drake and Cacchione, 1989). The applicability of this model is, therefore, wide except for the case of rapid change in hydrodynamic conditions.

Figure 36 Predicted suspended sediment concentrations, storm  
portion.





## 5. CROSS-SHORE SEDIMENT TRANSPORT

### 5.1 Introduction

The direction and magnitude of time-average sediment transport is the important factor in the determination of the sediment budget. Onshore transport is forced mainly by wave asymmetry and sometimes by upwelling. Gravity pulling, downwelling, amplitude modulated waves due to wave groupiness are known to provide offshore escape mechanism. Tidal currents can be in either onshore or offshore directions. The resulting direction of net transport is determined by the combinations of these forcings.

Swift et al. (1985) asserted that the fair-weather landward creep of sediments due to the wave asymmetry and the storm-induced seaward sweep of sediments represent the cross-shore sediment exchange process over the Long Island shoreface. They suggest the escaping mechanism during storms to be provided by downwelling. Shi (1983) reasoned that the forced long waves induced by the wave groupiness provide the offshore transport mechanism even under the fair-weather conditions.

In this chapter, we consider the direction of net sediment transport and the contributions to the directional transport by the flow components of different in time scales. The model developed through Chapter 4 only deals with mean concentration. The transport by quasi-steady flow is straightforward. The direction of the net transport is the direction of the transport of sediments carried by

the mean flow. The role of high frequency wave has been questioned by many researchers (e.g. Nielsen, 1979).

An energetics-based model sees sediment transport processes as the consumption of fluid energy by sediments. Bagnold (1963) applied his energetics-based bedload transport model for a stream flow to oscillatory flows. The transport rate is directly related to fluid power via an efficiency factor. The angle of repose of sediments and the slope of the bed also affect the transport rate. The available fluid power is the flux of tractive stresses which are represented by bottom shear stress here. If we maintain the quadratic stress law, we can deduce the third power relationship of the fluid power. Thus, bedload has third power dependency while suspended load transport has fourth power dependency because the suspension has advection mechanism opposing the settling of particles.

The periodic fluctuation of fluid velocity is the main forcing under oscillating flow. For the wave environments, perturbation in terms of time scale has been attempted (e.g. Bowen, 1980; Bailard and Inman, 1981; Bailard, 1981). In this context, we regard only the first order perturbation, which is consistent with our model for combined boundary layer flow.

An energetics approach is concerned with velocity moments. Questions have been raised about the direct relevance of the measurements of some moments to sediment transport (e.g. Guza and Thornton, 1985). Working with the data from Duck'85 experiments,

which span both fair and storm weather conditions, we are able to calculate the immersed weight sediment transport rate. Because there is no way for an energetics model to resolve the phase of the flow, the calculated transport rate is evaluated by comparing with flux measurement. At the end of this Chapter, a semi-quantitative sediment transport model is given.

## 5.2 An energetics model

Bagnold (1956) postulated that the sediment transport rate is proportional to the fluid power available:

$$I = K \Omega \quad (5.1)$$

Here,  $I$  is transport rate and  $\Omega$  is the fluid power available. Again, the transport is via both bedload and suspended load transport:

$$I = I_b + I_s = (K_b + K_s) \Omega \quad (5.2)$$

The subscripts  $b$  and  $s$  denote bedload and suspended load, respectively. In vertically two-dimensional steady flow, he reasoned to get

$$K_b = \frac{\epsilon_b}{\tan \phi - \tan \beta} \quad (5.3)$$

$$K_s = \frac{\epsilon_s \cdot (1 - \epsilon_b)}{w_{sf}/\bar{U}_s - \tan \beta} \quad (5.4)$$

Here, the balance between turbulent diffusion and the settling of sediments are assumed for the suspended sediment transport.  $\epsilon$  is the efficiency,  $\tan \beta$  is the bed slope,  $\tan \phi$  is the angle of

repose,  $w_{sf}$  is the settling velocity, and  $\bar{U}_s$  is the mean flow velocity.

The above idea was extended to the oscillatory flows (Bagnold, 1963). Because of the horizontally two-dimensional features of the oscillatory flows, the transport rate in the direction  $\theta$  is given by

$$I = K' \Omega u_\theta / U_o \quad (5.5)$$

where  $u_\theta$  is the velocity in the direction  $\theta$  measured at the same height as the orbital velocity  $U_o$ . Bailard and Inman (1981) extended this to the total load transport. They treated both the instantaneous transport rate  $\vec{I}_t$  and the coefficient  $\vec{K}_t$  as vectors:

$$\vec{I}_t = \vec{K}_t \Omega \quad (5.6)$$

Here, the subscript  $t$  denotes the instantaneous values. For the bedload transport, they regarded the contributions coming from two parts, that is, a velocity induced transport directed parallel to the instantaneous velocity  $\vec{u}_t$  and a gravity-induced transport directed downslope. For  $\frac{\tan \beta}{\tan \phi} \ll 1$ , they derived

$$\vec{K}_{bt} = \frac{\epsilon_b}{\tan \phi} \left( \frac{\vec{u}_t}{|\vec{u}_t|} + \frac{\tan \beta}{\tan \phi} \hat{i} \right) \quad (5.7)$$

Bailard (1981) extended the same arguments for the suspended sediment transport:

$$\vec{k}_{st} = \epsilon_s \frac{|\vec{u}_t|}{w_{sf}} \left( \frac{\vec{u}_t}{|\vec{u}_t|} + \epsilon_s \tan \beta \frac{|\vec{u}_t|}{w_{sf}} \hat{i} \right) \quad (5.8)$$

Assuming quadratic shear stress

$$\vec{\tau}_t = \rho C_D |\vec{u}_t| \vec{u}_t \quad (5.9)$$

where  $\rho$  is the fluid density and  $C_D$  is a drag coefficient, the local rate of energy dissipation becomes

$$\begin{aligned} \Omega &= \vec{\tau}_t \cdot \vec{u}_t \\ &= \rho C_D |\vec{u}_t|^3 \end{aligned} \quad (5.10)$$

Here, we have to note that the formulation given by equation (5.9) is different from the shear stress obtained from our wave-current boundary layer model given by equation (3.99). Now, combining equations (5.7), (5.8), and (5.10) and substituting into equation (5.6), we get

$$\begin{aligned} \vec{\tau}_t &= \rho C_D \left[ \frac{\epsilon_b}{\tan \phi} \left( |\vec{u}_t|^2 \vec{u}_t + \frac{\tan \beta}{\tan \phi} |\vec{u}_t|^3 \hat{i} \right) \right. \\ &\quad \left. + \frac{\epsilon_s}{w_{sf}} \left( |\vec{u}_t|^3 \vec{u}_t + \frac{\epsilon_s}{w_{sf}} \tan \beta |\vec{u}_t|^5 \hat{i} \right) \right] \end{aligned} \quad (5.11)$$

Bowen (1980) postulated that the velocity is decomposed into basically the mean and the sinusoidal oscillatory flows. Guza and Thornton (1985) argued about the assumption of sinusoidal flows and instead proposed the use of random sea model. In the same context, the forcings are decomposed according to their time scales. On the inner continental shelf, the complication of hydrodynamics are represented by a quasi-steady motion, low-frequency motion related to the wave-groupiness, and the high-frequency motion related to the gravity waves.



### 5.3. Velocity moments

Because the agitation of sediments is mainly given by the stress exerted by waves, it is tempting to normalize the terms in the equation (5.11) by the wave orbital velocity,  $U_m$ .

$$U_m^2 = 2 (\langle u_w^2 \rangle + \langle v_w^2 \rangle) \quad (5.12)$$

Corresponding to the wave orbital velocity, define a magnitude of mean current.

$$\bar{u}_t^2 = u_c^2 + v_c^2 \quad (5.13)$$

Then, we can compare the strength of current with wave by the following parameters.

$$\delta = \frac{\bar{u}_t}{U_m} \quad (5.14)$$

$$\delta_u = \frac{u_c}{U_m} \quad (5.15)$$

$$\delta_v = \frac{v_c}{U_m} \quad (5.16)$$

Now, define higher moments.

$$\psi_0 = \frac{\langle |\vec{u}_t|^2 \rangle}{U_m^2} \quad (5.17)$$

$$\psi_1^* = \frac{\langle |\vec{u}_t|^2 u_w \rangle}{U_m^3} \quad (5.18)$$

$$\psi_1' = \frac{\langle |\vec{u}_t|^3 \rangle}{U_m^3} \quad (5.19)$$

$$\psi_2^* = \frac{\langle |\vec{u}_t|^3 u_w \rangle}{U_m^4} \quad (5.20)$$

$$\psi_3 = \frac{\langle |\vec{u}_t|^5 \rangle}{U_m^5} \quad (5.21)$$

Then, the x-component of equation 5.11 becomes

$$\langle I_x \rangle = \rho C_D U_m^3 \left( \frac{\epsilon_b}{\tan \phi} \left[ \psi_0 \delta_u + \psi_1^* + \psi_1' \frac{\tan \beta}{\tan \phi} \right] + \frac{\epsilon_s}{w_{sf}} \cdot U_m \left[ \psi_1' \delta_u + \psi_2^* + \psi_3 \tan \beta \cdot \frac{\epsilon_s}{w_{sf}} \cdot U_m \right] \right) \quad (5.22)$$

Skewness terms  $\psi_1^*$  and  $\psi_2^*$  determine the contribution of periodic flows in the sediment transport through bedload and suspended load, respectively.  $\psi_0$  represents the agitation of bed materials by wave

stresses, whereas  $\psi_1'$  and  $\psi_3$  appear to be related to turbulent energy dissipation. The magnitude of steady current transport relative to wave carriage and the direction in on-offshore advection is represented by the magnitude and the sign of  $\delta_u$ .

Gravitational effects depend mainly on the slope of bottom. Near bottom, turbulence term  $\psi_1'$  enhances the gravitational effects, where as the angle of repose ( $\tan \phi = 0.47$ ) gives restriction to this activity. Away from bottom, gravity flows become complicated by many factors such as turbulent diffusion, wave advection, and settling of sediment particles due to gravity. For the calculation of immerse-weight transport rate, we adopted  $\epsilon_b = 0.21$ ,  $\epsilon_s = 0.025$ ,  $\tan \phi = 0.63$ ,  $\tan \beta = 0.01$ , and  $w_{sf} = 0.0065$  m/sec following Bailard (1981). Drag coefficients are calculated based on Sternberg's (1968)  $C_D(1.0 \text{ m}) = 4.1 \times 10^{-3}$ , thus  $C_D(0.2 \text{ m}) = 7.3 \times 10^{-3}$ . Here,  $C_D$  does not cover waves but currents.

#### 5.4. Application of the energetics model to field data

Table 8 shows the velocity moments calculated for the low energy condition. For bedload transport,  $\psi_0$  and  $\psi_1^*$  are of the same order of magnitude. Because  $\delta_u$  representing relative strength of current to wave is less than 0.1, the mean transport  $\psi_0\delta_w$  for bedload is smaller than the wave transport term  $\psi_1^*$  by an order of magnitude. For suspended load,  $\psi_1'\delta_u$  is also smaller than  $\psi_2^*$ . This implies that the net transport is governed by waves. Figure 37 shows the time variation of immersed weight transport rate calculated. Most of the times, the directions of transport by mean flow and waves are the same. The calculation based on the average values of velocity moments show that the onshore transport prevails, seemingly related to the wave asymmetry.

Table 9 tabulates the calculated velocity moments under high energy condition, moments representing transport by mean flow  $\psi_0$  and  $\psi_1'$  are both higher than  $\psi_1^*$  and  $\psi_2^*$  by two order of magnitudes. As the storm activity increases, the  $\delta_u$  value increases in magnitude by an order of magnitude. This seems to be related to downwelling. Overall sediment transport rate is proportional to  $U_m^3$  which increases by several factors toward the onset of storm. Total rate of transport is increased by two orders of magnitude. Figure 38 shows the time variations of calculated transport rate. Offshore transport by mean current is dominant. Onshore transport by waves is overwhelmed by the offshore transport by mean flow.

Table 8. Calculated moments for fair weather portion

Hour	$\psi_0$	$\psi_1^*$	$\psi_1'$	$\psi_2^*$	$\psi_3$	$\delta_u$	$U_m$
0	0.5102	-0.1610	0.7265	-0.4002	2.3403	-0.0452	0.1347
4	0.5086	-0.0938	0.7496	-0.2409	2.6780	-0.0523	0.1257
8	0.5004	-0.0111	0.7401	-0.0482	2.5315	0.0097	0.1322
12	0.5204	-0.3024	0.8721	-0.8202	5.2399	-0.1218	0.1222
16	0.5061	-0.2032	0.7507	-0.4548	2.7676	-0.0716	0.0942
20	0.5264	0.0228	0.7365	0.0295	2.1350	0.0388	0.1010
24	0.5036	-0.0007	0.6895	-0.0408	1.8578	0.0363	0.0974
28	0.5114	0.1083	0.7343	0.2188	2.3106	0.0468	0.0875
32	0.5200	0.0485	0.7488	0.0703	2.3935	0.0499	0.0873
36	0.5312	-0.2187	0.7385	-0.4601	2.0654	-0.0739	0.0900
40	0.5201	-0.2074	0.7462	-0.4618	2.3557	-0.0694	0.0787
Average	0.5137	-0.0926	0.7484	-0.2371	2.6068	-0.0230	0.1046

\*  $U_m$  is in m/sec.

Figure 37 Immersed weight transport rate for suspended load, fair weather portion. The unit is in W/m.

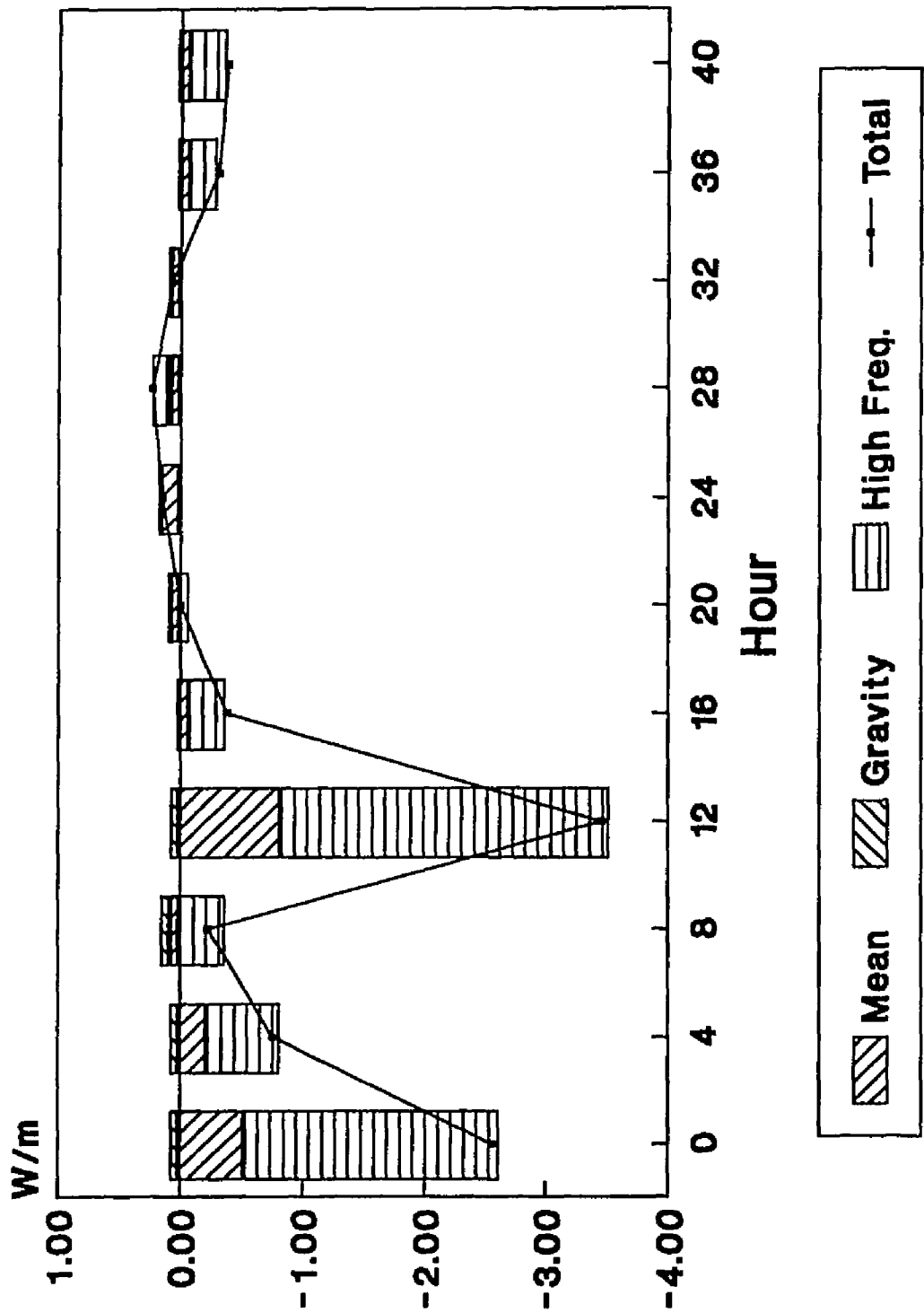


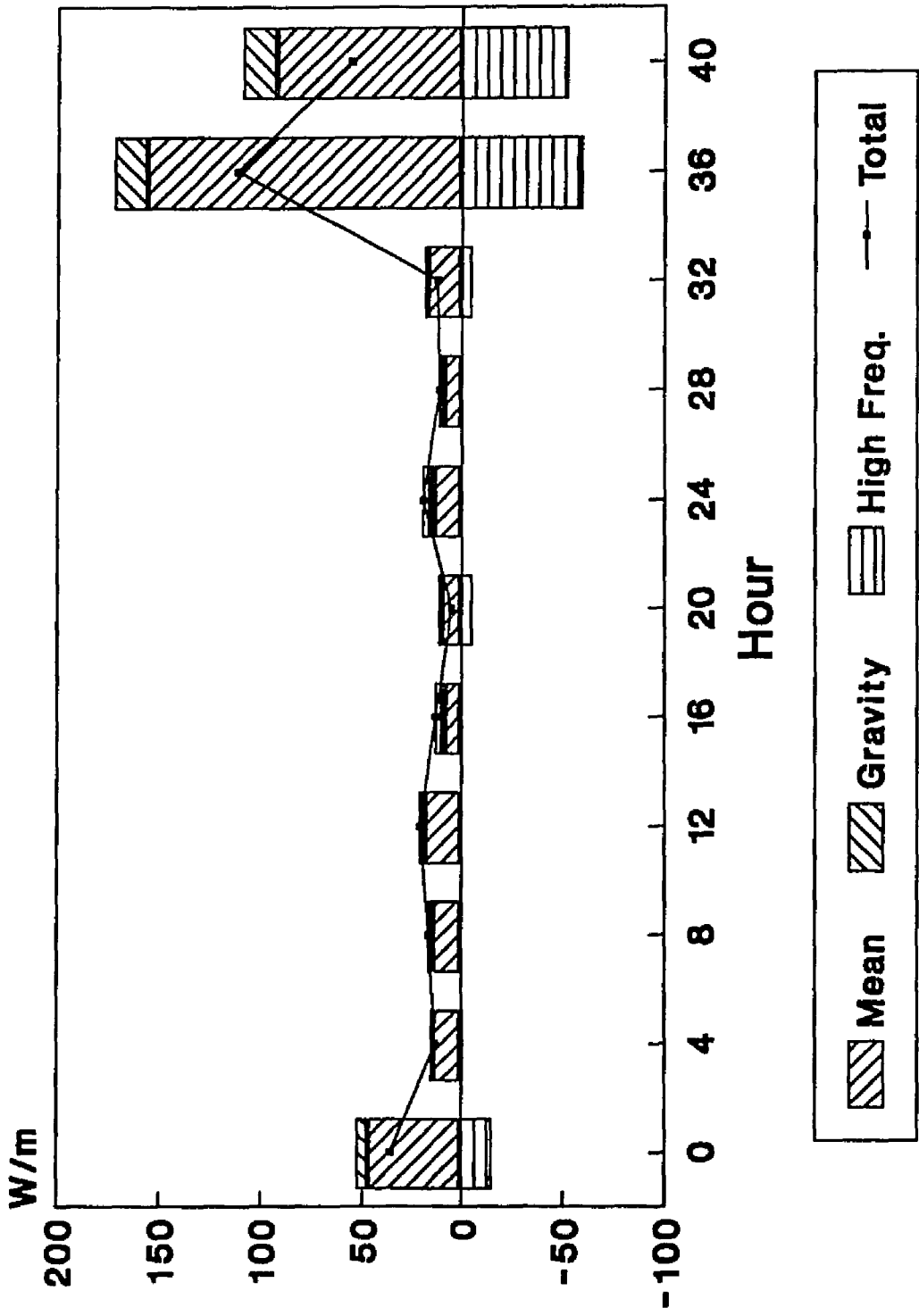
Table 9. Calculated moments for storm weather portion

Hour	$\psi_0$	$\psi_1^*$	$\psi_1'$	$\psi_2^*$	$\psi_3$	$\delta_u$	$U_m$
0	0.6740	-0.0557	0.7240	-0.1119	1.1770	0.2139	0.4443
4	0.6340	-0.0088	0.6774	-0.0224	1.1376	0.1710	0.3481
8	0.6596	-0.0024	0.7165	-0.0276	1.2588	0.1965	0.3378
12	0.6972	0.0022	0.7481	-0.0301	1.2541	0.2210	0.3433
16	0.5542	0.0175	0.5829	0.0224	1.0101	0.1236	0.3438
20	0.5635	-0.0095	0.5811	-0.0269	0.9025	0.1027	0.3837
24	0.6022	0.0208	0.6351	0.0273	1.0170	0.1341	0.3792
28	0.5572	-0.0020	0.5856	-0.0038	0.9400	0.1022	0.3662
32	0.7299	-0.0125	0.8148	-0.0497	1.4725	0.1986	0.3416
36	0.9800	-0.0693	1.1475	-0.1475	2.0030	0.3050	0.4925
40	0.6773	-0.0463	0.7103	-0.0802	1.0391	0.1635	0.5639
Average	0.6663	-0.0151	0.7203	-0.0409	1.2011	0.1756	0.3949

\*  $U_m$  is in m/sec.



Figure 38 Immersed weight transport rate for suspended load, storm portion. The unit is in W/m.



## 5.5 Discussion

Models of cross-shore sediment exchange processes over a shoreface have been developed by several researchers. Niedora et al. (1984) concentrate on the bedload transport under storm events and develop a model in which coastal storms induce offshore transport of sediments over the entire shoreface. They relate the source of power to the initial stage of storms yielding high local waves and offshore bottom currents due to downwelling. Swift et al. (1985) depicted the different mechanisms between fair weather and storm weather processes. They related the fair weather onshore transport to asymmetrical shoaling waves and the storm weather offshore transport to suspension by storm waves and subsequent carriage by wind-driven offshore flow.

Inman and Bowen (1963) demonstrated the possibility of an offshore transport due to ripple asymmetry and resulting differences in wave-induced vortices. Horikawa et al. (1977) classified sediment transport patterns due to wave action into four types according to the dominant transport mode and the role of ripples. Nielsen (1979) depicted possible shifts of phase angle between instantaneous suspended sediment concentration and instantaneous velocity, resulting in the transport in the opposite direction with respect to the net current or wave-induced mass transport. Shi and Larsen (1984) discuss the effect of wave groupiness which causes the net offshore transport. Wright (1987) examined the diabathic transport mechanisms and showed the roles of variable sources of

power such as waves, rip currents, wind-induced currents, tidal currents, gravity, and wave-current interactions.

From the calculated immersed weight transport rate, the role of waves seems to be substantial in case of low energy flow conditions. To give more details on this, sediment flux at the height of 15 cm from the bottom is calculated as the product of the cross-shore velocity measured at 20 cm above bottom and the concentration measured at 15 cm above bottom. Decomposing and averaging over burst period, the flux is again decomposed into the mean transport and transport by wave.

$$\langle q_x \rangle = u_c C_m + \langle u_w C_p \rangle \quad (5.23)$$

Under both the high and the low energy conditions, the net flux is governed by the transport of mean concentration by mean current (Figures 39 and 40). Comparing with the net transport rate (Figures 37 and 38), we see the trends are the same both for the transport rates calculated from energetics model and the fluxes calculated from the measurement of suspended sediment concentration and flow velocity.

Direct comparison of the flux and the transport rate may not be valid. But, we can compare two results at least on the qualitative basis. Our main purpose is to reveal the direction of sediment transport process. In this context, we believe that the transport rate calculated gives satisfactory explanation on the relative contributions of advective mechanisms and the direction of net

Figure 39 Suspended sediment flux, fair weather portion. The unit is in  $\text{g}/\text{cm}^2/\text{sec}$ .

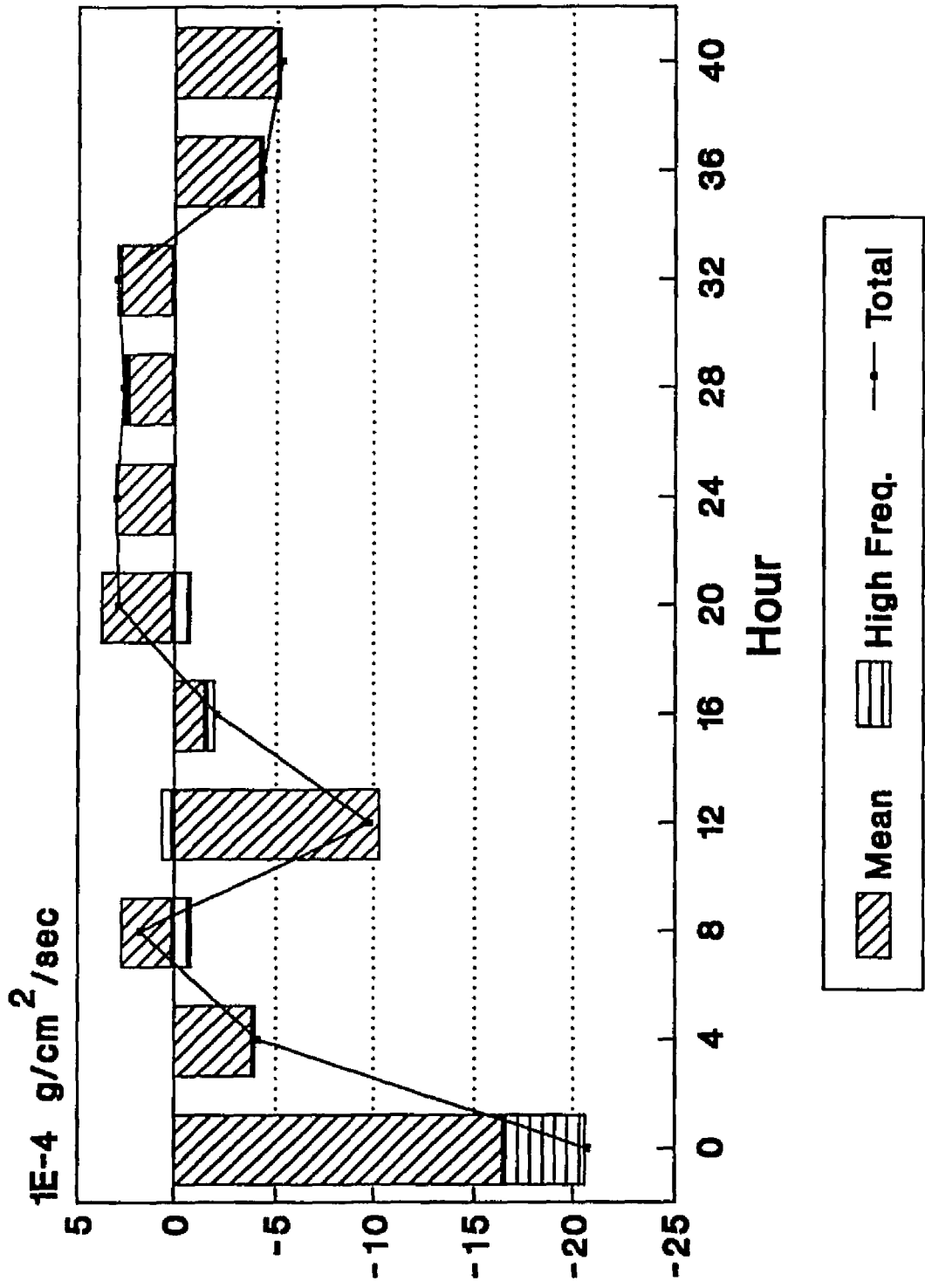
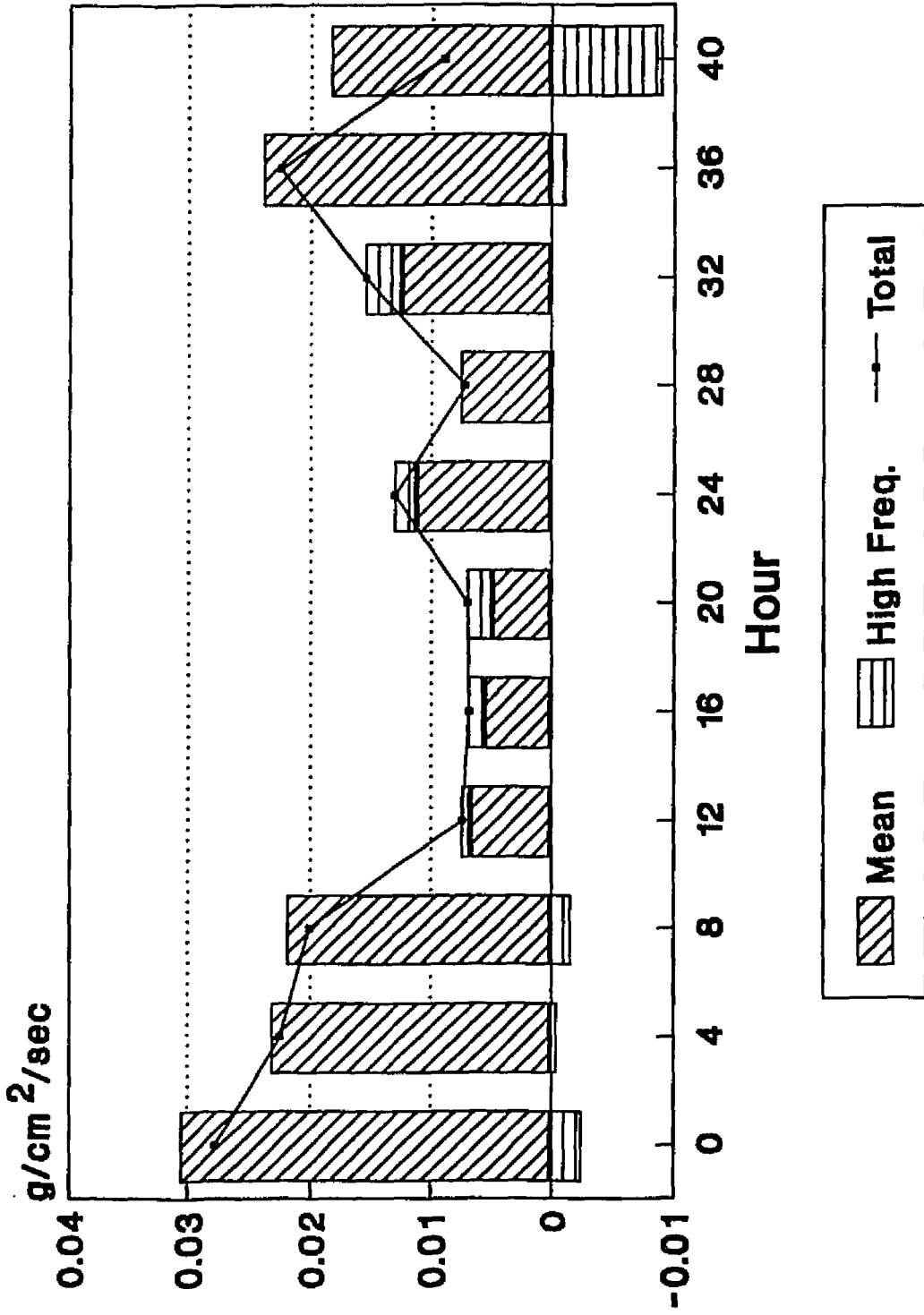


Figure 40 Suspended sediment flux, storm portion. The unit is in  $\text{g/cm}^2/\text{sec}$ .





transport. However, the parameters in the model are site specific thus we need to obtain the values from empirical data. And, it is hard to model higher moments even for simple equilibrium cases (see, for example, Bailard, 1981). The calibration of model parameters is limited by the quantity and the quality of data available. This model is a depth integrated model, thus it provides no details on the vertical distribution of suspended sediment flux. We can compensate this by using a different view such as the model developed in the previous chapters.

The mean transport rate is the depth integration of the product of mean velocity and mean concentration. the mean velocity is given in the equations (3.71) and (3.75), whereas the mean concentration is given by the equations (4.31) and (4.32). Then, the net cross-shore transport rate  $\langle Q_x \rangle$  is

$$\langle Q_x \rangle = \langle Q_x \rangle_{-\delta} + \langle Q_x \rangle_{+\delta} \quad (5.24)$$

Here, the subscripts  $-\delta$  and  $+\delta$  represent the integration upto the top of the wave boundary layer,  $\delta_w$ , and the integration from  $\delta_w$  to the mean sea surface,  $h$ . The transport rate inside the wave boundary layer is given as

$$\begin{aligned} \langle Q_x \rangle_{-\delta} &= \int_{z_r}^{\delta_w} u_c C_m dz \\ &= \int_{z_r}^{\delta_w} \frac{u_{*2}}{u_{*1}} \frac{u_{*2,x}}{\kappa} \ln\left(\frac{z}{z_0}\right) C_r \left(\frac{z}{z_r}\right)^{-w_{sf}/\kappa(u_{*1}+V)} dz \end{aligned}$$

$$- B^* \int_{z_r^*}^{\delta_w^*} (z^*)^{A^*} \ln(z^*) dz^* \quad (5.25)$$

where

$$z^* = z/z_0 \quad (5.26)$$

$$A^* = - w_{sf} / \kappa (u_{*1} + V) \quad (5.27)$$

$$B^* = \frac{u_{*2}}{u_{*1}} \frac{u_{*2,x}}{\kappa} z_0 C_r \left(\frac{z_0}{z_r}\right)^{A^*} \quad (5.28)$$

Solving equation (5.25), we have

$$\begin{aligned} \langle Q_x \rangle_{-\delta} = & \frac{B^*}{A^* + 1} \left[ \delta_w^* \left( \ln(\delta_w^*) - \frac{1}{A^* + 1} \right) \right. \\ & \left. - z_r^* \left( \ln(z_r^*) - \frac{1}{A^* + 1} \right) \right] \quad (5.29) \end{aligned}$$

The transport rate above the wave boundary layer is given by

$$\begin{aligned} \langle Q_x \rangle_{+\delta} = & \int_{\delta_w}^h u_c C_m dz \\ = & \int_{\delta_w}^h \frac{u_{*2,x}}{\kappa} \ln\left(\frac{z}{z_1}\right) C_m(\delta_w) \left(\frac{z}{\delta_w}\right)^{-w_{sf}/\kappa(u_{*2}+V)} \\ = & D^* \int_{\delta_w^*}^{h^*} (z^*)^{C^*} \ln(z^*) dz^* \quad (5.30) \end{aligned}$$

where

$$z^* = z/z_1 \quad (5.31)$$

$$C^* = - w_{sf}/\kappa(u_{*2}+V) \quad (5.32)$$

$$D^* = \frac{u_{*2,x}}{\kappa} z_1 C_m(\delta_w) \left(\frac{z_1}{\delta_w}\right) C^* \quad (5.33)$$

The solution is

$$\begin{aligned} \langle Q_x \rangle_{+\delta} = & \frac{D^*}{C^* + 1} \left[ h^* \left( \ln(h^*) - \frac{1}{C^* + 1} \right) \right. \\ & \left. - \delta_w^* \left( \ln(\delta_w^*) - \frac{1}{C^* + 1} \right) \right] \end{aligned} \quad (5.34)$$

The transport rate from the energetics model is given by

$$\langle Q_x \rangle_{\text{energetics}} = \frac{\rho_w C_D U_m^4 \frac{\epsilon_s}{sf} \psi_1' \delta_u}{(\rho_s - \rho) g N} \quad (5.35)$$

Bailard (1982) provides the available bed material,  $N = 0.6$ . In Figures 41 and 42, the transport rate predicted from the energetics model is compared with  $\langle Q_x \rangle$  for low- and high energy conditions, respectively. Both fair and storm conditions show that the energetics model gives the same direction of transport but the amount is low by an order compared with the transport rate,  $\langle Q_x \rangle$ .

Figure 41 Comparison of transport rates calculated by the integration of flux and the energetics approach, fair weather portion. The unit is in g/cm/sec.

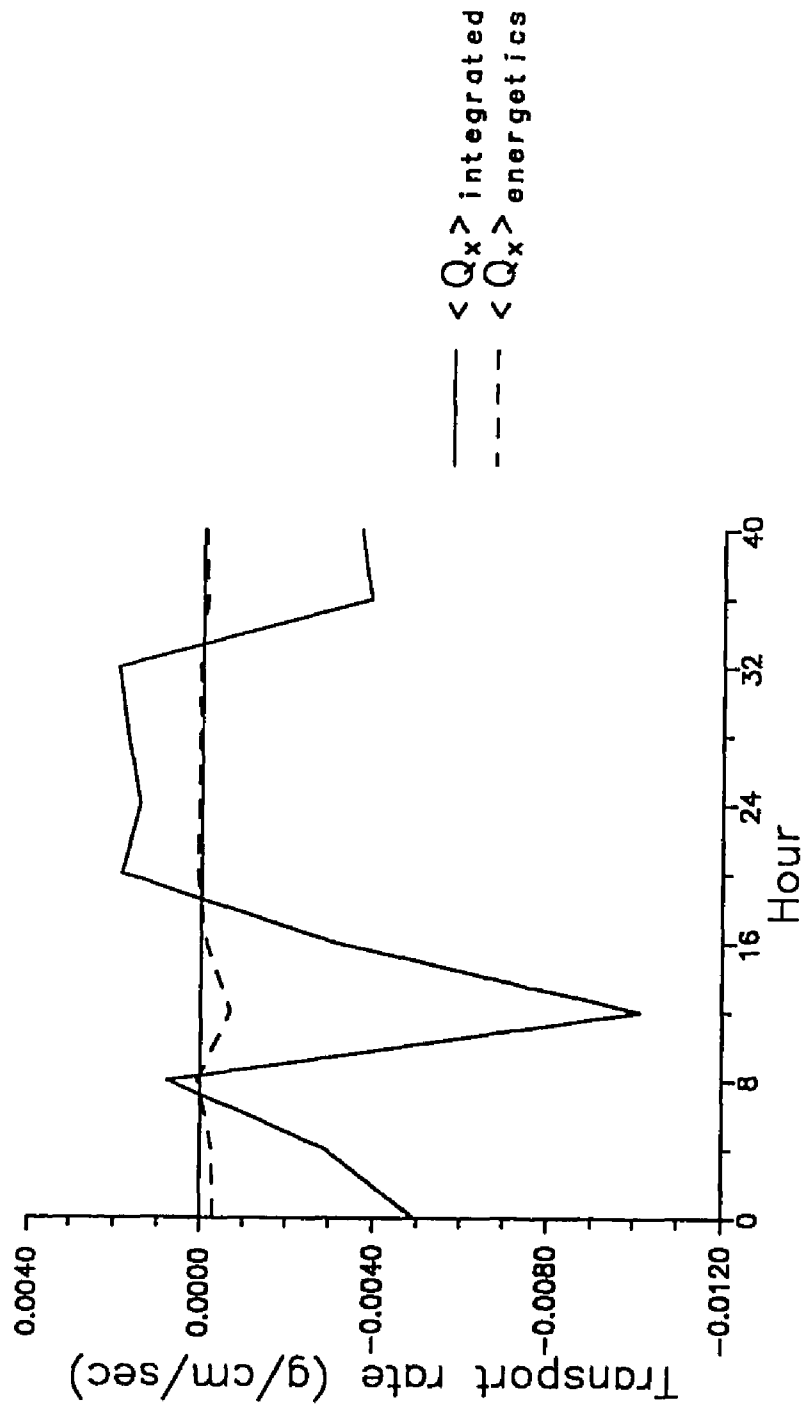
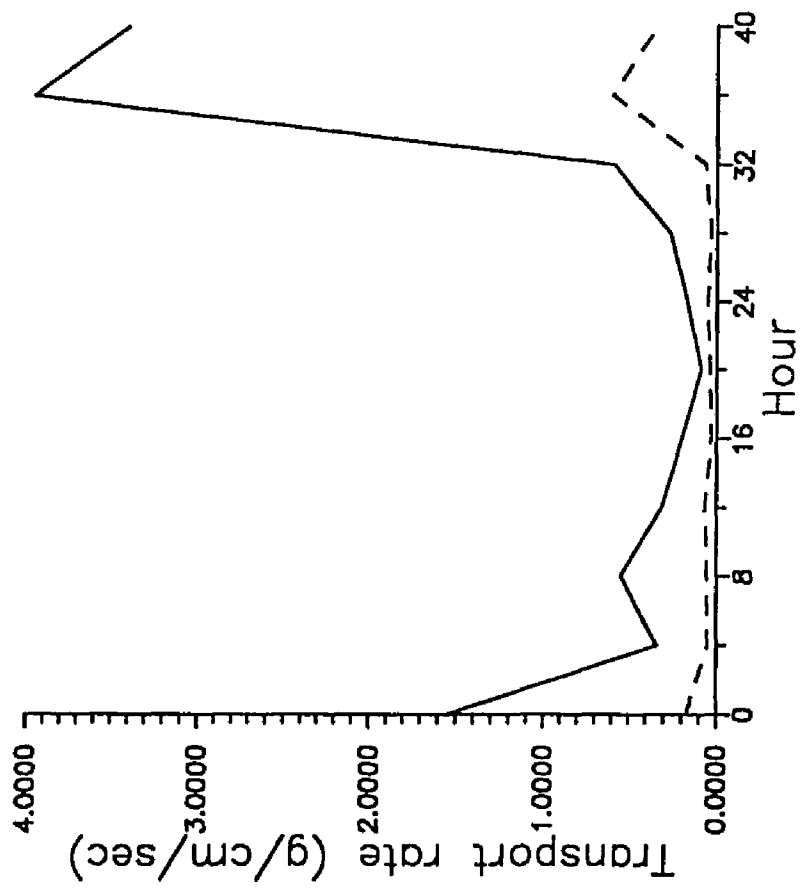


Figure 42 Comparison of transport rates calculated by the integration of flux and the energetics approach, storm portion. The unit is in g/cm/sec.



—  $\langle Q_x \rangle$  integrated  
- - -  $\langle Q_x \rangle$  energetics

Figures 43 and 44 shows the ratios between the transport rates inside and outside the wave boundary layer. The increase of the ratio is apparent for the high energy condition. The ratio vary between 1 and 10. This notes that the transport rate predicted from the energetics model is low by an order. The coefficients, especially the efficiency factor  $\epsilon_s$  and  $\epsilon_b$ , are given by the calculations in the surf zone. Because the dynamics over a shore face is different from the dynamics inside the surf zone, we have to calibrate the coefficients.

The cross-correlations between horizontal velocity and suspended sediment concentration give light to the study of the advection mechanism. Figure 45 shows the strong correlation between onshore velocity and high suspended sediment concentration thus implies the possible onshore transport by the wave advection. Both the transport rate (Figure 38) and the flux (Figure 40) show the dominant role of mean current over wave for transport under high energy condition. Therefore, we can conclude that the offshore transport by mean current supersedes the onshore transport by waves by an order under high energy condition.

Figure 46 shows that the sediment concentration is insignificantly related with cross-shore velocity. In addition to the low correlation coefficient, the lags between the advective velocity and the concentration implies that the role of waves for the transport is still not clear. We may use the first-order approximation for the flux calculation in case of high energy environment but a caution must be given for the low energy



Figure 43 The ratio between  $\langle Q_x \rangle_{+\delta}$  and  $\langle Q_x \rangle_{-\delta}$ , fair weather portion. The ratio is  $\langle Q_x \rangle_{-\delta} / \langle Q_x \rangle_{+\delta}$ .

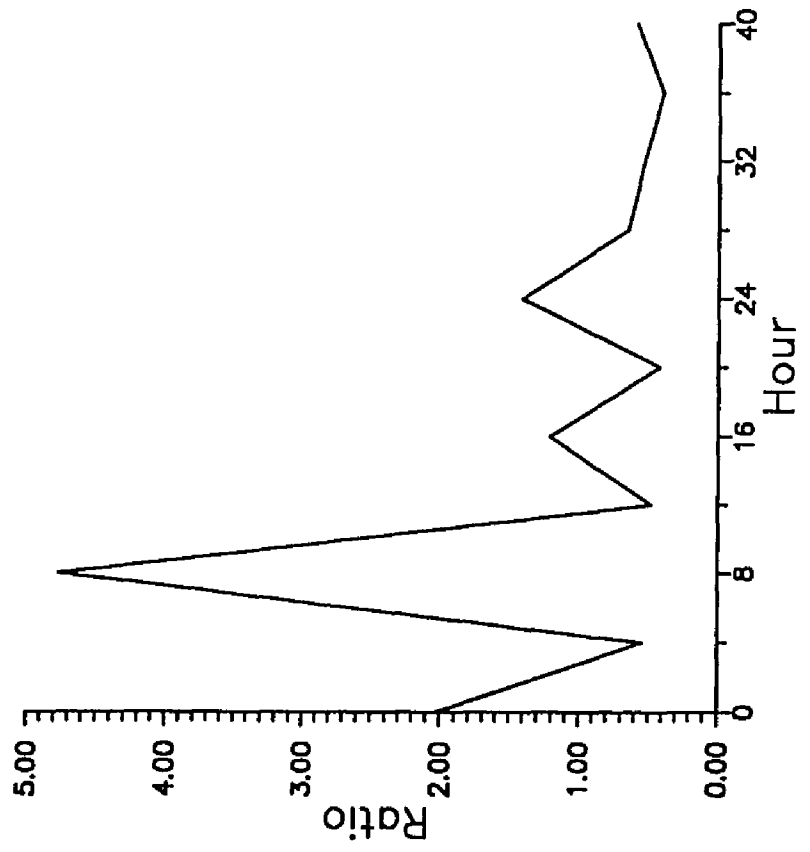


Figure 44 The ratio between  $\langle Q_x \rangle_{+\delta}$  and  $\langle Q_x \rangle_{-\delta}$ , storm portion. The ratio is  $\langle Q_x \rangle_{-\delta} / \langle Q_x \rangle_{+\delta}$ .

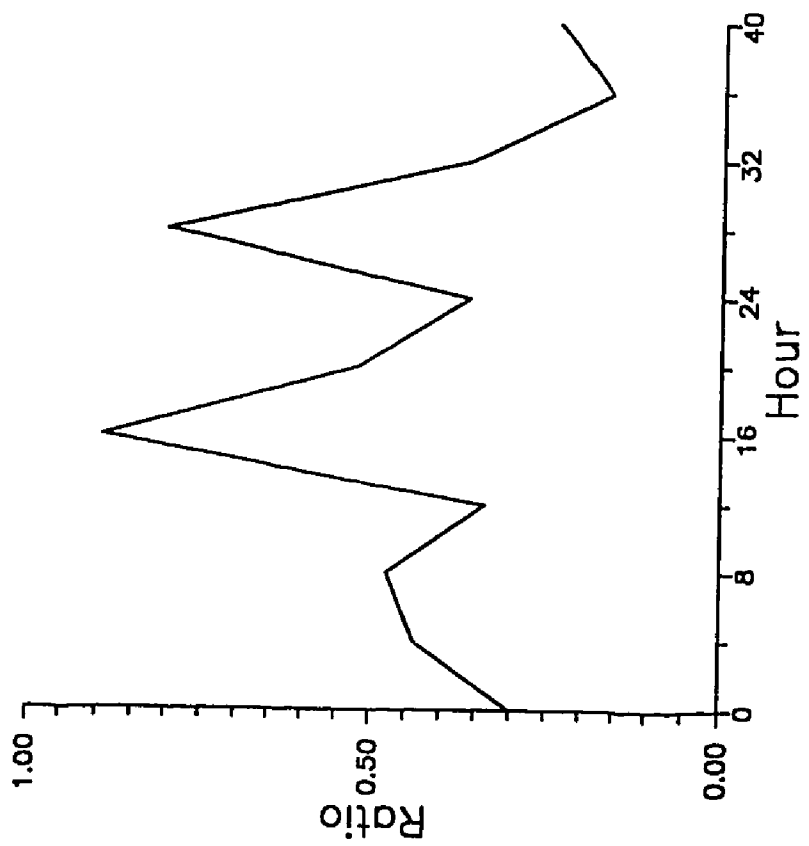


Figure 45 Cross-correlations between cross-shore velocity and suspended sediment concentration, storm condition.

Cross  
Correlation  
U vs. C

Duck'85  
Storm

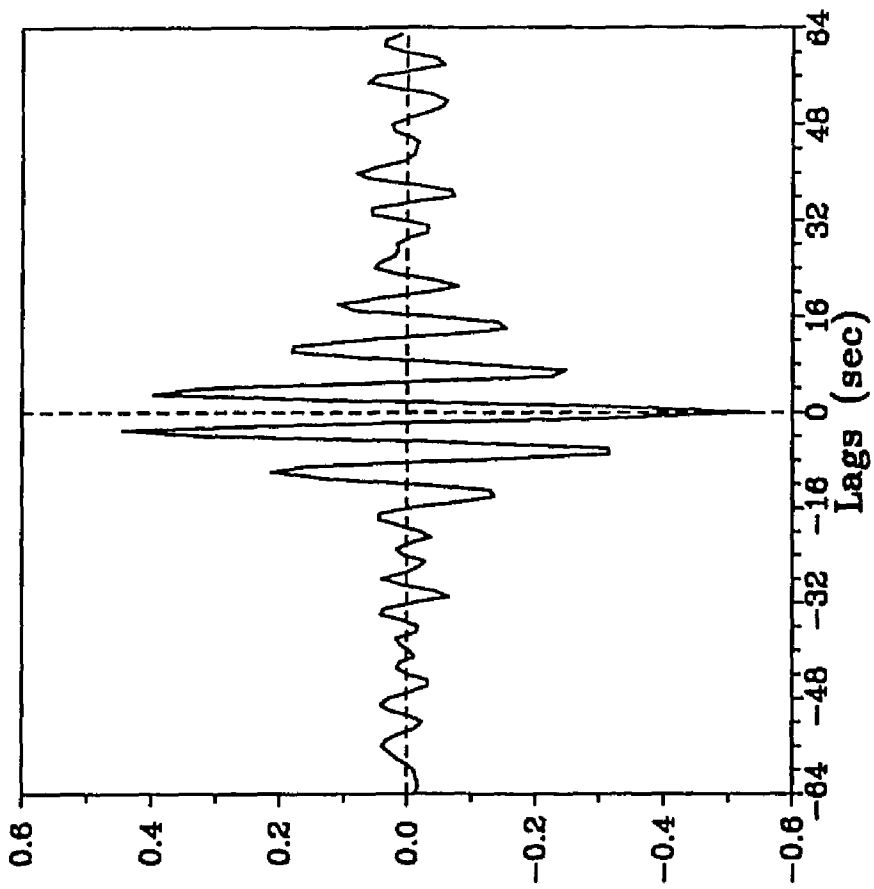
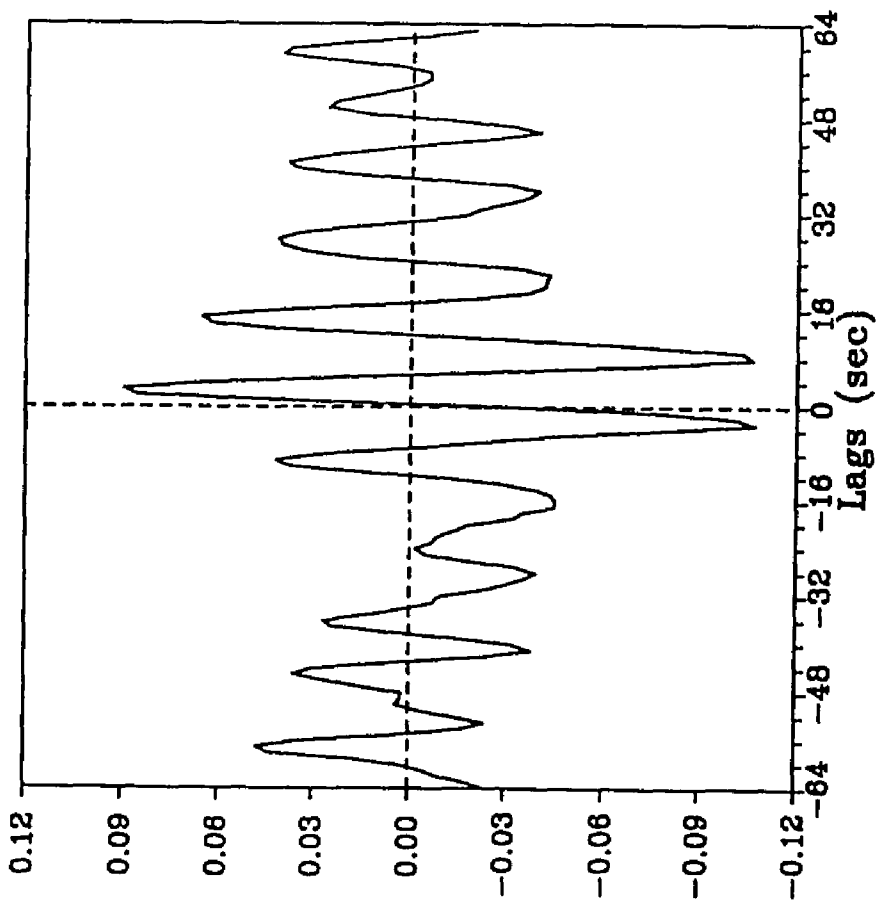


Figure 46 Cross-correlations between cross-shore velocity and  
suspended sediment concentration, fair weather condition.

Cross  
Correlation  
U vs. C

Duck'85  
Fair weather





environment case. However, there is no criteria to determine the applicability of the approximation of flux. Because an energetics model can not resolve the phase relationships, it is possible the transport by waves under low energy condition may be overestimated. The transport rate for high energy condition is high by an order of magnitude compared to the transport rate for low energy condition. Thus, still with the uncertainty of the role of mean flow and waves under fair weather condition, the transport rate under the low energy condition is also estimated by the first order approximation, that is, the product of mean concentration by mean flow velocity. A norm for the suspended sediment transport under low energy condition is that the direction varies but the net transport is usually onshore.

## 6. SUMMARY AND CONCLUSION

The data set from the Duck'85 experiment span from fair to storm weather conditions. During the storm period, waves propagate toward shoreline and force onshore transport while wind-driven offshore currents dominate the offshore transport. Under fair weather conditions, the mean flow has variable sources such as tidal currents, mass transport, and amplitude modulated low frequency waves. The contribution and directionality of each flow components are complex.

Wave boundary layer model shows that the distribution of eddy viscosity outside boundary layer does not affect much on the prediction of maximum bottom shear stress. The simple eddy viscosity assumption gives almost the same prediction of bottom shear stress as the prediction from more complicated distribution function for eddy viscosity.

A simple two-layer time-invariant eddy viscosity model, in which thin wave boundary layer is nested within the bottom of thick current boundary layer, satisfactorily reproduce bottom shear stress and current. The change in angle between wave propagation and current direction affects the bottom shear stress in such a way that the bottom shear stress is minimum with perpendicular and maximum with parallel wave to current. The change in bottom shear stress is about an order of magnitude increase toward the onset of storm.

The lags between bottom stress exerted on the bed materials and the responding sediment suspension complicate the applicability of diffusion model in case of fair weather condition. The high cross-correlation with zero time lag is observed for the storm weather processes. The variations of the mean concentration conform with the variations of mean shear stresses under both the high and the low energy conditions. This validates the use of diffusion model for the mean concentration. The diffusivity originates mostly from turbulence in case of storm events whereas the effect of bedform geometry and wave advection become important modification factors. The modification of turbulent diffusion from the other factors such as vortex bursting and sediment-induced stratification are resolved into a velocity scale  $V$  for which an empirical formulation is given for a wide range of energy conditions. The diffusivity is given by

$$\begin{aligned} \nu_{ts} &= \kappa (u_{*1} + V) && \text{for } z \leq \delta_w \\ &\kappa (u_{*2} + V) && \text{for } z \geq \delta_w \end{aligned} \quad (6.1)$$

where

$$V = -0.25 u_{*1} + 1.4 \quad (6.2)$$

The total diffusion is greater than turbulent diffusion under low energy condition and smaller under high energy condition.

The revision of the laboratory data of Kalkanis (1964) and Abou-Seida (1965) results in the linear relationships between the reference concentration,  $C_r$ , and the excess Shields parameter,  $\theta_{ex}$ .

$$C_r = 0.09 \theta_{ex} \quad (6.3)$$

This suggests the use of the linear relationships between  $C_r$  and the excess shear stress,  $S$ .

$$C_r = \frac{\gamma \cdot C_b \cdot S}{1 + \gamma \cdot S} \quad (6.4)$$

The test over a set of different reference concentration model shows that the resuspension coefficient,  $\gamma$ , varies with different flow conditions. Under the high flow conditions, the  $\gamma$  calculated from the measurements at different levels are invariant. The decrease in  $\gamma$  with increasing flow intensity is observed, which may be related with the armoring effect. Especially, with rapid increase flow intensity, the reduction in  $\gamma$  value is apparent. The data set, however, does not provide enough background to give any quantitative expression of  $\gamma$ , suggesting necessity of more data. The  $\gamma$  is given as 0.0003 for high energy condition and 0.002 for low energy condition. The model developed shows good agreement with the measured concentration. The limitation of the model is that the model does not resolve the horizontal advection and that the model is not working well in case of possible particle interaction.

With uncertainty of the contribution of mean flow for the suspended sediment transport under fair weather environment, the energetics model suggests that the onshore transport by waves might prevail for low-energy transport but the magnitude is low by an order of magnitude compared with the high-energy transport. The flux calculated from the measurement and the cross-correlation between the cross-shore velocity and concentration indicates the overestimation of the role of waves for the transport under low energy condition. Storm related strong mean current, related to the prevailing northeaster, is responsible to the offshore transport of sediments and dominate the process. The estimated transport rate from the integration of suspended sediment flux suggests that the energetics model can be used for the the study of sediment transport over an inner continental shelf only if the coefficients such as  $\epsilon_b$  and  $\epsilon_s$  be calibrated.

LITERATURE CITED

- Abou-Seida, H.M., 1965, Bedload function due to wave action. Rep. HEL-2-11, Hydraul. Eng. Lab., Univ. California, Berkeley, California, 78 pp
- Abramowitz, M. and Stegun, I., 1964, Handbook of mathematical functions, Nat'l Bureau of Standards Applied Math. Ser. 55, 1046 pp
- Adams, C.E. and Weatherly, G.L., 1981, Some effects of suspended sediment stratification on an oceanic bottom boundary layer. Jour. Geophys. Res. v.86, p 4161-4172
- Bagnold, R.A., 1956, The flow of cohesionless grains in fluids, Phil. Trans. Roy. Soc. London, A249, p 234-297
- Bagnold, R.A., 1963, Beach and nearshore processes. Part I. Mechanics of marine sedimentation. (ed by Hill, M.N.) The sea, Interscience, v.3, p 507-528
- Bailard, J.A., 1981, An energetics total load sediment transport model for a plane sloping beach. Jour. Geophys. Res. v.86, p 10938-10954
- Bailard, J.A., 1982, Modeling on-offshore sediment transport in the surfzone. Coast. Eng. 1981, ASCE, p 1419-1438

- Bailard, J.A. and Inman, D.L., 1981, An energetics bedload model for a plane sloping beach; local transport. Jour. Geophys. Res. v.86, p 2035-2043
- Bhattacharya, P.K., 1971, Sediment suspension in shoaling waves. Ph.D. Thesis, Univ. Iowa, Iowa, 100 pp
- Bowen, A., 1980, Simple models of nearshore sedimentation; beach profiles and longshore bars. (ed. by McCann, S.B.) The coastline of Canada, Geol. Surv. of Canada, Paper 80-10, p 1-11
- Brevik, I., 1981, Oscillatory rough turbulent boundary layers. Jour. Waterways, Port, Coastal and Ocean Div., ASCE, v.107, p 175-188
- Businger, J.A. and Arya, S.P.S., 1974, Height of the mixed layer in the stably stratified planetary boundary layer. Advances in Geophysics, Academic Press, New York, p 73-92
- Cacchione, D.A. and Drake, D.E., 1982, Measurements of storm-generated bottom stresses on the continental shelf. Jour. Geophys. Res. v.87, p 1952-1961
- Chappell, J. and Eliot, I.G., 1979, Surf-beach dynamics in time and space - an Australian case study and elements of a predictive model. Mar. Geol. v.32, p 231-250

- Clark, T.L., Lesht, B., Young, R.A., Swift, D.J.P., and Freeland, G.L., 1982, Sediment resuspension by surface-wave action: An examination of possible mechanisms. Mar. Geol. v.49, p 43-59
- Clauser, F.H., 1956, The turbulent boundary layer. (ed. by Dryden, H.L. and von Karman, Th.) Advances in applied mechanics, v. IV, Academic Press, New York, p 1-51
- Collins, J.I., 1963, Inception of turbulence at the bed under periodic gravity waves. Jour. Geophys. Res. v.68, p 6007-6014
- Csanady, G.T., 1982, Gradation in the coastal ocean. D. Reidel, Dordrecht, Holland, 279 pp
- Dobbins, W.E., 1943, Effect of turbulence on sedimentation, ASCE Trans. Paper No. 2218, p 629-678
- Drake, D.E. and Cacchione, D.A., 1985, Seasonal variation in sediment transport on the Russian River Shelf, California. Cont. Shelf Res. v.4, p 495-514
- Drake, D.E. and Cacchione, D.A., 1989, Estimates of the suspended sediment reference concentration ( $C_a$ ) and resuspension coefficient ( $\gamma_0$ ) from near-bottom observations on the California Shelf. Cont. Shelf Res. v.9, p 51-64



- Einstein, H., 1950, The bed-load function for sediment transportation in open channel flow. U.S.Dept. of Agriculture, Soil Conservation Service Tech. Bull. 1026, 70 pp
- Glenn, S.M., 1983, A continental shelf bottom boundary layer model: The effects of waves, currents, and a moveable bed. Sc.D. Thesis, Mass. Inst. Tech., Woods Hole Oceanogr. Inst., Mass., 237 pp
- Glenn, S.M. and Grant, W.D., 1987, A suspended sediment stratification correction for combined wave and current flows. Jour. Geophys. Res. v.92, p 8244-8264
- Graf, W.H., 1971, Hydraulics of sediment transport. McGraw-Hill, New York, 513 pp
- Grant, W.D. and Madsen, O.S., 1979, Combined wave and current interaction with a rough bottom. Jour. Geophys. Res. v.84, p 1797-1808
- Grant, W.D. and Madsen, O.S., 1982, Moveable bed roughness in unsteady oscillatory flow. Jour. Geophys. Res. v.87, p 469-481
- Grant, W.D., Williams III, A.V., Glenn, S.M., and Cacchione, D.A., 1983, High frequency bottom stress variability and its prediction in the CODE region. Tech. Rep. 83-19, Woods Hole Oceanogr. Inst. and CODE Tech. Rep. 15, 72 pp

- Green, M.O., 1987, Low-energy bedload transport by combined wave and current flow on a southern Mid-Atlantic Bight shoreface, Ph.D. Thesis, The College of William and Mary, 162 pp
- Gross, T.F. and Nowell, A.R.M., 1983, Mean flow and turbulence scaling in a tidal boundary layer. Cont. Shelf Res. v.2, p 109-126
- Guza, R.T. and Thornton, E.B., 1985, Velocity moments in nearshore. Jour. Waterways, Ports Coastal and Ocean Eng., ASCE v.111, p 235-256
- Hattori, M., 1969, The mechanics of suspended sediment due to standing waves. Coast. Eng. in Japan v.12, p 69-81
- Hinze, J.O., 1959, Turbulence, McGraw-Hill, New York, 586 pp
- Homma, M. and Horikawa, K., 1963, Suspended sediment due to wave action, Proc. 8th Intn'l Conf. Coastal Eng., p 168-193
- Homma, M., Horikawa, K., and Kajima, R., 1965, A study on suspended sediment due to wave action. Coast. Eng. in Japan v.8, p 85-103
- Horikawa, K., 1981, Coastal sediment processes. Ann. Rev. Fluid Mech. v.13, p 9-32
- Horikawa, K. and Watanabe, A., 1968, Laboratory study on oscillatory boundary layer flow. Coast. Eng. in Japan v.11, p 13-28

- Hunt, J.N., 1969, On the turbulent transport of a heterogeneous sediment. *Quart. Jour. Mech. and Applied Math.* v.22, p 235-246
- Inman, D.L. and Bagnold, R.A., 1963, Beach and nearshore processes. Part II. Littoral processes. (ed. by Hill, M.N.) *The sea*, Interscience, v.3, p 529-553
- Jonsson, I.G., 1963, Measurements in the turbulent wave boundary layer. *Proc. 10th Congr. IAHR, London*, v.1, Paper 1.12, p 85-92
- Jonsson, I.G., 1966, Wave boundary layer and friction factors. *Proc. 10th Coast. Eng. Conf., ASCE*, p 127-148
- Jonsson, I.G., 1980, A new approach to oscillatory rough turbulent boundary layers. *Ocean Eng.* v.7, p 109-152
- Jonsson, I.G. and Carlsen, N.A., 1976, Experimental and theoretical investigations in an oscillatory turbulent boundary layer. *Jour. Hydraul. Res.* v.14, p 45-60
- Kachel, N.B. and Smith, J.D., 1986, Geological impact of sediment transporting events on the Washington Continental Shelf. (ed. by Knight, R.J. and McLean, J.R.) *Canadian Soc. Petroleum Geologist, Memoir II*, p 145-162
- Kajiura, K., 1968, A model of the bottom boundary layer in water waves. *Bull. Earthquake Res. Inst., Japan*, v.46, p 75-123

- Kalinske, A.A. and Pien, C.L., 1943, Experiments on eddy-diffusion and suspended material transportation in open channels. Trans. AGU Papers, Hydrology, p 530-536
- Kalkanis, G., 1964, Transportation of bed material due to wave action. Tech. Memo. No. 2, U.S. Army Corps of Engineers, Coastal Eng. Res. Center, 38 pp
- Kamphuis, J.W., 1975, Friction factor under oscillatory waves. Jour. Waterways, Harbors and Coastal Eng. Div., ASCE, v.101, p 135-144
- Kennedy, J.F. and Locher, F.A., 1972, Sediment suspension by water waves. (ed. by Meyer, R.E.) Waves on beaches and resulting sediment transport, Academic Press, New York, p 249-295
- Lane, E.W. and Kalinske, A.A., 1941, Engineering calculations of suspended sediment. Trans. AGU v.20, p 603-607
- Larsen, L.H., Sternberg, R.W., Shi, N.C., Marsden, M.A.H., and Thomas, L., 1981, Field investigations of the threshold of grain motion by ocean waves and currents. (ed. by Nittrouer, C.A.) Sedimentary dynamics of continental shelves, Elsevier, Holland, p 105-132
- Lavelle, J.W. and Mofjeld, H.O., 1983, Effects of time-varying viscosity on oscillatory turbulent channel flow. Jour. Geophys. Res. v.88, p 7607-7616

- Lesht, B.M., Clarke, T.L., Freeland, G.L., Swift, D.J.P., and Young, R.A., 1980, An empirical relationship between the concentration of resuspended sediment and near-bottom wave-orbital velocity. *Geophys. Res. Lett.* v.2, p 1049-1052
- Long, G.E., 1981, A simple model for time-independent stably stratified turbulent boundary layers. Spec. Rep. No. 95, Dept. Oceanogr., Univ. Washington, Washington, 170 pp
- Longuet-Higgins, M.S. Stewart, R.W., 1964, Radiation stresses in water waves; a physical discussion with applications. *Deep Sea Res.* v.11, p 529-562
- Mason, c., Birkemeier, W.A., and Howd, P.A., 1987, Overview of Duck85 nearshore processes experiment. (ed. by Kraus, N.) *Coastal sediments '87*, ASCE, p 818-833
- Mellor, G.L. and Yamada, T., 1974, A hierarchy of turbulence closure models for planetary boundary layers. *Jour. Atmosph. Sci.* v.31, p 1791-1806
- Monin, A.S. and Yaglom, A.M., 1971, *Statistical fluid dynamics*. MIT Press, Cambridge, Mass., 769 pp
- Myrhaug, D., 1982, On a theoretical model of rough turbulent wave boundary layers. *Ocean Eng.* v.9, p 547-565

- Niedora, A.W., Swift, D.J.P., Hopkins, T.S., and Ma, C.-M., 1984,  
Shoreface morphodynamics on wave-dominated coasts. Mar. Geol.  
v.60, p 331-354
- Nielsen, P., 1979, Some basic concepts of wave sediment transport.  
Inst. Hydrodyn. Hydraul. Eng., Tech. Univ. Denmark, Ser. Paper  
No.20, 160 pp
- Nielsen, P., 1981, Dynamics and geometry of wave-generated ripples.  
Jour. Geophys. Res. v.86, p 6467-6472
- Nielsen, P., 1983, Entrainment and distribution of different sand  
sizes under water waves. Jour. Sed. Petrol. v.53, p 423-428
- Nielsen, P., Green, M.O., and Coffey, F.C., 1982, Suspended sediment  
under waves. Coastal Studies Unit Tech. Rep. No 82/6, Univ.  
Sydney, Australia, 151 pp
- O'Brien, M.P., 1933, Review of the theory of turbulent flow and its  
relation to sediment-transportation. Trans. AGU, Rep. and  
Papers, Hydrology, p 487-491
- Press, W.H., Flannery, B.P., Tenkolsky, S.A., and Vetterling, W.T.,  
1986, Numerical recipes. Cambridge Univ. Press, London, U.K.,  
818 pp

- Rodi, W., 1980, turbulence models and their application in hydraulics - a state of the art review. IAHR State-of-the-Art Paper, DELFT, Holland, 104 pp
- Rouse, H., 1939, Experiments on the mechanics of sediment suspension. (ed. by Hartog, J.P.D. and Peters, H.) Proc. 5th Intn'l Congr. for Applied Mech., Wiley and Sons, New York, p 550-554
- Seymour, R.J., 1986, Nearshore autosuspending turbidity currents. Ocean Eng. v.13, p 435-447
- Shi, N.C., 1983, Reverse sediment transport induced by amplitude modulated waves. Ph.D. Thesis, Univ. Washington, Washington, 121 PP
- Shi, N.C. and Larsen, L.H., 1984, Reverse sediment transport induced by amplitude modulated waves. Mar. Geol. v.54, p 181-200
- Shi, N.C., Larsen, L.H., and Downing, J.P., 1985, Predicting suspended sediment concentration on continental shelves. Mar. Geol. v.62, p 255-275
- Sleath, J.F.A., 1970, Measurements close to the bed in a wave tank. Jour. Fluid Mech. v.42, p 11-123
- Sleath, J.F.A., 1987, Turbulent oscillatory flow over rough beds. Jour. Fluid Mech. v.182, p 369-409

- Smith, J.D., 1977, Modeling of sediment transport on continental shelves. (ed. by Goldberg, E.D., McCave, I.N., O'Brien, J.J.O., and Steele, J.H.) The sea, Wiley Interscience, v.6, p 539-577
- Smith, J.D. and McLean, S.R., 1977, Spatially averaged flow over a wavy surface. Jour. Geophys. Res. v.82, p 1735-1746
- Snedecor, G.W. and Cochran, W.G., 1967, Statistical methods, 6th ed., Iowa State Univ. Press, Iowa, 593 pp
- Soulsby, R.L. and Dyer, K.R., 1981, The form of the near-bed velocity profile in a tidally accelerating flow. Jour. Geophys. Res. v.86, p 8067-8074
- Sternberg, R.W., 1968, Friction factors in tidal channels with differing bed roughness. Mar. Geol. v.6, p 243-261
- Sternberg, R.W., Cacchione, D.A., Drake, D.E., and Kranck, K., 1985, Suspended sediment transport in an estuarine tidal channel in San Francisco Bay, California. Mar. Geol. v.71, p 237-258
- Swift, D.J.P., Niedora, A.W., Vincent, C.E., and Hopkins, T.S., 1985, Barrier island evolution, Middle Atlantic Shelf, U.S.A., Part I: Shoreface dynamics. Mar. Geol. v.63, p 331-361
- Tennekes, H. and Lumley, J.L., 1972, A first course in turbulence, MIT Press, Mass., 300 pp



- Tooby, P.F., Wick, G.L., and Isaacs, J.D., 1977, The motion of a small sphere in a rotating velocity field: A possible mechanism for suspending particles in turbulence. Jour. Geophys. Res. v.82, p 2096-2100
- Vanoni, V.A., 1941, Some experiments on the transportation of suspended load. Trans. AGU Papers, Hydrology, p 608-621
- Vincent, C.E., Young, R.A., and Swift, D.J.P., 1981, Bed-load transport under waves and currents. Mar. Geol. v.39, p 71-80
- Wang, H. and Liang, S.S., 1975, Mechanics of suspended sediment in random waves. Jour. Geophys. Res. v.80, p 3488-3494
- Wiberg, P. and Smith, J.D., 1983, A comparison of field data and theoretical models for wave-current interactions at the bed on the continental shelf. Cont. Shelf Res. v.2, p 126-136
- World Meteorological Organization (WMO), 1976, Handbook on wave analysis and forecasting, WMO-No.446, WMO, Geneva, Switzerland, 97 pp
- Wright, L.D., 1987, Shelf-surfzone coupling: Diabathic shoreface transport. (ed. by Kraus, N.) Coastal Sediments '87, ASCE, p 25-40

Wright, L.D., Boon, J.D., Green, M.O., and List, J.H., 1986,  
Response of the mid shoreface of the southern Mid-Atlantic Bight  
to a "Northeaster". Geo-Mar. Let. v.6, p 153-160

Wright, L.D., May, S.K., Short, a.D., and Green, M.O., 1985,  
Prediction of beach and surfzone morphodynamics: Equilibria,  
rates of change, and frequency response. Proc. 19th Coast. Eng.  
Conf., Houston, Texas, Sep. 1984, p 2150-2164

Yalin, M.S., 1977, Mechanics of sediment transport. 2nd ed.,  
Pergamon Press, Oxford, U.K., 298 pp

VITA

SUNG CHAN KIM

Born in Uljin, Korea on 20 March, 1954. Entered the Department of Oceanography at Seoul National University, Korea, and graduated in 1977 with a Bachelor of Science. After serving in the Korean Army as a private for three dull years, returned to the graduate program in the same department. Received Master of Science in Oceanography in 1982. Was employed for the next one and half year by the Department of Oceanography at Inha University, Incheon, Korea, as a research assistant. With the scholarship from the Ministry of Education, Korean Government, decided to see the big world. In August 1983, began Ph.D. program at the Virginia Institute of Marine Science.